

Republic of Iraq  
Ministry of Higher Education  
and Scientific Research  
Al-Nahrain University  
College of Science  
Physics Department



# Construction and Characterization of Pseudospark High Power Plasma Switch

**A Thesis**

Submitted to the College of Science / Al-Nahrain University  
in a partial fulfillment of the requirements for the Degree of  
Doctor of Philosophy in Physics

**BY**

***Basma H. Hamad Al-Shammary***

B.Sc. Physics / College of Science / Al-Nahrain University/2001  
M.Sc. Physics / College of Science / Al-Nahrain University/2003

**Supervised by**

***Prof. Dr. Ahmed K. Ahmed      and      Dr. Kamal H. Lateef***

**April 2014**

**Jamad Al-Thani 1435**

# Supervisors Certification

We certify that this thesis entitled “**Construction and Characterization of Pseudo-Spark High Power Plasma Switch**” was prepared by "**Basma Hussain Hamad** " under our supervision at the College of Science/ Al-Nahrain University as partial fulfillment of the requirements for the degree of Doctor of Philosophy in Physics.

Signature:

Name: Dr. Ahmad K. Ahmad

Academic rank: Professor

Date:    /    / 2014.

Signature:

Name: Dr. Kamal H. Lateef

Academic rank: Chief Researcher

Date:    /    / 2014.

In view of the recommendations, I forward this thesis for debate by the examining committee.

Signature:

Name: Dr. Thamir Abdul-Jabbar Jumah

Academic rank: Asst. Professor

Title: Head of Physics Department

Date:    /    /2014

## Committee Certification

We examination committee certify that we have read the thesis entitled " *Construction and Characterization of Pseudo-Spark High Power Plasma Switch* " and examined the student, " *Basma Hussain Hamad* " in its content ,and that in our opinion it is accepted for the Partial Fulfillment of the Requirements for the Degree of Doctor of Philosophy in Physics.

*Signature:*

**Name : Dr. Bahaa T. Chiad**

**Title: Professor**

**Date: // 2014**

**Address: Dept. of Physics  
College of Science  
University of Baghdad  
(Chairman)**

*Signature:*

**Name: Dr. Raad A. Khamis**

**Title: Professor**

**Date: // 2014**

**Address: Laser Unit,  
Department of Applied Science  
University of Technology  
(Member)**

*Signature:*

**Name : Dr. Mohammed A. Z. Habeeb**

**Title: Asst. Professor**

**Date: // 2014**

**Address: Dept. of Physics  
College of Science  
Al-Nahrain University  
(Member)**

*Signature:*

**Name: Dr. Ramiz A. AL-Ansari**

**Title: Asst. Professor**

**Date: // 2014**

**Address: Dept. of Physics  
College of Science for Women  
University of Baghdad  
(Member)**

*Signature:*

**Name : Dr. Raad Hameed Majeed**

**Title: Asst. Professor**

**Date: // 2014**

**Address: Dept. of Physics  
College of Education (Ibn al Haitham)  
University of Baghdad  
(Member)**

*Signature:*

**Name : Dr. Ahmad K. Ahmad**

**Title: Professor**

**Date: // 2014**

**Address: Dept. of Physics  
College of Science  
Al-Nahrain University  
(Supervisor)**

*Signature:*

**Name: Dr. Kamal H. Lateef**

**Title: Chief Researcher**

**Date: // 2014**

**Address: Department of Renewable  
Energy, Ministry of Science &  
Technology  
(Supervisor)**

I, here by certify upon the decision of the examining committee.

*Signature:*

**Name : Dr. Hadi M. A. Abood**

**Title: Asst. Professor**

**Address: Dean of the College of Science  
Al-Nahrain University  
Date: // 2014**

*Dedication To my Parents  
and my Husband .....*

# Acknowledgment

Firstly, all praise goes to *Allah* for His uncountable blessing. I would like to express my sincere thanks and deep gratitude to *Prof. Dr. Ahmad K. Ahmad* and *Dr. Kamal H. Lateef* for supervising the present work and for their support and encouragement throughout the research.

I would like to thank *Prof. Dr. Bahaa T. Chiad* (Department of Physics/Baghdad University) for his valuable assistance during the work.

My special thanks are also due to *Mr. Ahmad KH. Kadhim* and *Mr. Natheer B. Mahmood* for helping me in this work.

I am grateful to the Head of the Department of Physics at Al-Nahrain University *Dr. Thamir A. Jumah* for his valuable support and cooperation.

Last but not least, I would like to record my deep affection and thanks to *my mother* for her moral support and patience throughout this work.

*Basma*

# Content

<b>Contents</b>	<b>Page</b>
Acknowledgments	i
Abstract	ii
Content	iii
List of Symbols	v
Abbreviations	vi
List of Tables	vi
<b>Chapter One: Introduction</b>	
1.1 Gas discharge phenomena	1
1.2 Glow discharge	3
1.3 Mechanism of breakdown of gases	5
1.3.1 Townsend mechanism	6
1.4 Paschen's law	9
1.5 Review of pulsed power switches	11
1.5.1 Spark gaps	17
1.5.2 Thyratrons	17
1.5.3 Pseudospark switch (PSS)	19
1.6 Mechanism and configuration of pseudospark discharge	20
1.6.1 Pre-discharge	22
1.6.2 Hollow cathode discharge	22
1.6.3 High current main discharge	23
1.6.4 Decay of plasma	23

1.7 Literature Review	24
1.8 Thesis Aim	27
<b>Chapter Two: Construction and Measuring Technique</b>	
2.1 Introduction	28
2.1.1 Type and pressure of the gas	29
2.1.2 Distance between the electrodes	30
2.1.3 Matching electrodes axes	31
2.2 Construction procedure of pseudo spark switch chamber	31
2.2.1 Construction of electrodes chamber	32
2.2.2 The insulator choice	35
2.2.3 O- ring rubber groove design	35
2.3 The pumping system and gas flow controller	35
2.4 The electrical circuits	36
2.4.1 A pseudospark switch	36
2.4.2 Trigger circuit	37
2.4.3 The main electrical circuits	40
2.5 Dummy load and shunt resistor	45
2.6 The measurements and calculations of reactance and impedance of the system	45
2.7 The erosion of the electrodes	49
2.8. Construction of Shunt resistor	51
2.8.1. Design considerations	52
2.8.2. Results and discussion	54
2.9. Dummy load manufacturing	56

2.9.1. Design considerations	57
2.9.2. Results and Discussion	58
<b>Chapter Three: Results, Discussion and Conclusions</b>	
3.1. Introduction	61
3.2. The trigger pulse shape	61
3.3. The breakdown voltage of the gas	65
3.4. Pseudospark switch characteristic	67
3.4.1. Anode voltage waveform	67
3.4.2 Conduction current waveform of PSS	71
3.5. Current Pulse Parameters	77
3.5.1. The Rise time	77
3.5.2. The effect of capacitor values	79
3.5.3. Jitter time	82
3.5.4. The inductance of the PSS	83
3.6. Conclusions	84
3.7. Suggestion for Future Work	85
<b>References</b>	86

## List of Symbols

A, B & C	constants
$A^+$	positive ion
C	capacitor
D	diameter of bore hole
d	distance between two electrodes
E	applied electric field
e	electron charge
$e^{\alpha d}$	electron avalanche
f	frequency
h	planck constant
I	current
L	inductance
l	length of coil
m	mass of electron
N	number of turns of coil
n	number of electrons leaving the cathode through distance x
P	electrical power
$p$	gas pressure
Q	flow rate
R	resistance
$r_0$	radius of gas vessel volume
$r_1$	radius of 1 <sup>st</sup> layer of coil

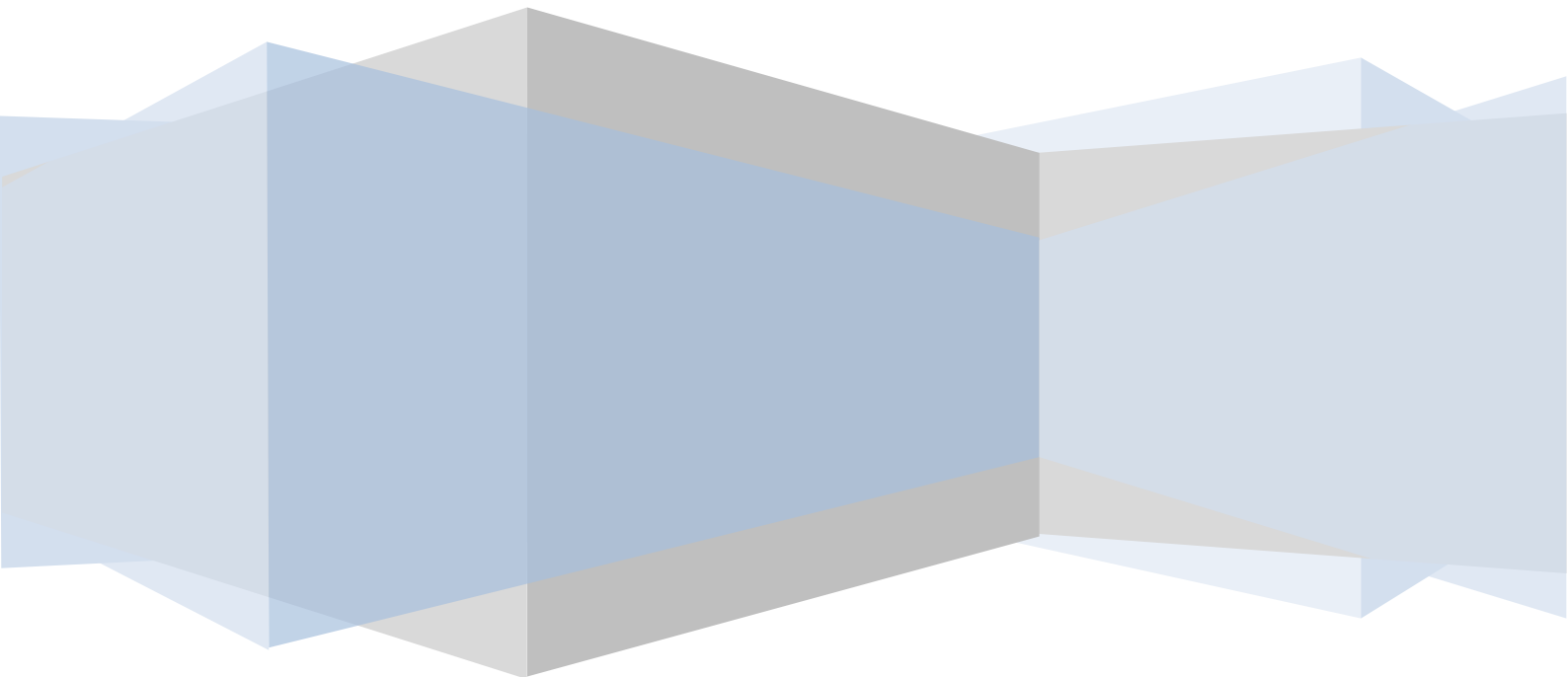
$r_6$	radius of 6 <sup>th</sup> layer of coil
t	time
$t_{rec}$	minimum limit of recovery time
$U_L$	Energy
V	voltage
V	volume of the chamber
v	velocity of electron
$X_L$	reactance due to inductance
Z	impedance
$\alpha$	Townsend 1 <sup>st</sup> ionization coefficient
$\gamma$	Townsend 2 <sup>nd</sup> ionization coefficient
u	velocity of photons
$\omega$	angular frequency

## Abbreviations

<b>AC</b>	<b>Alternative Current</b>
<b>BLT</b>	<b>Back Light Thyatron</b>
<b>CVR</b>	<b>Current View Resistor</b>
<b>DC</b>	<b>Direct Current</b>
<b>FWHM</b>	<b>Full Width Half Maximum</b>
<b>TEA-CO<sub>2</sub></b>	<b>Transversely Excited Atmospheric CO<sub>2</sub> Laser</b>
<b>PSS</b>	<b>Pseudo Spark Switch</b>
<b>PVC</b>	<b>Poly Vinyl Chloride</b>

# **Chapter One**

## **Introduction**



## **1. Introduction:**

### **1.1. Gas Discharge Phenomena:**

Discharge can be created by applying a potential difference between two electrodes in a gaseous medium. Electric field generated between these two electrodes (anode and cathode) causes ionization of neutral gas particles and creates a conducting path. This phenomenon is called breakdown of the gaseous medium [1].

Electric field lines between the anode and the cathode depend on the geometry of the electrodes. The simplest configuration, where the electric field is almost uniform, is two plane electrodes with a small gap in between compared to the size of electrodes. Figure 1.1 shows voltage-current characteristics of a DC low pressure electrical discharge with plane electrodes [1,2]. Dark discharge region is where discharge formation begins, however the discharge does not contain enough energized particles to lead to breakdown formation.

This discharge is dark because there are no energy level transitions of electrons causing visible light emission. During background ionization regime of the dark discharge, individual ions and electrons created by cosmic rays and other forms of natural ionizing radiation are swept out by increasing voltage; during saturation regime, all the background ionized charged particles are removed and moreover electrons do not have enough energy to cause ionization [3].

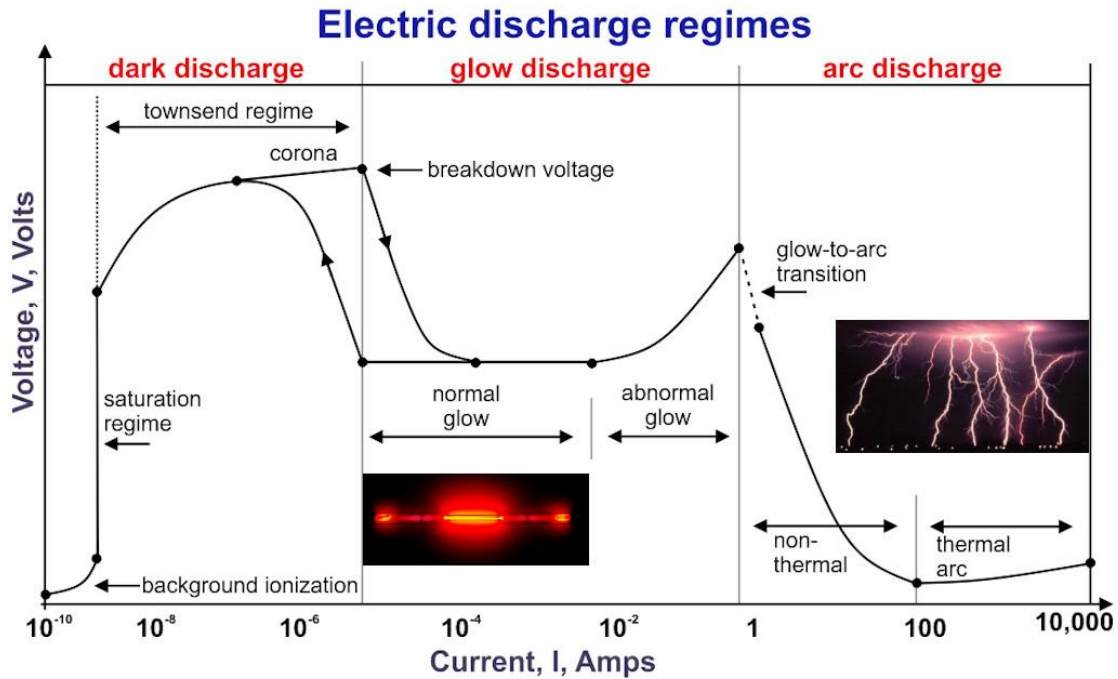


**Figure 1.1: I-V characteristic gas discharge [1].**

Townsend regime is where ionization caused by electric field starts, and the current increases exponentially with the increasing voltage. Between Townsend regime and the breakdown, corona discharges may occur as a result of local electric field concentrations on the electrode surfaces around sharp edges. Corona discharges can be visible or dark depending on the level of current supplied [3].

Glow discharge region is one of the main interests of this research. This region starts with the breakdown and ends with the arc formation. Glow discharge will be explained in detail in the next section.

Processes leading to the breakdown and glow discharge formation can be classified into two groups: (a) Gas processes in which ionization by electron and ion collisions is effective; (b) cathode processes in which electrons are liberated from the cathode. Cathode processes are also called secondary processes where electron emission is effective. Experimental results in the literature indicate that the cathode material affects the breakdown phenomenon

and play a major role in breakdown formation. Secondary processes can be caused by different types of energy radiations like photoelectric emission where light energy contributes to electron release, or thermionic emission where thermal energy is main cause of electron emission, or field emission where emission due to electric field occurs [1,3].

Arc discharges region are intense, highly luminous, and high current density discharges. High current densities up to kilo amperes per square centimeter are easily achieved by arc discharges; however their concentrated nature causes high erosion rates of the electrodes [4].

## 1.2. Glow Discharge:

The glow discharge is a luminous low pressure discharge which has widespread industrial applications like analytical chemistry, micro-electronics fabrication, lasers, and lamps [2]. For the electrical discharge structure mentioned in previous section; current increases exponentially with applied voltage up to the breakdown voltage. At the breakdown voltage, if the current supplied through the voltage source is sufficient, the gas will breakdown leading to the glow discharge regime. Figure 1.2, represent an ideal sketch showing the regions of the normal glow discharge [1].

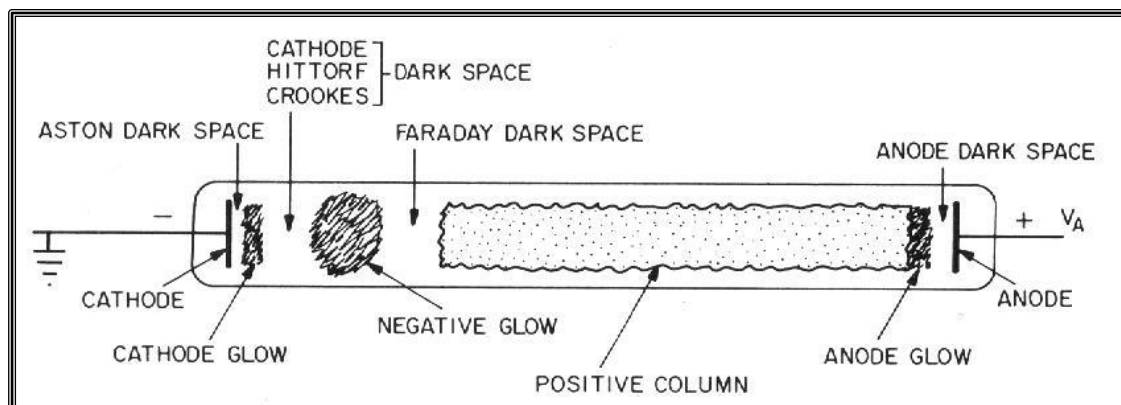


*Figure 1.2: Regions of normal glow discharge [1].*

The glow discharge can be divided into several categories:

Cathode: Electrically conducting metal whose secondary electron emission coefficient is very important for the discharge formation.

Aston Dark Space: Next to the right of cathode, Aston dark space is a thin dark region which contains slow electrons that are too low in energy to excite the gas.

Cathode Glow: Bright region close to the cathode with high ion number density, this region may cling to cathode and block Aston dark space.

Cathode Dark Space: Dark region to the right of cathode glow with high ion density and positive space charge.

Cathode Region: Most of the voltage drop across the discharge appears between cathode and the right of the cathode dark space. This region is called cathode region and the voltage drop in this region is referred as cathode fall. Most of the power dissipation occurs in this region. Length of this region is adjusted so that minimum power dissipation can be achieved.

Negative Glow: The brightest region with intense excitation of atoms. Electrons accelerated in the cathode region produce light emitting processes. This region is usually longer than the cathode glow.

Faraday Dark Space: Electron number density decreases in this region. Net space charge is very low and electric field is small.

Positive Column: This region is quasi-neutral. As the length of the discharge tube is increased at constant pressure, length of cathode region remains constant. Positive column is a long, uniform glow.

Anode Glow: Bright region close to anode that is not always present.

Anode Dark Space: Dark region next to anode with high negative space charge.

During the normal glow discharge operation both the voltage across the electrodes and the current density through the plasma remain almost constant while the current delivered by the supply increases. This regime continues until

the plasma covers the entire cathode surface in order to deliver total current at constant current density. After this point both the voltage and the current density increase significantly leading to the abnormal glow discharge. At the end of the abnormal glow regime, the electrodes become sufficiently hot and the cathode emits electrons thermionically. If power source can supply sufficient current, glow-to-arc transition occurs at this point.

Glow discharge is the self-sustained continuous DC discharge consisting of a cold cathode, which emits electrons as a result of secondary emission mostly induced by positive ions [5].

### **1.3. Mechanism of Breakdown of Gases:**

At normal temperature and pressure, the gases are excellent insulators. At higher electric fields, charged particles may gain sufficient energy between collisions to cause ionization on impact with neutral molecules. It is known that during an elastic collision, an electron loses little energy and rapidly builds up its kinetic energy which is supplied by an external electric field. On the other hand, during elastic collision, a large part of the kinetic energy is transformed into potential energy by ionizing the molecule struck by the electron. Ionization by electron impact under strong electric field is the most important process leading to breakdown of gases [5, 6]. The electron gains energy due to acceleration in the electric field, where elastic collisions are the most dominant in low kinetic energy till reaching to sufficient kinetic energy to cause inelastic collisions making ionization in the medium, which will flow the current between the two electrodes:

$e + A \rightarrow A^+ + e + e$  (Inelastic collisions) and  $e + A \rightarrow A^* + e$  (excitation)  
where  $A$  represents a neutral atom or molecule in the gas,  $A^+$  is the positive ion and  $A^*$  excited atom [6].

### 1.3.1. Townsend Mechanism:

The variation of current as a function of voltage was studied firstly by Townsend (1939) [7]. He considered a two parallel electrodes having gas as an insulating medium and separated by a distance  $d$  as shown in figure 1.3. When no electric field is set up between the electrodes, a state of equilibrium exists between electrons and positive ions generation due to the decay processes. This state of equilibrium will be disturbed the moment a high electric field is applied. He found that the current at first increases proportionally as the voltage is increased and then remains constant, at  $I_0$  which corresponds to the saturation current. At still higher voltages, the current increases exponentially.

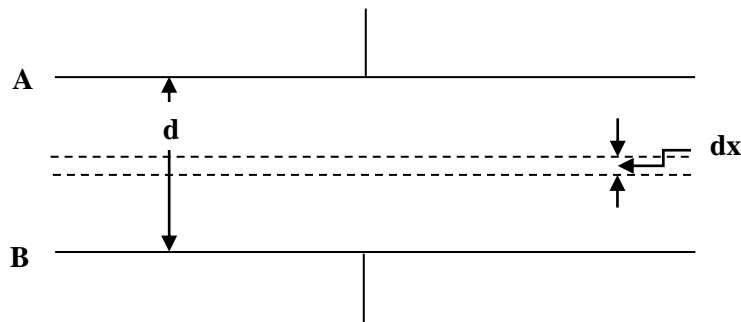


*Figure 1.3: Two parallel electrodes [7].*

The variation of current as a function of voltage is shown in figure 1.4. The exponential increase in current is due to ionization of gas by electron collision. As the voltage increases  $I$  increases and hence the electrons are accelerated more and more and between collisions these acquire higher kinetic energy and, therefore, knock out more and more electrons [7].

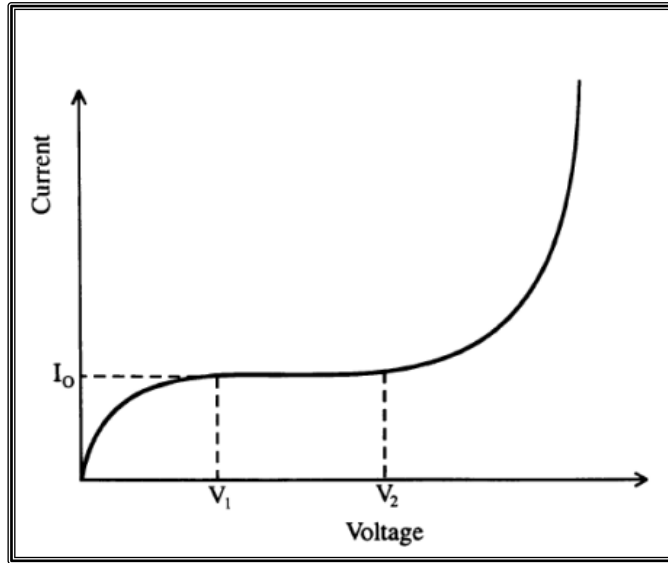


**Figure 1.4: Current vs. voltage relationship developed by Townsend [7].**

To explain the exponential rise in current, Townsend introduced a coefficient  $\alpha$  known as *Townsend's first ionization coefficient* and is defined as the number of electrons produced by an electron per unit length of path in the direction of field. Let  $n_0$  be the number of electrons leaving the cathode and when these have moved through a distance  $x$  from the cathode, these become  $n$ . Now when these  $n$  electrons move through a distance  $dx$  they produce additional  $dn$  electrons due to collision. Therefore,

$$dn = \alpha n dx \dots\dots\dots(1-1)$$

Integrating this equation over the distance  $d$ , from cathode to anode gives:

$$n = n_0 e^{\alpha d} \dots\dots\dots(1-2)$$

In terms of current at the anode:

$$I = I_0 e^{\alpha d} \dots\dots\dots(1-3)$$

where  $I_0$  is the current leaving the cathode.

The term  $e^{\alpha d}$  is called the *electron avalanche* and it represents the number of electrons produced by one electron in travelling from cathode to anode.

The ionization coefficient is actually dependent on the electron energy distribution in a gas, which depends only on E/P, where E is the applied electric field and P is the gas pressure. Therefore the relation can be written as [8]:

$$\frac{\alpha}{P} = F\left(\frac{E}{P}\right) \dots \dots \dots (1-4)$$

Townsend suggested that a second mechanism must be affecting the current. He postulated that the additional current must be due to the presence of positive ions and the photons. The positive ions will liberate electrons by collision with gas molecules and by bombardment against the cathode. Similarly, the photons will also release electrons after collision with gas molecules and from the cathode after photon impact. Townsend suggested ( $\gamma$ ) known as *Townsend second ionization coefficient* which is defined as the number of electrons released from cathode per incident positive ion, the steady state current, equation (1-3), accounting for both Townsend coefficients, can be rewritten as [7,8]:

$$I = I_0 \frac{e^{\alpha d}}{1 - \gamma(e^{\alpha d} - 1)} \dots \dots \dots (1-5)$$

Experimental values for  $\gamma$  have been determined from equation (1-5) for known values of E, P, gap distance, and  $\alpha$ . Values for  $\gamma$  are highly dependent on cathode surface properties. Low work function materials will produce greater emissions. The value of  $\gamma$  is small at low values of E/P and higher at greater values of E/P. This is to be expected since at high values of E/P there will be a greater number of positive ions and photons with energies high enough to eject electrons from the cathode [5,7].

$$I = I_0 \frac{e^{(pd)F\left(\frac{v}{pd}\right)}}{1 - \gamma(e^{(pd)F\left(\frac{v}{pd}\right)} - 1)} \dots \dots \dots (1-6)$$

As the gap voltage increases, the electrode current at the anode increases according to equation (1-5). The current will increase until at some point the denominator of equation. (1- 5) becomes zero, or

$$\gamma (e^{\alpha d} - 1) = 1 \dots\dots\dots (1-7)$$

At this point, equation (1-5) predicts that the electrode current becomes infinite. This is defined as the transition from self-sustained discharge to breakdown.

Theoretically, the value of the current becomes infinite, but in practice it is limited by the external circuit and voltage drop across the gap. A self-sustaining discharge occurs when the number of ion pairs produced in the gap by the passage of one electron avalanche is large enough that the resulting positive ions, on bombarding the cathode, are able to release one secondary electron and cause a repetition of the avalanche process. The discharge may also be self-sustaining as a result of the secondary electron photoemission process [7].

#### 1.4 Paschen's Law:

Paschen's law stating that the amount of potential difference required for a gas to breakdown is a function of pressure and gap distance product ( $pd$ ).

$$V_{breakdown} = F(pd) \dots\dots\dots (1-6)$$

It was first stated by F. Paschen in his paper at 1889.

If there exists different lengths of discharge paths between anode and cathode, Paschen minimum can occur at long-paths for low-pressures and short-paths for high pressures. The shape of Paschen's curve indicates two different  $pd$  product values for the same breakdown voltage, one on the right-hand side, and one on the left-hand side of Paschen minimum. High power plasma switches aiming to hold-off very high voltages are developed on both sides of Paschen

curve, indicating either high or low pressure range operation. Thyratrons and pseudo sparks operate on the left-hand side of the Paschen's curve [9,10].

In general, the equations for breakdown are given by:

Breakdown voltage:

$$V_{breakdown} = \frac{Bpd}{c + \ln F(pd)} \dots \dots \dots (1-6)$$

Breakdown field strength:

$$E_{breakdown} = \frac{Bp}{(c + \ln F(pd))} \dots \dots \dots (1-7)$$

where:

$$c = \ln \left[ \frac{A}{\ln(1 + \frac{1}{\gamma})} \right] \dots \dots \dots (1-8)$$

where  $\gamma$  is the secondary ionization coefficient, for air :

$A = 15 \text{ cm}^{-1} \text{ Torr}^{-1}$ ,  $B = 365 \text{ Vcm}^{-1} \text{ Torr}^{-1}$  and  $\gamma = 10^{-2}$ , hence  $c = 1.18$ .

Figure 1.5 shows the breakdown voltage as a function of  $pd$  product [9]:

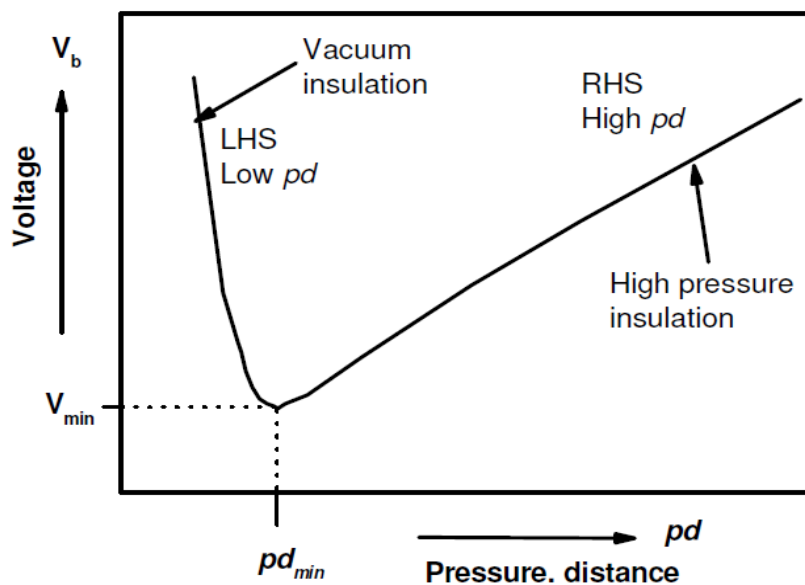


**Figure 1.5: Paschen's curve [9].**

## 1.5 Review of Pulsed Power Switches:

Pulsed power systems are the technology of storing energy in capacitive or inductive form over a relatively long period of time (usually milliseconds to minutes) and then discharging it into a load over a much shorter time period (usually  $\mu\text{s}$  to ns) as an electrical energy by closing or opening power switches. Power generation, power switches, pulse forming network, and the load are the major components of a pulsed power system.

Many types of high voltage and nanosecond pulse generators are commercially available currently. However, the performance of these generators varies broadly and they should be chosen according to load requirements, such as output voltage, pulse width, rise time, repetition rate, and peak power. The fundamental purpose of all pulsed power system is to convert a low-power, long-time input into a high-power short-time output [6].

In simplest terms, a pulsed power system includes an energy storage stage, a load, and a pulse forming stage between these two stages as shown in figure 1.6. The pulse forming stage can be a single high power switch that transfers the stored energy to the load or a more complex system based on a network of high power switches.

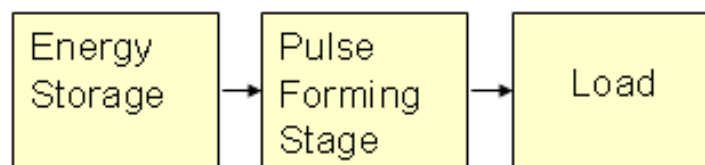


***Figure 1.6: Pulsed power system block diagram***

Power switches, between the storage devices and the loads, play an indispensable role in the generation of pulsed power. The shape, rise time, and magnitude of the generator output pulse depend strongly on the properties of the power switches. Moreover, the maximum power capacity and power density that the power switches could handle also limit the performance of pulse

generators. Switches are generally categorized into closing switches for capacitive storage devices and opening switches for discharging inductive storage devices.

Gas switches and semiconductor switches are two common types of closing switches. Gas switches are highly employed in high power pulse generators. They are easy to use, can handle relatively large currents, and can be also triggered accurately. Several kinds of gas switches such as ignitron, thyatron, pseudospark switch, and spark gap are reported in literature [6,7]. Their operating gas pressure and hold-off voltage ranges are shown in Figure 1.7.

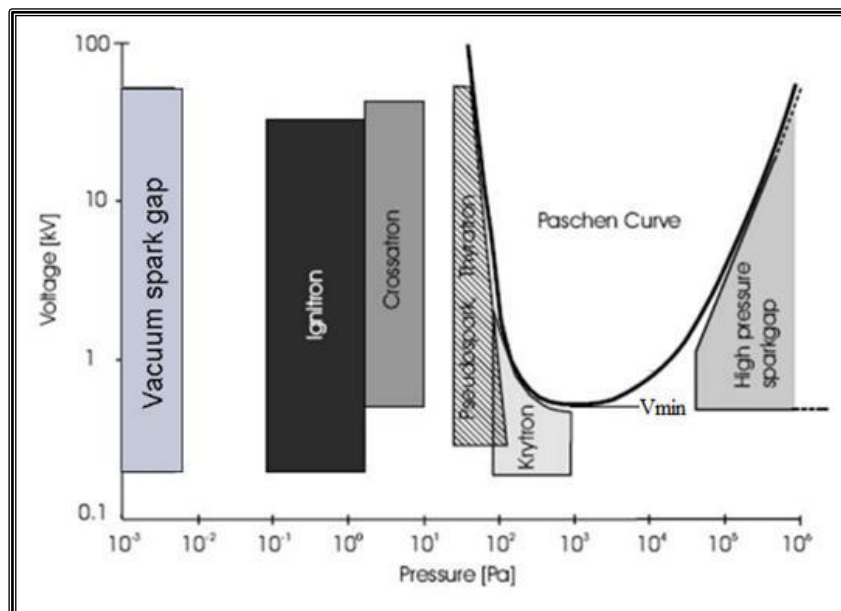


**Figure 1.7: Range of gas pressure and operating voltages for different types of gas switches [6]**

Among these, pseudospark switch taking advantage of hollow cathode effect stands out because of its reduced electrode erosion, high power capability, and long lifetime. Generally the operation of pseudospark switch is described in four different periods: pre-discharge, hollow cathode discharge, high current super-emissive discharge, and the decay of the discharge plasma [6,8]. In order

to make use of the pseudospark discharge, a precise triggering system is required for the switch.

Although the specific terminology of the pulsed power switch is sometimes different, the parameters that are used to evaluate the switch performances have much in common. The regular switch parameters are described below [12]:

Hold-off Voltage: The maximum voltage that can be provided between the electrodes of the switch without breakdown. It is also called stand-off voltage, self-breakdown voltage or blocking voltage sometimes. The

value of the hold-off voltage is determined by the medium property between the electrodes and the dielectric strength of the insulating envelope outside the switch. In some special cases, the switch is charged up rapidly in pulse mode with voltage higher than the DC hold-off voltage, which is called over-voltage [12].

Peak Current: The highest current conducting capability of the switch. The usual units are amperes (A), or kilo amperes (kA). It is limited by the medium conducting property and the geometry of the electrodes. Especially in the gas switch, the hollow structure of the switch cathode improves the peak current. The hollow cathode mode of the pseudospark switch will be discussed in detail later.

Delay Time: The time interval between the application of a trigger command and the initiation of switch conduction. This time interval is composed of processes which involve the generation of the initial charge carriers and the pre-breakdown phases to establish conducting channels between the electrodes. In addition, the inductance of the switch itself and the pulsed power system also increases the delay time of the switching.

Jitter Time: The statistical variations of the delay time. This time is usually measured in ns or  $\mu$ s. The sufficient energy is required to accelerate the carriers and transport them to the gap to establish “switch-on” and sustain the conduction. Because the initial charge will have some initial velocity distribution, some of the carriers will cross the gap later than others, resulting in switching “jitters”. Thus, the initial conditions are very important and some switches use “keep alive” discharges, lasers or electron beams to reduce jitters [12].

These devices help to insure consistent behavior of the initiation process, particularly when timing is critical.

Recovery Time : The time for the recovery of the dielectric properties of the switch so that voltage can be reapplied at some rate ( $dV/dt$ ). The recovery process relates to the plasma kinetic characteristics of the conducting medium which include the charge density, mobility, temperature, recombination, attachment, mean free paths, and applied fields, etc [11].

Forward Drop : The voltage drop across the switch impedance during the “turn on” phase. When the switches work for high current or high frequency operations, the heat problem caused by the forward drop becomes serious, and a cooling system is necessary[12].

Repetition Rate : The rate at which the switch can be operated without degradation of characteristics. The usual units are Hertz (Hz) or kilohertz (kHz). The rate is limited by the switch recovery time and forward drop.

Life Time: The number of operation times, sometimes called “shots”, beyond which the switch cannot work properly [12].

The definitions of those switch parameters above could be a guide when we choose and design switches for the real applications. These parameters are commonly mentioned for switch characterization evaluations.

As mentioned in the introduction, high power switches are the most important components of the pulse forming stage of a pulsed power system. They are used to transfer large amounts of stored energy as high amplitude, short duration pulse to the load. Therefore, they must meet high voltage/current and short rise/recovery time requirements of the load. These requirements are usually voltages between several tens of kilovolts to megavolts and rise times as short as nanoseconds up to microseconds. Plasma switches have been used for their good transition properties and high voltage stand-off (hold-off) capabilities for decades in pulsed power systems. Closing plasma switches like gas filled spark gaps, ignitrons, thyratrons are reviewed in literature in detail [13, 14].

Solid-state switches are also finding increasing applications in pulsed power systems with their compact house-keeping requirements and long lifetimes. However, their limited hold-off voltage and peak current capabilities are still making them unable to handle the parameters of large pulsed power systems. Closing solid-state switches when operated within specifications have very long lifetimes, however one-time formation of an arc is catastrophic unlike plasma switches where this will only cause reduction of lifetime [15]. Table 1.1 summarizes some parameters for primary gas-phase closing switches like spark gaps, thyratrons and pseudo sparks as well as solid-state closing switches like thyristor.

**Table (1-1): Summary of Gas-Phase and Semiconductor Switches for Pulsed Power Applications [15]**

<b>Switch</b>	<b>Hold-off Voltage (kV)</b>	<b>Peak Current (kA)</b>	<b>Forward Drop (V)</b>
<b>Spark Gap</b>	<b>100</b>	<b>10 to &gt;1000</b>	<b>20</b>
<b>Thyratron</b>	<b>30</b>	<b>1-10</b>	<b>150</b>
<b>Pseudospark</b>	<b>35</b>	<b>5-100</b>	<b>200</b>
<b>Thyristor</b>	<b>1-5</b>	<b>1 to 50</b>	<b>2</b>

### **1.5.1. Spark Gaps:**

Self-breakdown spark gaps can be described as the simplest closing switches with two electrodes inserted in a gaseous medium. Upon application of required voltage, transition of the gas from a good insulator to a good conductor (open to close) is achieved [15].

In order to achieve better estimation of delay, and to be able to synchronize spark gaps in series or in parallel, several trigger mechanisms can be used. Triggered spark gaps include spark gaps that utilize a trigger electrode between anode and cathode, electron beam triggered spark gaps and laser triggered gas filled spark gaps [13]. Spark gaps can hold-off very high voltages and currents; however, arc formation can be very erosive at high currents, thus altering electrode characteristics. As a result, repeatability and lifetime are main limitations for this type of switches [15].

### **1.5.2. Thyratrons:**

Although first idea for thyratron was stated as early as 1918's [16], hydrogen thyratrons have emerged during World War II as an input switch for power modulators for radars, and other applications. Hydrogen thyratron was

developed by Germeshausen. Thyratrons are low-pressure plasma switches with a typical geometry as shown in Figure 1.8.

Thyratrons work on the left-hand side of the Paschen curve which provides high stand-off voltages. Upon application of a positive trigger pulse to the grid, plasma formation is achieved in the grid-cathode region. This leads to closing of the switch by initiating the breakdown in grid-anode region and later connecting these two regions of plasmas [17].

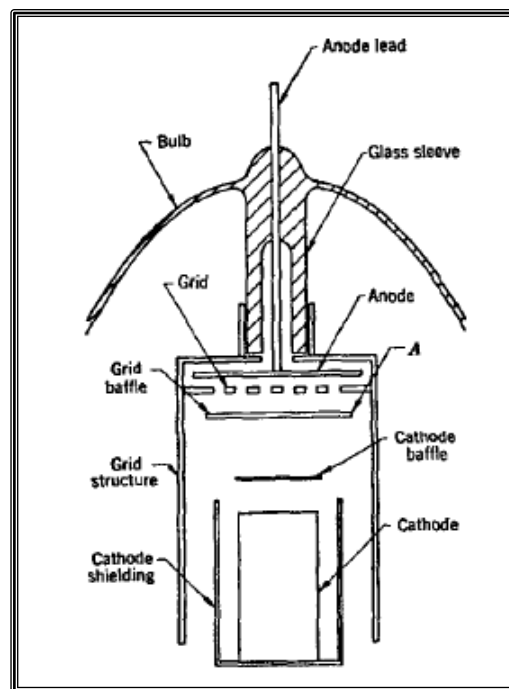


*Figure 1.8: Geometry of a hydrogen thyatron [17]*

Recovery of the switch is usually achieved by starting deionization by keeping the anode voltage slightly negative. Thermionic cathodes which require external heating are used to increase peak current levels. High lifetime specifications are achieved by usage of hydrogen reservoir [12].

Early thyratrons used mercury vapor as filling gas which was replaced by hydrogen because of two big advantages. First, cathode destruction voltage for hydrogen is much higher which improves standoff voltage and lifetime

parameters. Second, it has much lighter ionic mass which means much less recovery time and higher repetition rates. However, hydrogen has the disadvantage of being a chemically active atom which causes unwanted impurities in the gas. Hydrogen reservoirs containing metal hydrides which lead to reversible reaction with hydrogen as a function of temperature are the solution to this problem. These reservoirs accompany a heater to control the mentioned reversible reaction [14]. Later many improvements like ceramic envelope and multi gap thyratrons have led to very high power ratings with hydrogen thyratrons.

One of the most important advantages of hydrogen thyratrons is their long lifetimes. This is due to glow discharge operation rather than arc which is the case for spark gaps. Glow discharge operation causes less erosion because of its diffused nature. Although thyratrons could not achieve high peak currents of spark gaps, they are still very widely used because of their very high repetition rate capabilities and long lifetimes in many repetitive pulsed power applications [18].

### **1.5.3. Pseudospark Switch (PSS):**

Pseudosparks are low pressure plasma switches similar to thyratrons but with much higher current rise capability. Usually, higher current densities cause shorter lifetimes due to electrode erosion. However, because of special properties of the pseudospark discharge, which can prevent arcing at very high current densities; these switches have lifetimes comparable to thyratrons [19].

Pseudosparks when first discovered [20] were regarded as intense electron beam generators. Later they attracted attention as high power switches with very short current rise times as well as high current peaks and long lifetimes. Moreover, low pressure operation providing short recovery times and, therefore, high repetition rates are attractive [21].

Pseudosparks have a special axisymmetric hollow cathode-hollow anode structure. At low pressures, mean free path of electrons is very long compared to the distance between the electrodes. Therefore, most of the electrons released at cathode arrive to anode without undergoing any ionizing collisions, which is the reason for increased breakdown voltage at low pressures (left-hand side of Paschen curve).

However, hollow geometry of electrodes provides other possible lengths of discharge paths between anode and cathode thus decreasing breakdown voltage as a result of hollow cathode effect [21,22]. Figure 1.9 shows electric field lines at the axis of hollow cathode- hollow anode geometry causing breakdown voltage drop at this region.

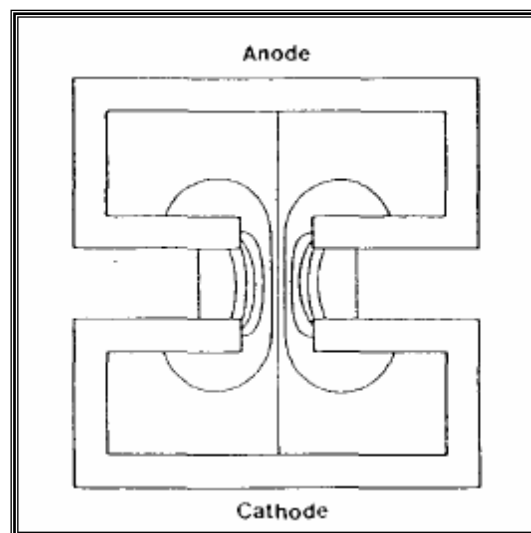


*Figure 1.9: Electric field lines on the axis of a typical pseudospark geometry [23].*

### **1.6. Mechanism and Configuration of Pseudo Spark Discharge:**

The pseudo spark discharge was first discovered in the late 1970's, as an axially symmetric, high voltage gas discharge operating at low pressure regime located on the left hand side of the Paschen curve as illustrated in Figure 1.10 [23], which is based on the principles of a hollow cathode discharge. The fundamental discharge configuration consists of planar anode and cathode, or multi-gap electrodes, as illustrated in Figure 1.11. The central hole in the

middle of the electrodes makes the effective distance of the discharge path a maximum in the region of the bore hole on the axial center of electrodes and cathode cavity. Thus the gas discharge is concentrated in the region around the axis of the central holes [24]. Then the high electric field ( $10^6$  V/m) concentrated in the central axis across the electrode gap and the charge carrier multiplication taking place in the hollow cathode causes the final ignition of high voltage high current gas breakdown. According to the previous research works [25], the pseudo spark discharge with a hollow cathode configuration can be divided into five different processes as illustrated in Figure 1.11.

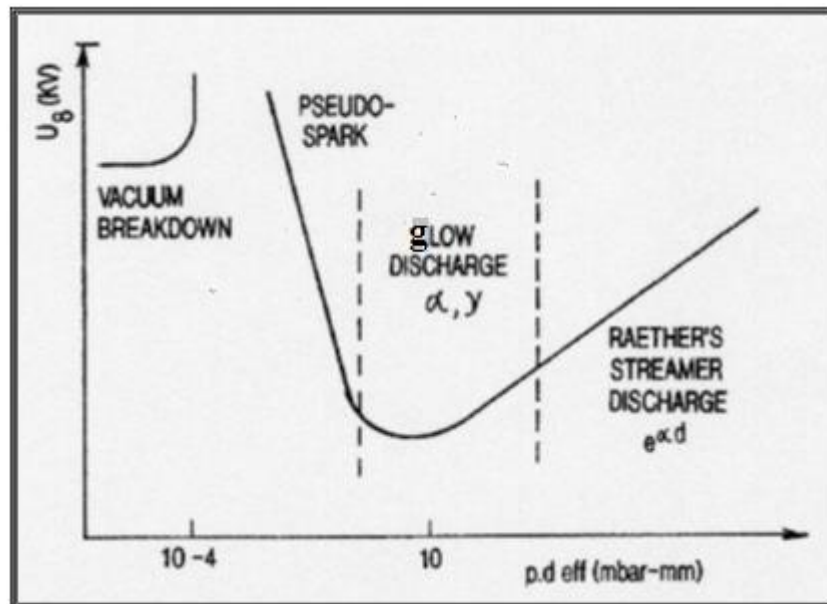


**Figure 1.10: Gas breakdown curve (Paschen's curve) under various pressure regions [22].**

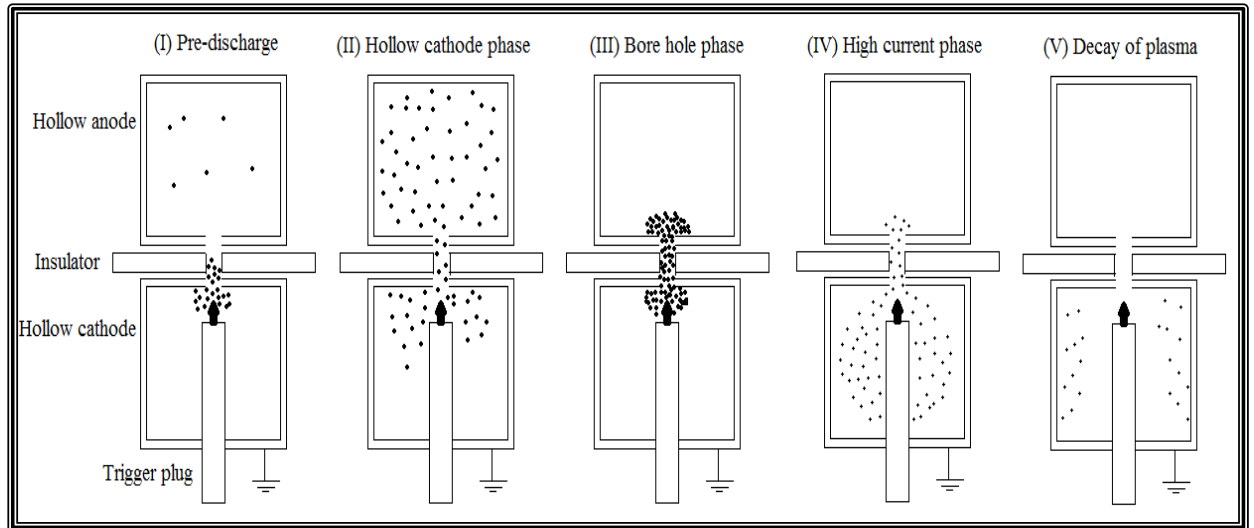


*Figure 1.11: Different stages in pseudo spark discharge.*

### **1.6.1 Pre-discharge:**

This stage is the initiation of pseudo spark discharge. The pseudo spark discharge originates from the large charge carrier multiplication in the region of hollow cathode. Thus the electrons released from the hollow cathode region generated by the particle impact or photo-effect depending on the trigger type cause a strong avalanche growth in the cathode backspace and accelerated into the gap between anode and cathode. Then dense plasma emerges at the center path in the inter gap region as illustrated in Figure 1.11 [24].

### **1.6.2. Hollow Cathode Discharge:**

In some research work, the hollow cathode discharge (phase II in Figure 1.11) and bore hole phase (phase III in Figure 1.11) are assumed to be one phase, since they are both characterized by ionization enhancement in the gap region and plasma propagation from cathode region toward anode space [25]. In this phase, the charge multiplication is further enhanced and the hollow cathode phase is filled with plasma working as a virtual cathode for the electron extraction from the cathode backspace. The extracted electrons from cathode backspace are accelerated and propagated under the effect of electric field

potential in the inter gap region between anode and cathode. This phase is characterized by the start of electron emission from pseudo spark discharge. Additionally, the voltage breakdown across the pseudo spark gap and increase in discharge current can be easily observed by electrical measurements in this phase [26].

### **1.6.3. High Current Main Discharge:**

This phase is of great interest in gas switching applications due to its capability to establish high current of kA within very short time of  $10^{-9}$ - $10^{-7}$  seconds, leading to a current rising rate of  $10^{10}$ - $10^{11}$  A/second. The mechanism for pseudo spark to achieve such a high current is still not well determined. In the work of Hartmann [27], the high current pseudo spark discharge is assumed to be a form of super dense glow discharge. In [27], gas particles are released from the cathode surface by ion impact and thermal desorption. The electrode surface is then heated by ion impact to a temperature of 3000-4000 K within 30-100 ns. Additionally, an estimation of field-enhanced thermionic electron emission (Schottky emission) was presented in [27] to show its capability to deliver the measured high current density. However, in some other works, the parameters of high current in pseudo spark are assumed to be mainly determined by the external circuit consisting of trigger, capacitance and inductance, and pulse charging mode.

### **1.6.4 Decay of Plasma:**

At this stage, the decay and recovery of plasma in pseudo spark is of specific interest due to their effect on the recovery strength and repetition rate of pseudo spark device. When the time interval between single shot of pseudo spark discharge exceeds the limit of decay and recovery time of plasma in given pseudo spark device, residual ionization in the gap can cause the

discharge to become unstable and breakdown of the gas occurs at lower voltages, i.e., during charging of the storage capacitors. During this phase, the main processes that remove the residual ionization in the pseudo spark device are plasma bulk recombination and diffusion toward the wall [28]. The research work presented in [29] shows that the bipolar diffusion of electrons inside the hollow cathode is the main limiting factor for the decay and recovery time of pseudo spark discharge. And the recovery time of pseudo spark device presented in [29] is fitted as a function of hollow cathode length and radius of gas volume in the given configuration:

$$t_{\text{rec}} \propto \left[ \left( \frac{2.405}{r_0} \right)^2 + \left( \frac{\pi}{L} \right)^2 \right] \dots \dots \dots (1-9)$$

where  $t_{\text{rec}}$  is the minimum limit of recovery time for a pseudo spark device,  $r_0$  is the radius of gas vessel volume in the given device, and  $L$  is the length of hollow cathode.

### 1.7. Literature Review:

Pseudospark discharge was first discovered in **1979** by **Christiansen and Schultheiss** [20] they designed electrical switches involving axially symmetric hollow electrodes at low pressure of  $\text{H}_2$  gas to produce an electron beam with a current density for more than  $10^6 \text{ A/cm}^2$  at 140 A total current . The design by **D. Bloess, et al (1982)** [30] suggests a basic model to describe and explain the initialization and the growth of the pseudospark discharge process in two phases (single-gap and multi-gap chambers) , and generate pinched electron beams with peak current up to 5kA with FWHM pulse of 2ns to 20 ns and densities greater than  $10^5 \text{ A/cm}^2$ .

**G. Mechtersheimer, et al [31] in 1986** developed a pseudospark switch triggered by a pulsed low pressure of  $\text{N}_2$  gas discharge, this switch works at high repetition rates of 100 kHz and fast rates of current rise time of up to

$5 \times 10^{11}$  A/s. After that **K. Frank et al (1988) [32]** demonstrated in their experiments that for several key high-power switching performance factors, the pseudospark and BLT switches are superior to either high-pressure spark gap switches or thyratrons or, in some cases, both. And the high performance has been demonstrated in peak current ( $>100$  kA), current rate of rise ( $>10^{12}$  A/s), switching precision, trigger efficiency, current reversal (100%), and recovery time. In **1989** a numerical modeling based on large parameters has been carried out to investigate the plasma formation in the hollow cathode region of the pseudospark discharge by **P. Choi, et al [23]**. Results show that a combination of varying ionization rates due to the field geometry and differing mobility of electrons and ions, leads to the formation of a highly localized space-charge field on axis behind the hollow cathode. Also, **in 1989 C. Kozlik, et al [33]** designed a pseudospark high-power switch for hold off voltages and peak current of 40 kV and 25kA respectively. Their results show the capability of switching pulse energies of up to 40J at a current rise rate of  $8 \times 10^{11}$  A/s and a current reversal of up to 95%.

**G. Babst and M. Schwertl in 1992 [34]** used a pseudospark switch to drive a copper-vapor laser with an input power of 3-7 kW at a repetition rate of 5-7 kHz. Their results show that no decrease in electrical data was observed in comparison with a thyatron it replaced. Switch performance after 60 h of operation ( $> 10^9$  pulses) shows that further development could lead to a simple alternative for thyratrons.

The results presented by **V.D. Bochkov, et al (1995) [35]** showed that the use of a blocking electrode offers the possibility of increasing the upper limit of the operating pressure for the pseudospark switch with the static breakdown voltage kept at the level of 20 kV and of obtaining operating regimes where the delay time weakly depends on the gas pressure. **In 1996, V.D. Bochkov et al [36]** presented their results of development of high-voltage switching device that depends on a low pressure discharge with a cold cathode. The emergence

of this switch was associated with the necessity to increase the commutation current in a classical hydrogen thyatron with a hot cathode, and the design of the new switch can be considered in some respects as an advancement of thyatron design.

A special design of pseudospark switch in which a high-emissivity insert is placed in the cathode cavity is described by **Yu. D. Korolev, et al in 2002 [37]**. They proved that the essential advantage of the switch with the high emissivity material is that the main discharge burning voltage of the switch (with the forward voltage drop) decreases.

**In 2005 A. W. Cross**, generated high brightness electron beams from a pseudospark discharge. Further beam experiments can be carried out to generate both short (<1 ns) and long (~100 ns) duration electron beam pulses [38]. The electric strength recovery process in the pseudospark switch in xenon and oxygen has been investigated by **Yu.D. Korolev, et al (2006)**. Their results showed, that different blocking schemes application increase the pulse repetition rate up to 10 kHz [39]. **K. Frank, et al (2007)** constructed multi-gap pseudospark switches, which can handle reliably the specifications of the pulse forming network (PFN) for the injection/extraction kicker magnet system of the future heavy ion synchrotron accelerator complex SIS100/300[40].

**D.V. Bochkov, et al (2009)** constructed SN-thyatron and achieved a goal to have principally novel switches, combining the best features of thyatrons, vacuum and spark gaps, solid state switches. The operation of SN-thyatron with high cathode (and/or anode) potential improves the characteristics of the switches, and in particular, extends operating environmental temperature range, improves stability and, simplifies circuitry [41]. Pseudospark switches were developed by **B. L. Meena, et al (2010)** in demountable setup with single gap for 25 kV hold off voltages and 5 kA peak currents respectively [42]. A small

sized plasma jet ( $\phi$ 28 mm–60 mm) has been developed by **M. Watanabe, et al (2011)** using a modified pseudo-spark discharge with 2 kA peak current [43].

**N. Kumar, et al (2012)** designed and developed pseudospark based electron gun, and this pseudospark discharge has been found to be a promising source of high brightness and high intensity electron beam pulses. The experimental investigation was carried out on axial and radial variations of the beam current inside the drift space of the gun [44].

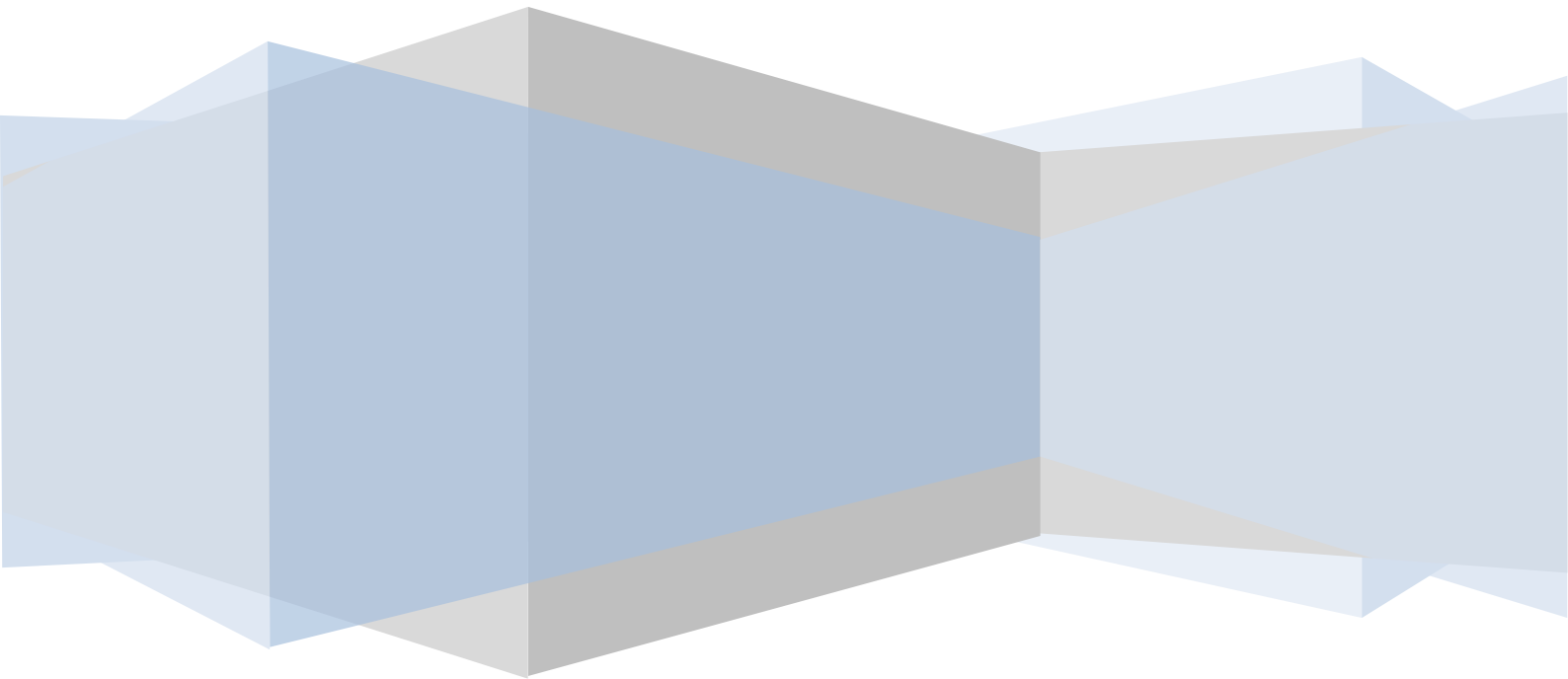
In 2013 **Y. D. Korolev, et al**, gave a summary of the experimental data as applied to high-current pseudospark switches and the interpretation of the processes in the stages of dense and super-dense glow discharge [45].

### **1.8. Thesis Aim:**

The aim of this work is to design and construct a high power pseudospark switch (PSS), and study its characteristics to be used later to run high power lasers. In this research, design of electrodes, fabrication, processing and switching behavior of the PSS are presented and discussed.

# **Chapter Tow**

**Construction and Measuring Technique**



## **2. Construction and Measuring Technique:**

### **2.1. Introduction:**

To understand how the pseudospark switch functions, we have to start with the "Paschen curve". The gas becomes conductive when it is converted into plasma. Plasmas are formed when energy is put into a collection of molecules faster than energy lost by radiation when the cations and electrons recombine. Recombination of the cations and electrons causes energy to be released as light; this is how fluorescent lights and neon signs work [30].

In a simple atmospheric pressure spark gap, as the potential difference between the electrodes is increased (or as the distance between the electrodes is decreased), electrons start to be emitted by the cathode and travel to the anode. As they travel, some of the electrons will collide with gas molecules, knocking electrons loose and forming cations and more free electrons. Near the electrodes, where the concentration of traveling electrons is highest, a faint glow caused by the recombination of ions and electrons will become visible. This glow is called a corona discharge and removes energy from the ionized gas at a high enough rate to prevent the formation of plasma. At higher voltages (or smaller gaps) the energy put into the molecules by electron collision exceeds the ability of the corona discharge to dissipate the energy and plasma is formed. The electric field between the electrodes will then separate the cations and electrons. The electrons will flow towards the anode, while the cations will flow towards the cathode. When the cations impact the cathode, they recombine with electrons from the surface of the cathode,

completing the electric circuit. In an atmospheric pressure spark gap, the flow of cations and electrons tends to be confined to a fairly narrow channel which is called a spark. At the point on the cathode where the spark connects, a large amount of heat is generated by the impacting cations, damaging the electrode surface (more current = more damage). Electrons impacting the anode surface do not cause much damage, since they are thousands of times lighter than the cations and thus have much less kinetic energy ( $1/2 mv^2$ ) [30,46].

The pseudo spark switches are used in pulsed laser systems such as (TEA-CO<sub>2</sub> laser system) as a low frequency switch or single shot system. But it is sufficient use for high frequency pulsed system, it can work under different frequencies with range (1 Hz - 40 kHz). Also the pseudospark switch has high hold off voltage for spark gap doesn't exceed few millimeters which makes it better than the thyatron and the classic spark gap switches [47,48].

The proposed design of the switch under study can be applied to many gases without a significant change in the parameters of discharge for example, possibly to use Ar, Ne, He as monoatomic gases and N<sub>2</sub>, H<sub>2</sub> as diatomic gases, as well as mixing of these gases in a very reliable manner.

We will address other basic parameters that affect the operation of the switch in the following paragraphs.

### **2.1.1. Type and Pressure of the Gas:**

From Paschen's curve described in chapter one the region of pseudospark pressure falls within the confined boundary between ( $P \cdot d \sim 10^{-3} - 7 \text{ mbar} \cdot \text{mm}$ ) where P is the pressure of gas and d is the distance between electrodes. While the classic spark gap works in high pressure region (right hand side of Paschen's curve), the effect of the gas type in this region is very significant [9].

It has been observed that the classic spark gap using inert gases for this purpose because the inert gases possesses high breakdown voltage that work is happening in a high pressure region. Therefore, it can be concluded that the diatomic gases be more appropriate in the pseudo spark switch operation. These gases have small ionization energy, so the breakdown of such gases giving a high abundance of electrons leads to increasing the current, but the current pulse width will be larger than that of inert gas switches [49,50].

### **2.1.2. The Distance Between the Electrodes:**

The pseudo spark switch operates within the range of very low pressure, leading to a rise in breakdown voltage for electrical discharge events and high hold off voltage as well. So, the distance between the poles is usually not more than several millimeters. This means that the distance ( $d$ ) has a significant effect on the stability of discharge, as well as on the breakdown voltage depending upon the region of the breakdown in Paschen's curve giving more stable and more fixed stability discharging.

Most of the studies in this field suggest that the central hole diameter must not exceed the distance between the electrodes [51]. That's where the discharge is more systematic when we achieve this condition. In the present work the diameter of the central hole is selected to be in harmony with the distance between the electrodes.

### **2.1.3. Matching Electrodes Axes:**

Many experiments show matching that the axes of the poles has a significant influence on the work of the switch and the stability of the discharge even on the jitter time, and on the specification of the measured pulse current flowing

through the switch [51]. In the case of a mismatch of axes arc-type discharge may distort the current pulse flowing and thus affects the shape of the current pulse and transmitted energy pulse from critical damping discharge to oscillation discharge. The central hole in the electrodes makes the effective distance of the discharge path a maximum in the region of the bore hole on the axial center of the electrodes and cathode cavity. It has been observed that the electrodes match has a clear effect on the jitter time. So we should consider this point in design, to reduce the differences in the axes matching. It should be taken into account the system as a whole is to have coaxial surfaces and is, smooth, free from manufacturing defects, leakages and clean of dust and impurities [51,52].

## **2.2. Construction Procedure of Pseudo Spark Switch Chamber:**

The design of switch chamber is compared with that of previous researches to manufacture models with good specifications based on a simple model for a single stage spark gap [52]. The pseudospark switch system has been constructed after studying and considering many designs, we reached to a simple, reliable design which is unique compared with other previous designs.

### **2.2.1. Construction of Electrodes Chamber:**

#### **1.The anode:**

It is a hollow dispenser of stainless steel with a central hole in its lower base, which allows the plasma discharge to pass through the cathode [53]. The upper base of the cylinder contains a metal ring from the same material to attach the anode via install screws with insulating material (Teflon) to avoid the case of

electrical conductivity between the poles. The dimensions of our pseudo spark chamber are illustrated in table 2.1.

## **2. The cathode:**

It is quite similar to the anode cylinder, but it has a slot to allow the gas discharge through the side of the lower base and welded with KF-16 link for tight gas inlet. In addition to that the center of the cathode contains a slot of 10 mm width to insert spark plug of the trigger unit as shown in figure (2.1).



*Figure 2.1: Plug of trigger unit*

## **3. The main gap:**

The main gap spacing is comparable to the bore hole diameter and can be determined from the thickness of the insulating material between the poles, which must have very high isolation to avoid breakdown. A glazing ceramic is used in our work, since it can withstand the high hold off voltage (more than 15kV dc and 35 kV peak pulse voltage at around 2.2 kHz)

**Table 2.1: The geometrical dimension of stain less steel pseudospark chamber**

<i>Geometric dimensions of the PS chamber</i>	
<i>Gap distance</i>	<i>~ 5mm</i>
<i>Electrode thickness</i>	<i>2mm</i>
<i>Central hole of the electron path</i>	<i>3mm</i>
<i>Inner diameter of the electrodes</i>	<i>65mm</i>
<i>Outer diameter of the electrodes</i>	<i>69mm</i>
<i>Length of hollow cathode &amp; hollow anode</i>	<i>65mm</i>
<i>Width of groove</i>	<i>2mm</i>
<i>Depth of groove</i>	<i>3mm</i>
<i>The distance from the tip of the plug to the cathode hole</i>	<i>5mm</i>
<i>O-ring diameter</i>	<i>3mm</i>
<i>Plug slot diameter</i>	<i>17mm</i>
<i>Distance between plug and KF-16 link</i>	<i>19mm</i>
<i>Diameter of the gas pump slot</i>	<i>3mm</i>
<i>The length of the link gear</i>	<i>10mm</i>
<i>The diameter of the upper and lower rings</i>	<i>110mm</i>

Figure 2.2 shows the schematic drawing of single-gap pseudospark chamber.



### **2.2.2. The Insulator Choice:**

The insulator used in our design is a glazed ceramic 70 mm in diameter and 3.5 mm in thickness. Glazing ceramics share many properties with both glasses and ceramics and have interesting properties like zero porosity, high strength, low thermal expansion, high temperature stability, high chemical durability, high resistivity, high breakdown voltage and high thermal conductivity to disperse the heat rapidly [54].

### **2.2.3. O-Ring Rubber Groove Design:**

The groove on the two surfaces of anode and cathode is about 2mm in diameter but the o-ring used in our design is about 3mm in diameter, so only 1/3 from the o-ring is inside the groove i.e. 1mm from the diameter o-ring. Also 16% from 1mm goes for vacuum pressing, so only 0.84 mm remains and from two sides (0.84+0.84)mm, we get 1.68mm which is the *Vacuum Accuracy* [55]. Now, all of dimensions of maximum main gap spacing are, 1.68 mm + 3.5mm (insulator's thickness).

### **2.3. The Vacuum Pumping System and Gas Flow Controller:**

The pseudospark switch is operated under the vacuum level of  $10^{-3}$  mbar. The whole experimental system was evacuated down to  $10^{-3}$  mbar by a two stage rotary vane vacuum pump 2.9 m<sup>3</sup>/h (Pfeiffer) within 10 minutes. The pressure was measured by analog Pirani gauge (Alcatel Pa111) as shown in figure 2.3:

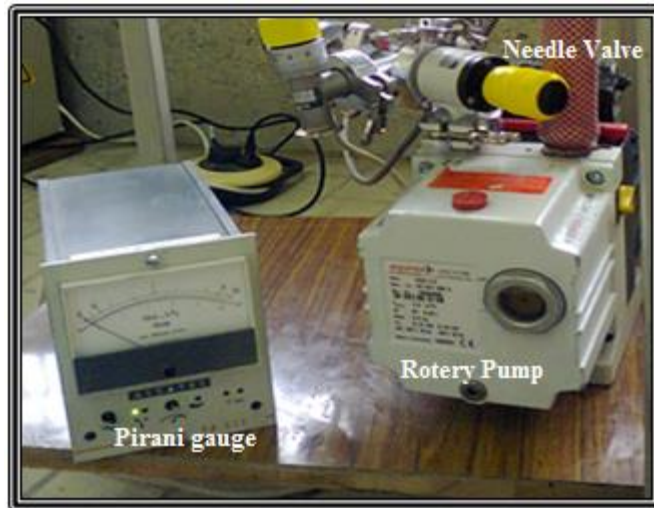


**Figure 2.3: Vacuum pump and Pirani gauge.**

We used Argon gas for discharging; such gas enters into the vacuum system through a mass flow controller. The mass flow rate of Argon can be adjusted accurately to control the operating pressure in vacuum system. The gas pressure of the chamber can be controlled at a very slow rate less than  $Q = 1.5$  mbar.ml/min according to equation (2-1) [26,56]:

$$Q = V \cdot \frac{dp}{dt} \dots \dots \dots (2-1)$$

where Q is the flow rate (mbar.ml/min), V the volume of chamber (liter), dp is the pressure difference (mbar) at the time difference dt (min).

**2.4. The Electrical Circuits:**

**2.4.1. A Pseudo Spark Switch:**

A pseudospark switch represents one of the most important elements of circuit controlling the electrical discharge in pulsed lasers. It is one of the best switches that withstand high voltage of more than (30 kV) and peak pulse current up to 5 kA with a rise time not exceeding several nanoseconds [49,56]. These characteristics are related to the main discharge parameters and ways to construct primary ionization triggered circuit and electronic accessories and gas pressure.

## 2.4.2. Trigger Circuit:

### 1. 555-Timer Circuit (Master-Slave):

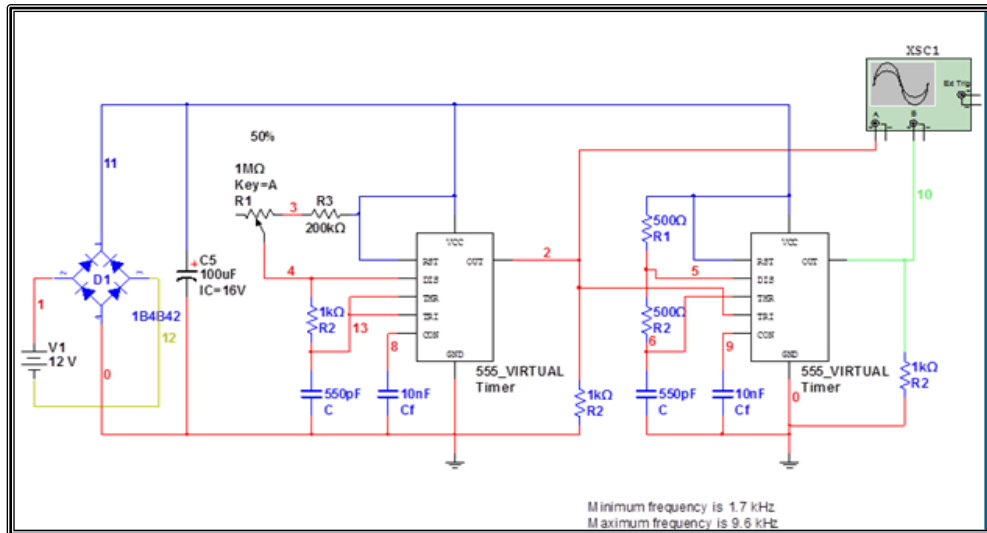
The switch needs to trigger one of the poles with the desired frequency, to open and close the course of the stream, compatible with synchronous resonance circuit. The trigger circuit consists of two complementary LM555CN type. The LM555CN is a highly stable device for generating accurate time delays or oscillation. In the time delay mode of operation (mono stable), the time is precisely controlled by one external resistor and capacitor. For a stable operation as an oscillator, the free running frequency and duty cycle are accurately controlled with two external resistors and one capacitor. The circuit must be triggered and reset on falling waveforms, where the desired frequency can be calculated from equation (2-2) [57]:

$$f = \frac{1.44}{(R_1+2R_2)C} \dots\dots\dots(2-2)$$

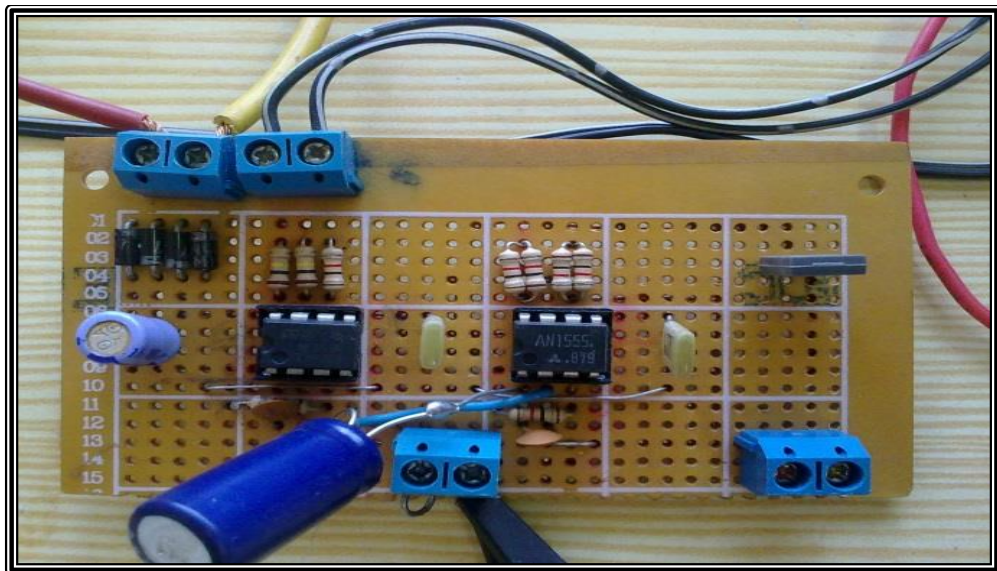
for a stable 555 oscillator the time of charge  $t_1$  and time discharge  $t_2$  are given by the equations (2-3):

$$t_1 = 0.693 (R_1+R_2) C \quad \& \quad t_2 = 0.693 R_2 C \dots\dots\dots(2-3)$$

During each cycle capacitor C charges up through both timing resistors, R1 and R2, but discharges itself only through resistor R2. The other side of R2 is connected to the *discharge* terminal, pin 7. As a result the positive square pulse width of about 3μs with frequency 2kHz is controlled by 1M Ω variable resistor as shown in figure 2.4 (a) and (b). The pulse width is calculated by the values of the capacitor and resistor. This pulse-phase type has been applied to Darlington pair circuit using 100 Vdc on one of the collectors of the two transistors.



(a)



(b)

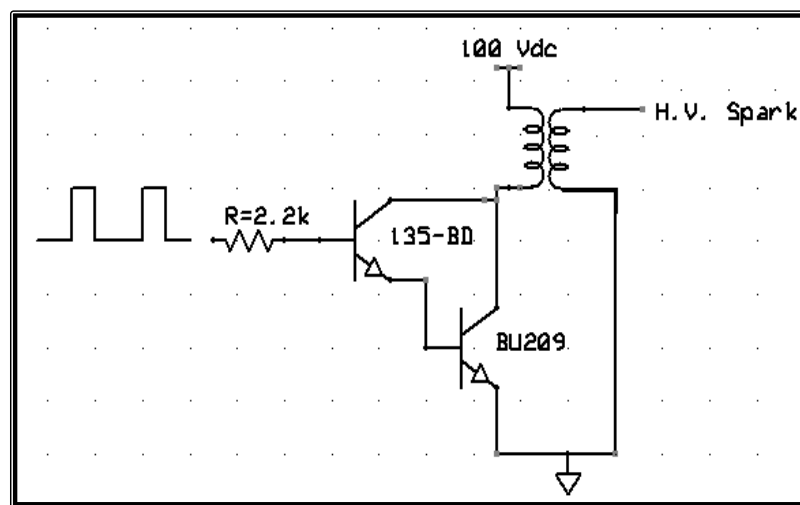
**Figure 2.4: Master-slave 555-timer trigger circuit (a) schematic drawing (b) Photograph picture**

## 2.The Power Transistor Circuit:

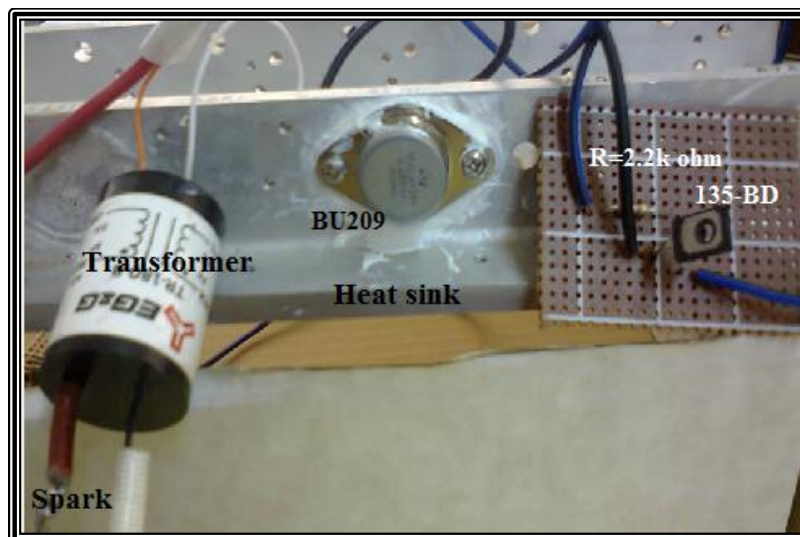
A very simple highly accurate reliable power circuit has been used in the trigger circuit as shown in figure 2.5(a) and (b). This power circuit consists of a Darlington pair of two transistors, one of 135-BD type to drive the other transistor BU209 type [58]. The applied voltage at the collector-emitter terminal is 100 dc volt and current 0.3A. This power circuit connected with trigger transformer (TR-180B EG&G type) 1kV:25kV to get the trigger pulse

which is used as ignitor to breaking down the gas to create the main breakdown current pulse.

The oscillator circuit has been separated from the base of 135-BD by a resistance of 2.2 k $\Omega$  to protect the electrical circuit. The use of Darlington pair gives a pulse of a desirable specification, also protects the circuit from a long period current flow which raises the temperature and then damages the circuit [59,60].



(a)



(b)

**Figure 2.5: Darlington pair circuit with the pulse transformer**  
**(a) schematic drawing (b) Photographic picture**

### 2.4.3. The Main Electrical Circuits:

#### 1. High voltage power supply:

The circuit designed for this work consists of a transformer of 10 kV, DC power supply and current of 0.5 A, the value of voltage is controlled through varic. A set of 14 kV diodes have been used as rectifier to convert the alternating current into a direct current. The designed power supply applying a continuous high voltage to the anode of the Pseudospark chamber and it was working efficiently for several hours.

#### 2. Charging resonant circuit:

Charging resonant circuit consists of an air core coil ( $L= 0.36H$ ) with resistance which does not exceed  $30 \Omega$ , its inert diameter is  $0.284 \text{ m}$ ,  $0.292 \text{ m}$  for outer diameter and  $0.23\text{m}$  length. Since the wire gauge is 20, so the increase in diameter of the coil is  $1.7 \text{ mm}$  for the two sides because the wire diameter is  $0.85 \text{ mm}$ . The coil contains 1334 turns with six layers. So, the value of its inductance can be calculated by equation (2-4) of the multilayers coil [61]:

$$L(\mu H) = \frac{31.6 N^2 r_1^2}{6r_1 + 9l + 10(r_6 - r_1)} \dots\dots\dots(2-4)$$

where :

$N$ : no. of turns

$r_1$ : radius of the 1<sup>st</sup> layer (m)

$r_6$ : radius of the 6<sup>th</sup> layer (m) [last one]

$l$ : length of coil (m)

This coil has many advantages, first chocking the current to certain value for gradual charging of the capacitor. The chocking of the current will induce inductive voltage that will be rise to be doubled with second pulse cycle as shown in figuer 2.6.

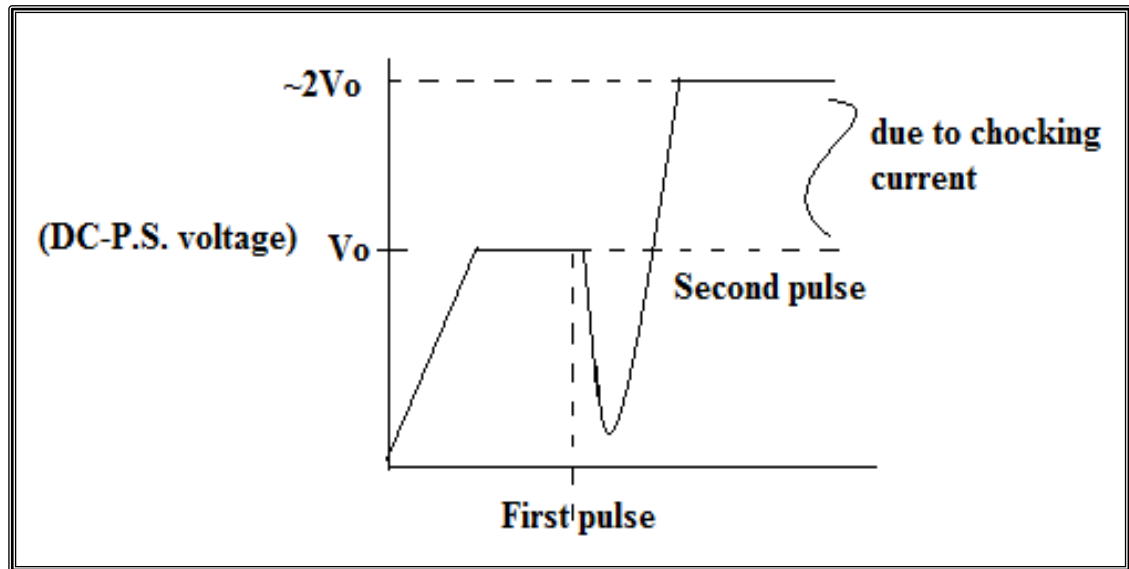


***Figure 2.6: Doubling voltage pulse due to multilayer air core coil.***

The storage energy in the coil is  $U_L = 1/2 LI^2$  which will be added to main energy from the power supply  $U = 1/2 CV_{DC}^2 + 1/2 LI^2$ . This amount of energy will appears as  $(2V_o)$ .

Such coil consists of six layers each layer contains about 220 - 222 turn and is isolated by electrical insulator. When resonant circuit shown in figure 2.7 works, the voltage reaches more than 20 kV between the layers of the coil. The inductance of coil calculated from equation (2-4), according to the values of its dimensions, is equal to 0.38 Henry.

The measured value by multimeter is 0.36 Henry. From values of capacitance and inductance, the applicable frequency range is found to be equal to 6.6 kHz, so that the trigger pulse frequency 2.2 kHz is suitable for operation. The coil is made in our labrotary.

The parallel high voltage hold off diode connecting with capacitor is to ensure no voltage goes inversely back to the power supply because the capacitor in the resonant circuit is charged to more than the value of power supply voltage. Also, in this circuit three capacitors of 0.5nF have been connected once in parallel and once in series to obtain different values of capacity (0.1, 0.25, 0.5, 1 and 1.5 nF) to study their effect on current waveform, rise time, and current pulse shape [51,62].

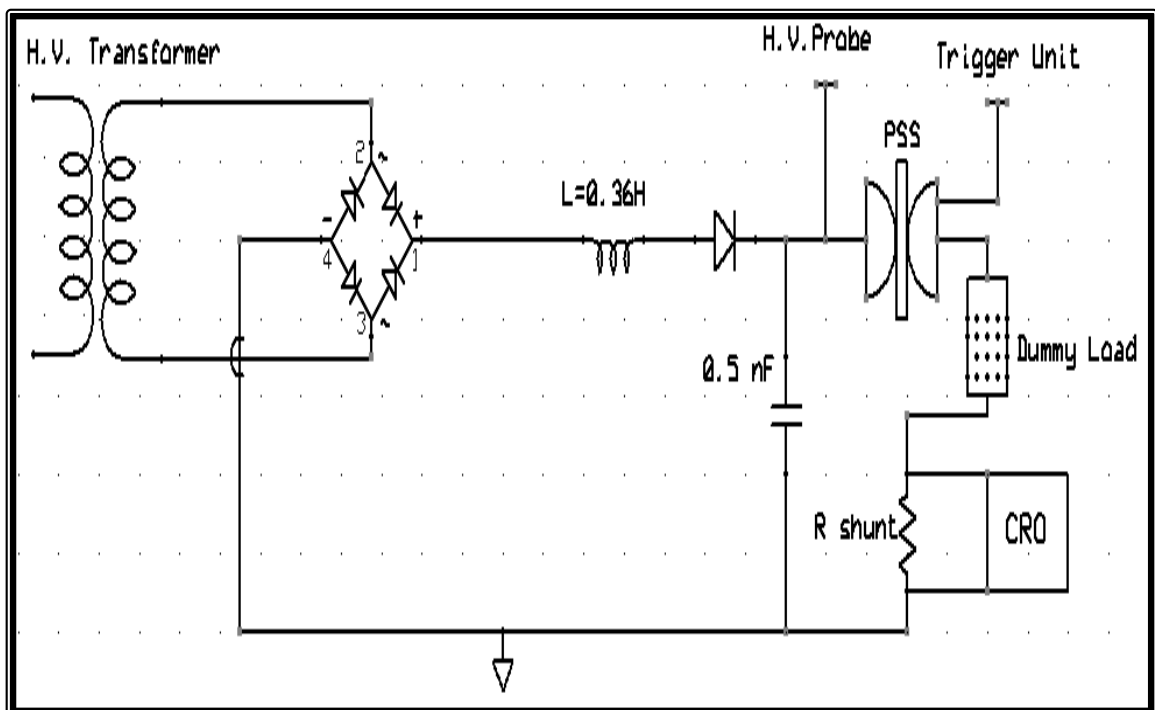


**Figure 2.7: The main discharge circuit diagram**

### 3. Analysis of the Electrical Circuit:

Figure 2.8 shows the two parts of charge and discharge circuit.

The charge part: Through LC- circuit the capacitor is charged through the coil at resonant time within the range of required frequency and must be compatible with the charging time where applicable [63]:

$$t = 2\pi\sqrt{LC} \dots\dots\dots(2-5)$$

where :

$t$  : charging time (sec)

$L$  : inductance of coil (H)

$C$  : charging capacitor (nF)

Now, as  $L=0.36$  H and  $C=1.5$ nF and  $f_{max} = 6.6$  kHz, the average charging current is given by,

$$I = CV*f_{max} \dots\dots\dots (2-6)$$

From the last equation for  $V = 18.5$  kV, the current is within the range of power supply ( $I \sim 0.2$  A), the maximum power extracted from the power supply will be less than 2kW, while our power supply designed for 5kW.

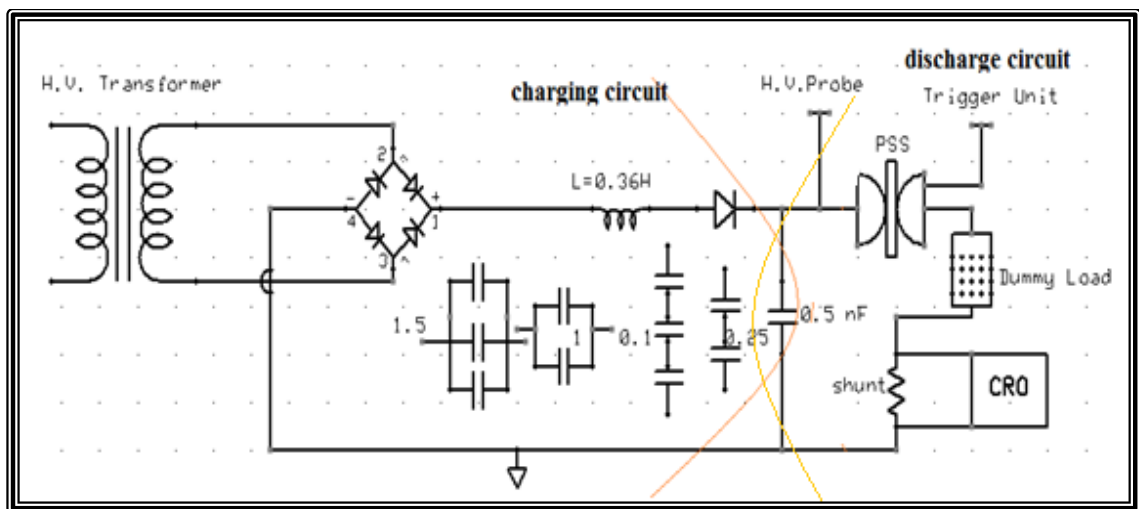


**Figure 2.8: The charge and discharge part circuit**

*The discharge part:* From the LRC-circuit the time of discharge can be calculated also from the equation (2-5), but in this time L will represent the inductance of the Pseudo-spark discharge part including the inductance of the earthing wires in to the ground. Its value is calculated from the anode voltage and current waveform using the relation below [64,65]:

$$L = \frac{V * t_{FWHM}}{I_{peak}} \dots\dots\dots(2-7)$$

where V is the anode voltage,  $I_{peak}$  is the peak current pulse and  $t$  is FWHM of the current pulsed width. The reactance  $X_L$  of the Pseudo-spark switch (PSS) is easily found from the relation:

$$X_L = 2\pi f L \dots\dots\dots(2-8)$$

From the values of L and C we can find the time of discharge and the discharge current from the equations (2-5) and (2-6).

**2.5. Dummy Load and Shunt Resistor:**

For our experiment we need two important apparatuses, dummy load for discharging the current through and shunt resistor to measure the current pulse through digital oscilloscope.

*1-Dummy load:* To determine the reactance of the Pseudo-spark switch and that of earthing wire to the ground we use a non-inductive dummy load instead of using conventional coil test circuit, this new technique gives us a good approach to find the accurate value of the inductance for the PSS. In this work our dummy load is made from char cool graphite material.

*2- Shunt resistor:* It is also called Current View Resistor (CVR). A shunt resistor is a high precision device used to measure DC and AC currents in an electrical circuit. Shunt resistors are used to measure high currents that would

potentially damage an ammeter or any device except precise or through Rogowski coil.

## 2.6. The measurements and calculations of reactance and impedance of the system:

### 1- With dummy load:

Inductive reactance  $X_L$  is a measure of the obstruction of inductance to current and it varies with the frequency of the electrical signal, it is measured in ohms. The inductance  $L$  of the PSS has been calculated from equation (2-7) and it is equal to 241 nH. The reactance of the PSS has been calculated from equation (2-8), and it is  $X_{L(PSS)} = 3.3 \text{ m}\Omega$ , which is very applicable to our high power switch.

$X_{L(total)} = X_{L(PSS)} + X_{L(dummy\ load)}$ ,  $X_{L(dummy\ load)} = \text{zero}$  where the dummy load is non-inductive ( $L=0$ ).

hence:  $X_{L(total)} = X_{L(PSS)} = 3.3\text{m}\Omega$ .

Impedance ( $Z$ ) is a measure of the overall opposition of a circuit to current, it consists of two components reactance and pure resistance [66].

$$Z = \sqrt{R_{total}^2 + X_{L(total)}^2} \dots \dots \dots (2-9)$$

where  $R_{total}$  is the resistance of the system which is equal to the sum of earth resistance and dummy load resistance,  $R_{total} = R_{dummy\ load} + R_{earth}$ , as well as the stray resistance due to wires and their connections, its value is very low and can be neglected. The earth resistance has been measured by using earth tester (KYORITSU-type, 4105A model) as shown in figure 2.9.  $R_{dummy\ load} = 32 \text{ }\Omega$  and

$R_{earth} = 3.97 \Omega$ , hence the  $R_{total} = 35.97 \Omega$ . Therefore, we can easily find  $Z$  which is equal to  $35.97 \Omega$ .



*Figure 2.9: Earth tester reading.*

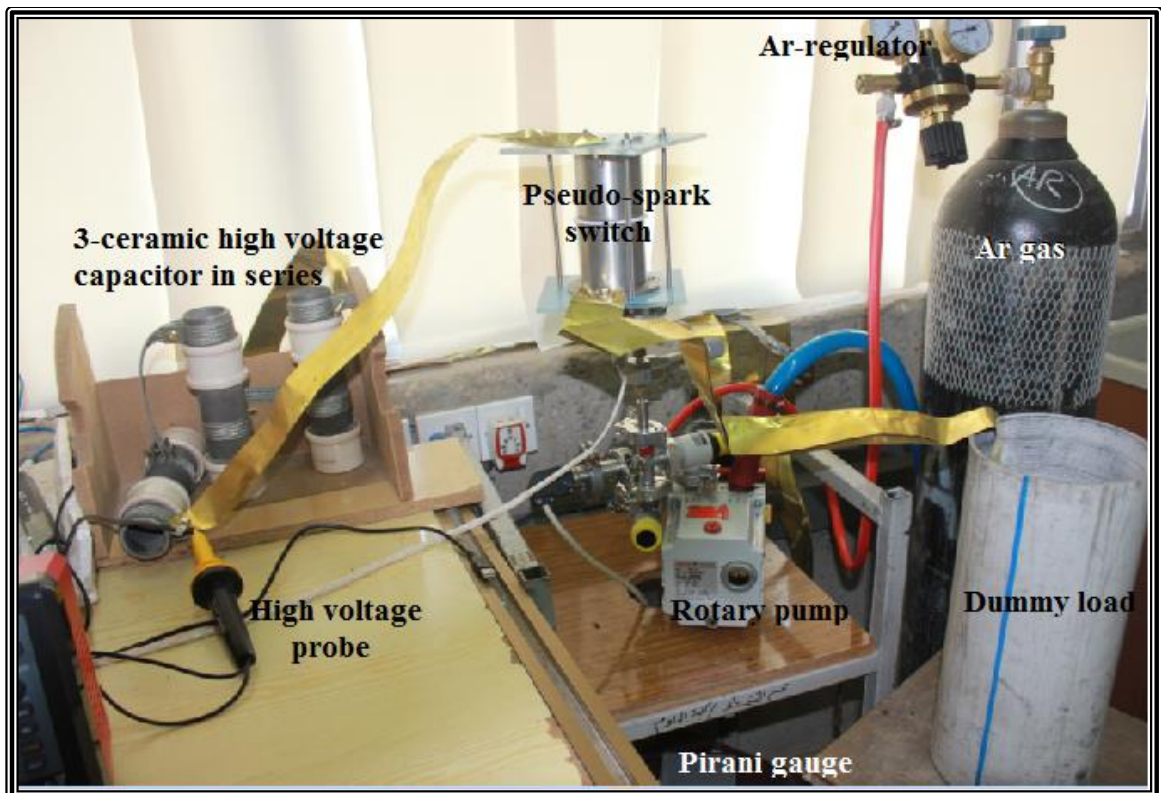


*Figure 2.10 The system circuit with dummy load.*

**2- With air core coil:**

Figure (2.11) shows the connection of an air core coil ( $L = 24\mu\text{H}$ ,  $R = 0.15 \Omega$ ) instead of the dummy load to determine  $L$ ,  $R$ ,  $X_L$  and  $Z$  of the (PSS). From the damping oscillation of the current waveform that was obtained during the operation, the current equation can be written as [67]:

$$I = I_P .exp (-\alpha t) \dots \dots \dots (2-10)$$

where  $I_P$  is the 1<sup>st</sup> peak value of the current pulse.

$$514\text{A} = 770\text{A} \exp (-\alpha (0.8\mu\text{s}) , \text{ or}$$

$$\alpha = 0.5 \times 10^6 \text{ sec}^{-1}, \text{ which represents the dumping factor.}$$

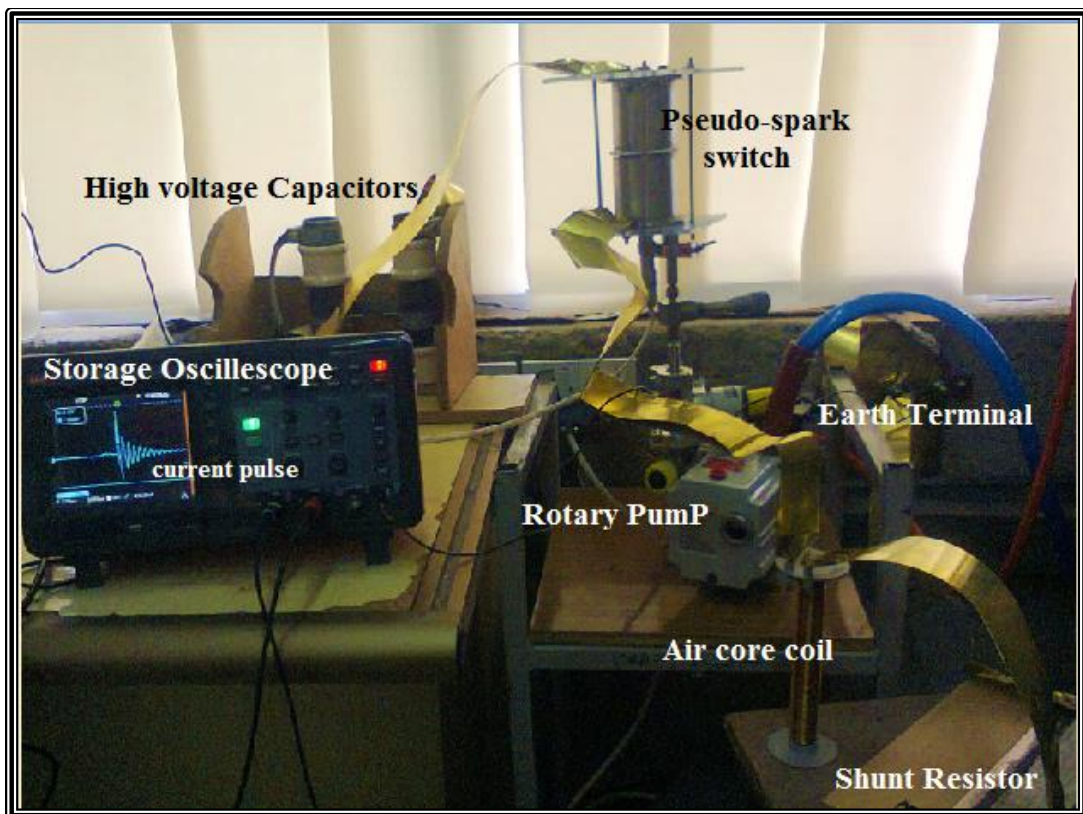


**Figure 2.11: The system circuit with air core coil**

$$\omega = 2\pi/T , \text{ since } T = 1\mu\text{s} \text{ then } \omega = 6.28 \times 10^6 \text{ sec}^{-1}.$$

The inductance of the PSS is calculated from:

$$L = \frac{V_{anode}}{I_P \omega \exp - \left(\frac{\pi \alpha}{2\omega}\right)} \dots\dots\dots(2-11)$$

Hence: L = 750 nH

and the PSS resistance is given by:

$$R = 2\alpha L \dots\dots\dots(2-12)$$

From above equation it is found that R = 0.75 Ω. The reactance of the PSS can be calculated from equation (2-8). Hence,  $X_{L(PSS)} = 10.3 \text{ m}\Omega$  and it is good for the high power switch.

The total reactance of the system is:

$$X_{L(total)} = X_{L(PSS)} + X_{L(coil)}, \text{ and } X_{L(coil)} = 0.3\Omega .$$

Hence,

$$X_{L(total)} = 0.310\Omega.$$

From equation (2-9), and in the same way as in dummy load calculations, we can obtain the resistance of the system ( $R_{total}$ ) which is equal to the sum of earth resistance, PSS-resistance and coil resistance:

$$R_{total} = R_{PSS} + R_{coil} + R_{earth} = 0.75 + 0.15 + 3.97 = 4.72 \Omega. \text{ Therefore, we can easily find } Z \text{ which is equal to } \sim 4.73 \Omega.$$

## 2.7. The Erosion of the Electrodes:

The erosion of the two electrodes depends on their material; the electrons which can hit the edges of the holes can make erosion in the material if the kinetic

energy is higher than the work function of the material. The anode voltage reaching around 30 kV can accelerate electrons, their energy is sufficient to make erosion.

When the central hole diameter ranges between 3-5 mm this will lead to change the cutoff voltage which cuts the current. This change will generate large effect on jitter time. Hence, the choice of the electrode material has a great effect on increasing the reliability of the switch and improving the voltage and current pulse parameters [63]. In this work stain less steel was used as electrodes, which seems to be good selection for high reliability characterized by withstanding high temperatures and low erosion rate. The discharge current pulse width has a significant effect on the electrode erosion. Due to the increases in pulse width, the accumulation time of energy increases; this will raise the temperature of the zone around the hole. Therefore, the erosion appears in the central hole of the electrodes as shown in figure 2.12 (a) and (b), after 100 hr. operation.

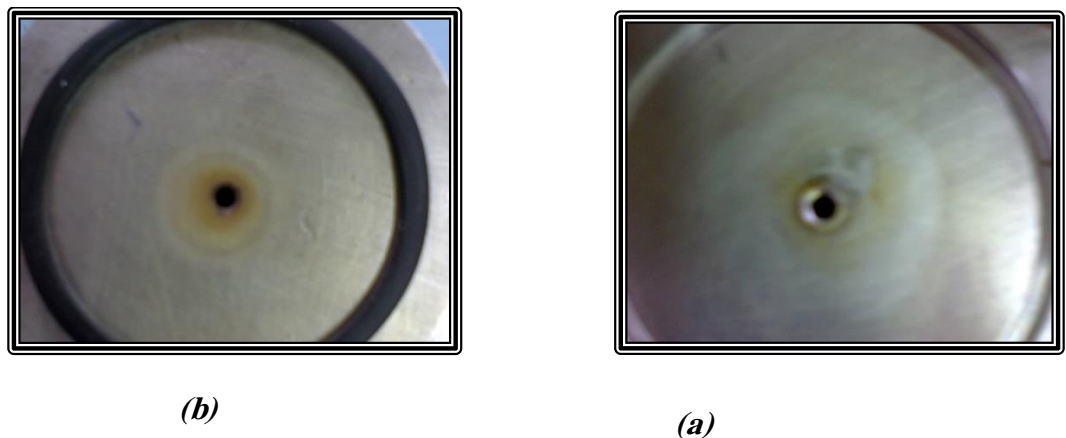


*Figure 2.12: The erosion of the two electrodes (a) cathode (b) anode*

## **2.8. Construction of Shunt Resistor:**

A shunt resistor is a high precision device used to measure DC and transient current in an electrical circuit. Shunt resistors are used to measure high currents

that would potentially damage an ammeter. This could be a result of the magnitude of the current passing through the circuit or the possibility of current spikes [68]. A shunt resistor typically looks different from a normal resistor, having two large terminals with one or more strips of metal connecting them. It works by measuring the voltage drop across a known resistance value. If the value of the shunt resistor is known, the potential across it can be measured via the voltage probe then the pulse that will appear at the oscilloscope screen represents the current pulse. Hence the current passing through the resistor will be affected by the resistor value and the induced inductance that may appear due to the resistor material itself. Moreover, not any small resistor can be used as current view resistor (CVR) unless it has very low inductance. For instance if the inductance of such a shunt resistor is in the range of 1nH, and the current pulse rise time is of about 100ps then the value of the reactance will be around  $60\Omega$ , so the power dissipation will be very high, moreover, the high inductance will distort the current pulse shape as well.

One of the major advantages of using such non-inductance resistor is the fact that it doesn't have any effect on the pulse shape behavior and the current rise time which are the most critical parameters. Such a high frequency circuit, reaches more than 10 GHz, the existence of inductance will rise rapidly due to rising frequency and then it affects the pulse shape. Moreover, it seems that the peak current pulse and its rise time cannot be seen by any other tool or measuring device without distortion, except the CVR of precise parameters [69].

### **2.8.1. Design Considerations:**

Several parameters are important to specify a shunt resistor. The resistance value is given by the voltage drop at the maximum current rating. The important parameters include the temperature coefficient of resistance and the

power rating. The power rating indicates the amount of electrical power that the resistor can dissipate at a given ambient temperature without damaging or changing the other resistor parameters [68,70].

Our design of shunt resistor is made of a large number of graphite rods (pencil rods) which is a diamagnetic material, these rod are connected in parallel with each other by using graphite paste on two stainless steel sheets of each rod shielded by PVC sleeve to avoid contacting between the rods and to keep them parallel as well. These sheets are fixed on a piece of wood as shown in figure 2.13.

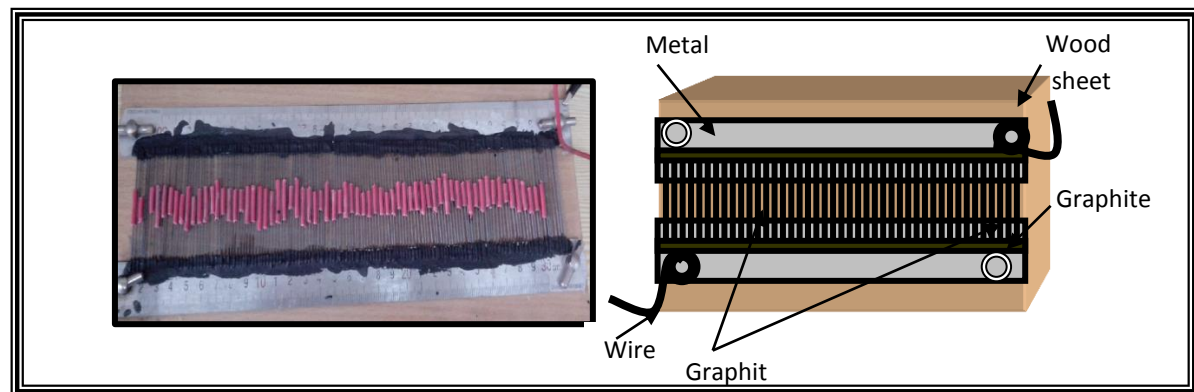


***Figure 2.13: Shunt resistor design.***

It is important to choose the position of the shunt in the circuit. When the circuit shares a common ground with the measurement device, often it is the shunt is placed as close to the ground as possible. Other ways more wire lengthening more inductance will rise in the high frequency, high voltage circuit. This design of current shunt resistor seems more reliable and accurate than other means of measurements duo to its precise and fixed parameters, the longtime of operation as well as its simplicity (any one can build it in the laboratory), and affordability. The resistance of one graphite rod is equal to  $r = 1 \Omega$ , measured by using the voltmeter. By adding around 140 piece of these rods

in parallel and connecting them together as shown in figure 3.1, the equivalent resistance will be equal to  $R=7.142 \text{ m}\Omega$ , which is a sufficient value for a shunt resistor to detect peak current of few kilo amperes and a high voltage up to few tenths of kilo volts without affecting other measuring devices such as oscilloscope. The equivalent resistor can be calculated from equation:

$$\frac{1}{R_{eq}} = \frac{1}{R_1} + \frac{1}{R_2} + \frac{1}{R_3} + \dots + \frac{1}{R_{140}} \dots \dots \dots (3-1)$$

The value of the shunt resistor has been measured by a simple electrical circuit shown in figure 2.14. The current and the voltage applied by a high precision electronic power supply have been measured using accurate multi-meter device.

By taking many measurements of current flow and voltage applied through the shunt resistor, one can calculate the average value of R.

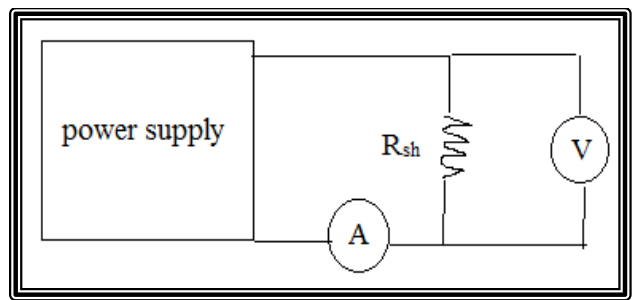


**Figure 2.14: Simple electrical circuit to measure the resistance of the shunt resistor.**

**2.8.2. Result and Discussion:**

The peak current pulse and its rise time are greatly affected by stray reactance of the resistors. Therefore the object of this design is to provide a non-inductive resistor which is simple, cheap and reliable [71, 72]. Moreover, the simple design of our CVR can withstand high current due to temperature stability, it can be used for high frequency pulse lasers. From the relation between the

voltage and current we can find the resistance of the shunt as shown in figure 2.15:

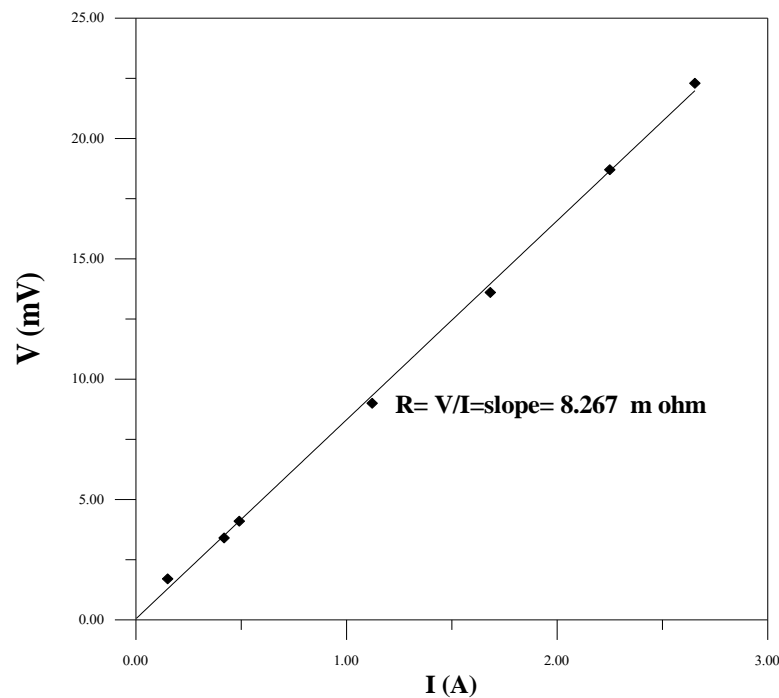


**Figure 2.15: The value of CVR from I-V linear**

From the above figure the value of  $R_{sh}$  is equal to  $8.267\text{m}\Omega$ , it is seen that this experimental value approaches theoretical value that is calculated from equation (3-1)  $R_{eq} = R_{sh} = 7.142\text{m}\Omega$ . Also,  $R_{sh}$  is measured by LRC-meter device and gives value equal  $6.68\text{ m}\Omega$ . Moreover, it's obvious that the carbon paste adds some additional resistance to the value of the carbon rods. The main value of the shunt resistor is calculated by taking the average value of the three above readings which is equal  $7.363\text{m}\Omega$ .

The shunt resistor was tested to measure high currents in two ways:

First, it was tested through the applying DC voltage up to 50 volts with  $I=15\text{ A}$ , then by using the relation  $P = IV$  it was found to afford high power ( $P = 750\text{W}$ ). After operated for many hours, it was found that the value of current and voltage remains unchanged. This means that we have a current view resistant

(CVR) which is not affected by those parameters so, no change appears in its internal temperature and the value of resistance remains constant. The power dissipated through this resistor is about 1.6W by applying the equation:

$$P_{\text{dissipated}} = I^2R = (15)^2 \times 7.363\text{m}\Omega = 1.656 \text{ watt}$$

This means that the dissipated power is very small if compared with the energy afforded by the resistance.

Second, shunt resistor was tested at the system of pseudo spark plasma switch to measure the current switch. It has been connected to measure the high current pulses at voltages passing through it for more than six hours using a high -voltage probe and digital storage oscilloscope. The current value of more than (1.5 kA) has been measured using CVR without being affected by the values of current and resistance and without raising temperature as shown in figure below:

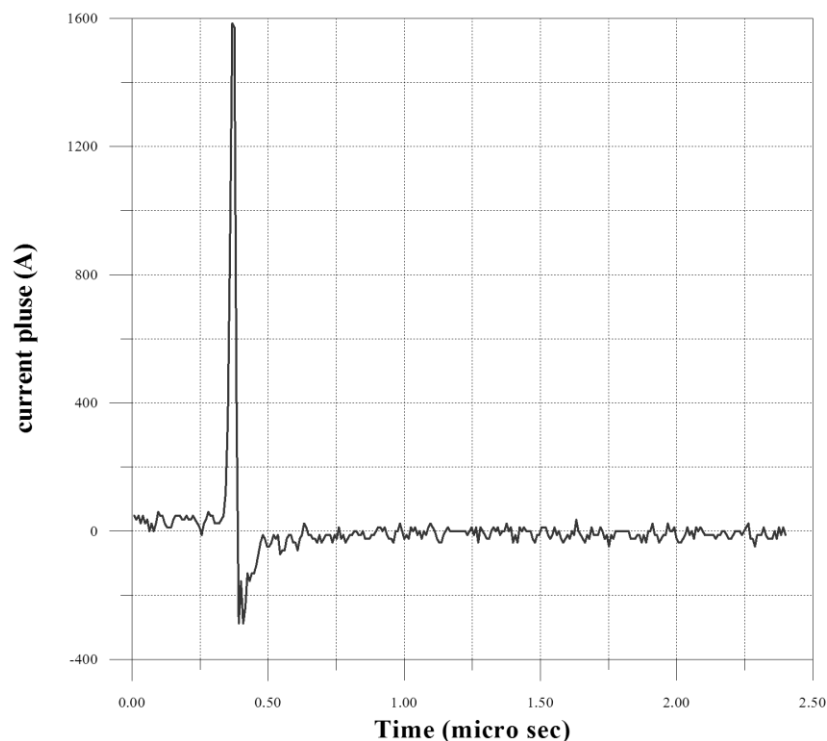


***Figure 2.16: The current pulse of peak 1.575 kA measured by shunt resistor***

Our CVR used in the PSS experiment has withstood more than 3.5kV as will be shown in chapter 4. We have designed and manufactured shunt resistance or the so-called current view resistor CVR of a diamagnetic graphite material to measure short rise time current pulse. Because the energy dissipated during the resistor is very small, it doesn't have effect on its value at the passage of current through it. Such a non-inductive resistance gives an excellent result for measuring high currents without being affected.

## **2.9. Dummy Load Manufacturing:**

Non inductive dummy load resistors are a must for bench testing in many devices such as audio amplifiers, load speaker and most importantly in switching mode device circuit testing i.e. Thyatron, spark gap, pseudo-spark gap circuits and as tanner in antenna radar circuit as well [73,74].

The problem in such circuits is that they operate at high frequencies, thus any tinny amount of inductance in the medium of the resistor can rapidly increase the reactance that is created due to the inductance of the material. This problem initiates the idea to find a reliable, non-inductive, high power and variable resistor.

The design and construction is very simple and can be done in any laboratory if the experimenter desires.

### **2.9.1. Design and Consideration:**

In our design a 5kg activated carbon powder has been used, the grain size of the powder ranged from (1-0.5) mm, a plastic pipe of 30 cm in diameter and 40 cm in length has been used as a container for the powder.

Two discs of aluminum were manufactured as a plug to close the two ends of the pipe tightly. Lower disc was pasted by using strong glue and the upper disc

plug of the plastic pipe container was screwed on the pipe to press the powder. Hence changing the value of the resistance of carbon powder depends on more pressing the powder to achieve minimum value of the dummy load resistance as shown in figure 2.17.

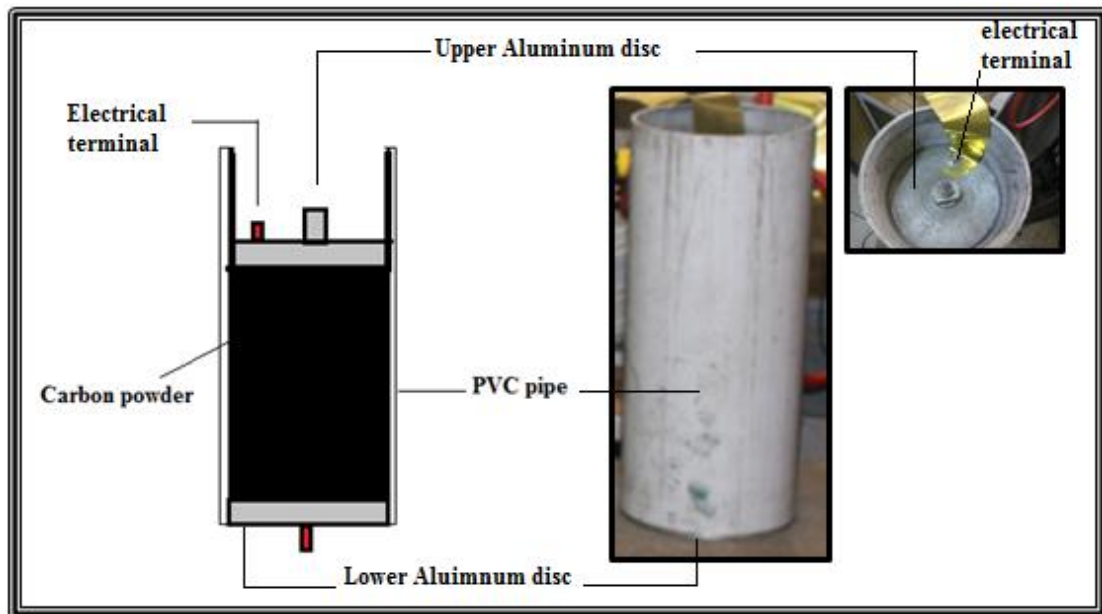


*Figure 2.17: The dummy load design*

After filling the plastic pipe with carbon and closing it with a screw aluminum disc to squeeze the activated carbon inside the pipe, a multi-meter device has been used to measure the resistance of the dummy load.

Therefore, pressing at carbon more reduces the length of the carbon column (20cm). Thus resistance decreases and vice versa, the dummy load resistance is increased by releasing the press on the carbon column inside the plastic pipe.

### **2.9.2. Results and Discussion:**

For certain carbon powder grain size, it is found the value of dummy load resistance obeys the empirical formula,  $R \propto P^{-1}$  where P is the pressure applied

by the Aluminum disc screw (see figure 2.18). The two aluminum discs of the dummy load have been linked to the terminals with good electrical conductors.

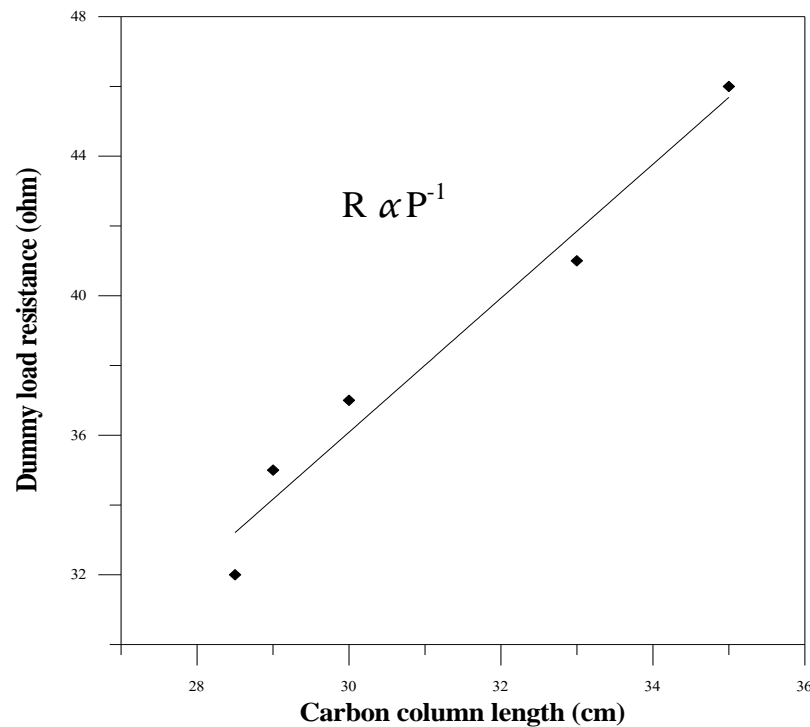


**Figure 2.18: The dummy load resistance as a function of carbon column length**

From figure 3.6 the fitting linear relation  $y = a x + b$  gives the constant  $a$  which represents the constant of an empirical formula  $R \propto P^{-1}$  then this relation will be  $R = 1.9 P^{-1}$ .

Also, the resistance of the dummy load has been found by a simple electrical circuit shown in figure 3.2, by measuring the voltage drop from the power supply using a multi-meter, and then applying Ohm's law.

Many readings of current flow through the dummy load have been taken to calculate the value of  $R$  for dummy load resistor. From plotting a graph between the voltage and current as shown in figure 2.19 it is found the value of  $R_{\text{dummy}}$  is equal to  $30.9 \Omega$ , it is seen that this experimental value approaches

measuring value ( $R_{\text{dummy}} = 32.1\Omega$ ) using multi-meter device, concluding that these two values are true.

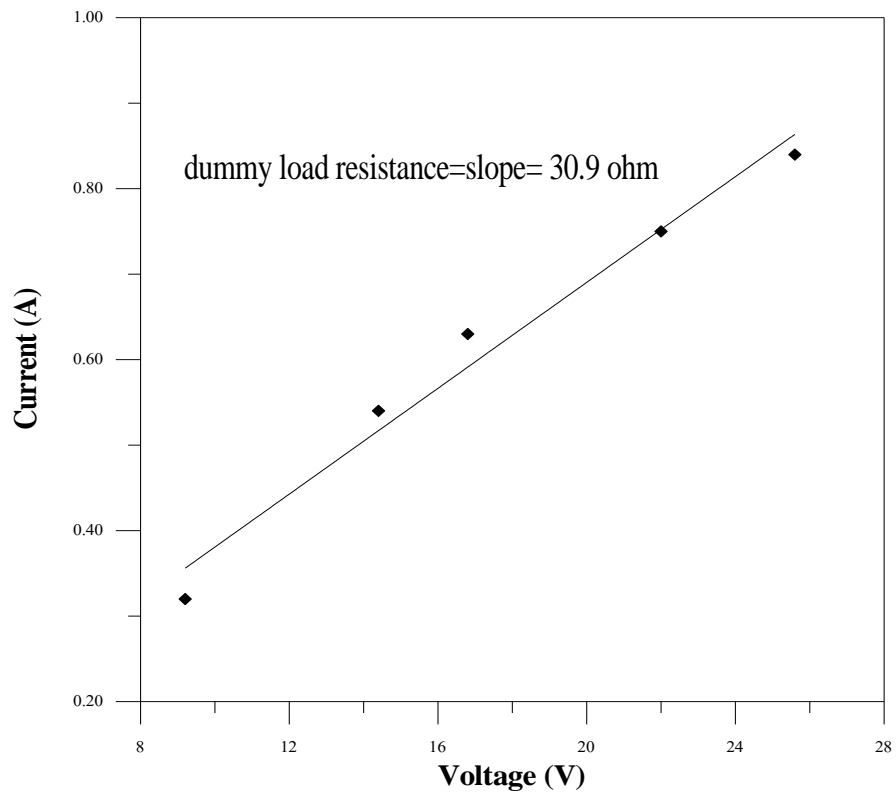
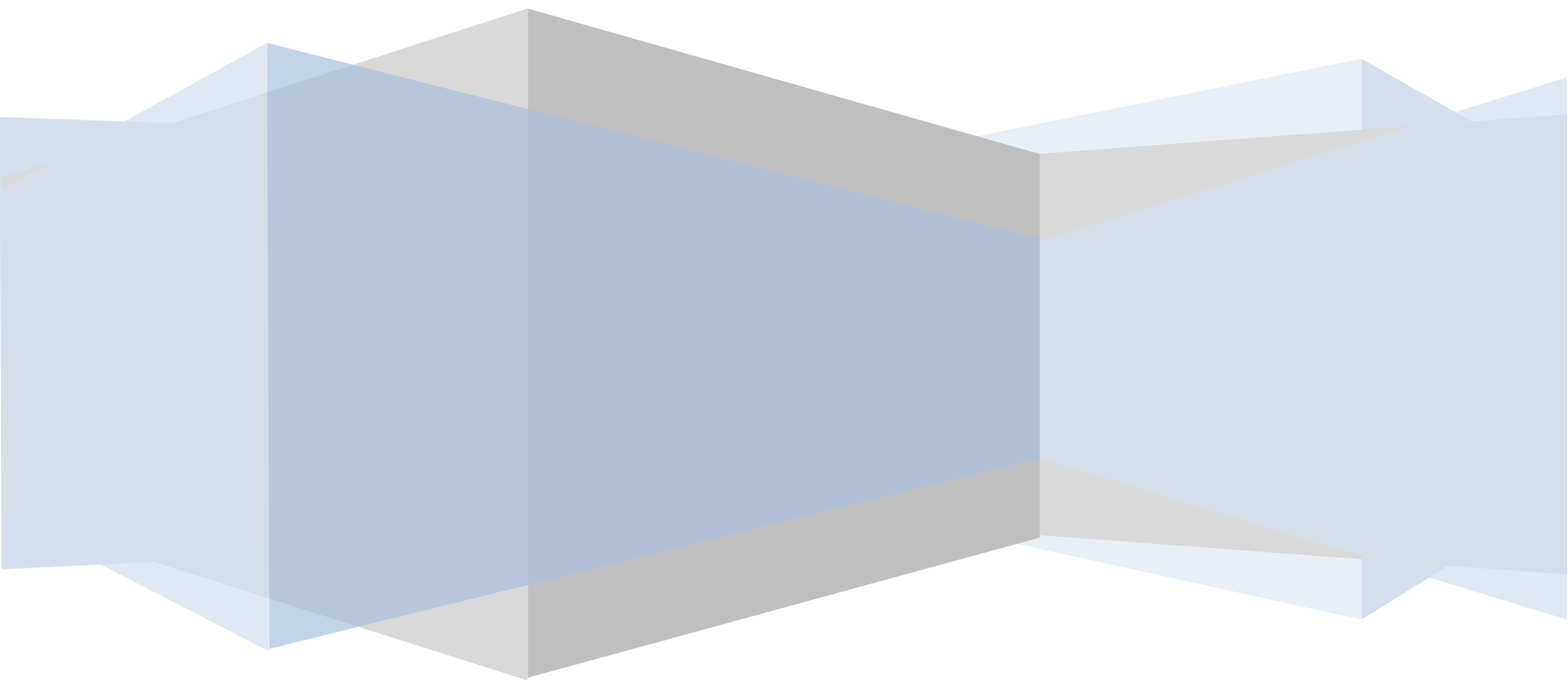


***Figure 2.19: The value of resistance of the dummy load from I-V linear relationship***

# **Chapter Three**

**Results, Discussion and Conclusions**



### **3. Results, Discussion and Conclusions:**

#### **3.1. Introduction:**

As stated earlier, the primary objective of this work is to design and construct pseudo spark switch (PSS) that has a scope for future improvement depending on the requirements of the specific applications.

In order to reach the final objective stated above, a series of experiments under different conditions have been done to operate PSS. To obtain a desirable operation of PSS system, many parameters were measured such as: breakdown voltage of used gas, trigger pulse shape, applied voltage to anode, current waveform, and rise time (at different values of high voltage capacitor). Also, the jitter time for the current peak to peak has been measured. All the presented experimental results in the following sections represent multi-shots mode. The current data is measured through shunt resistor. Both voltage and current data are collected by an oscilloscope through a USB cable and recorded by a computer.

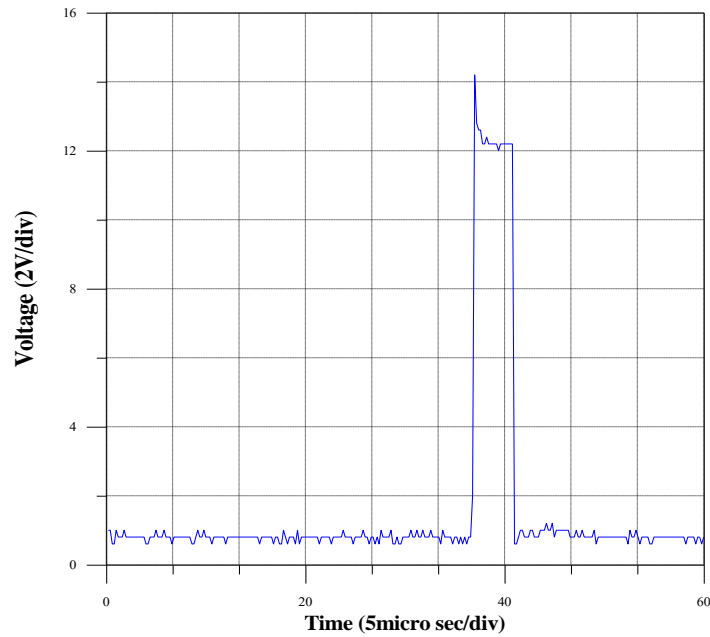
Our results are compared with the results of the other pseudospark switches designed by many researches.

#### **3.2. The trigger pulse shape:**

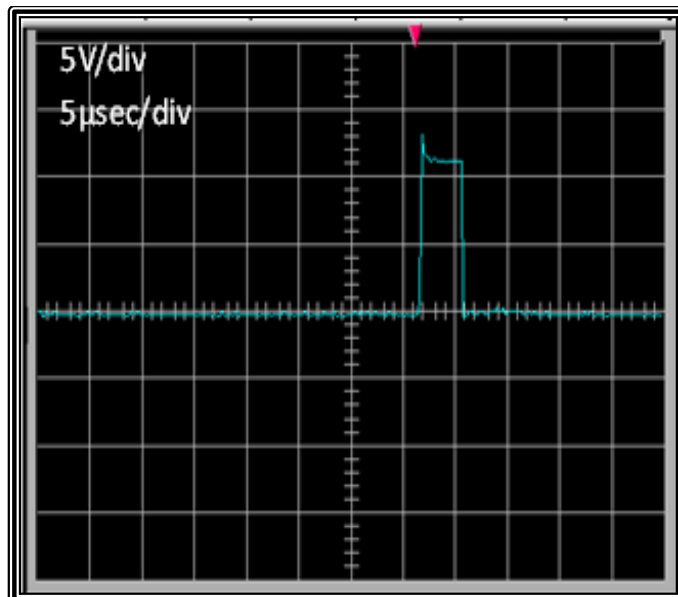
Data are acquired by a high speed oscilloscope with 300 MHz bandwidth, 2 GS/s sampling rate. With the aid of high power probe (Tektronix 1:1000 attenuation, 3 pF input capacitance, 20kV DC, 40 kV peak, 4 ns usable rise time) one can measure the high voltage pulses easily. At low gas pressure, the single electrons are not able to initiate the breakdown process in electrode system. A considerable pre-breakdown electron flow is required for this purpose. Hence a trigger unit which is placed in the cathode cavity, is needed to

provide a sufficient electrons flow into the main gap to ignite the main discharging.

The positive square pulse produced from the master-slave 555-timer (explained in chapter 2) is shown in figure 3.1 (a) and (b) with  $\sim 3\mu\text{sec}$  in width, 2.2 kHz in frequency, 13.7V and 0.75mA in current.



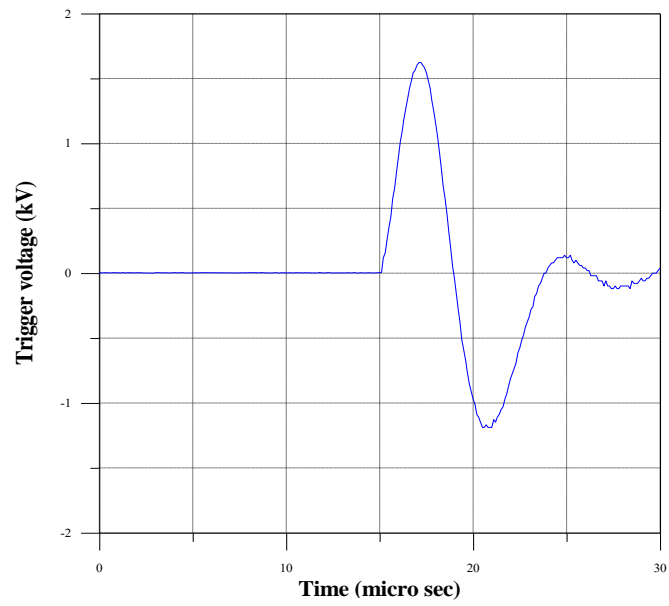
(a)



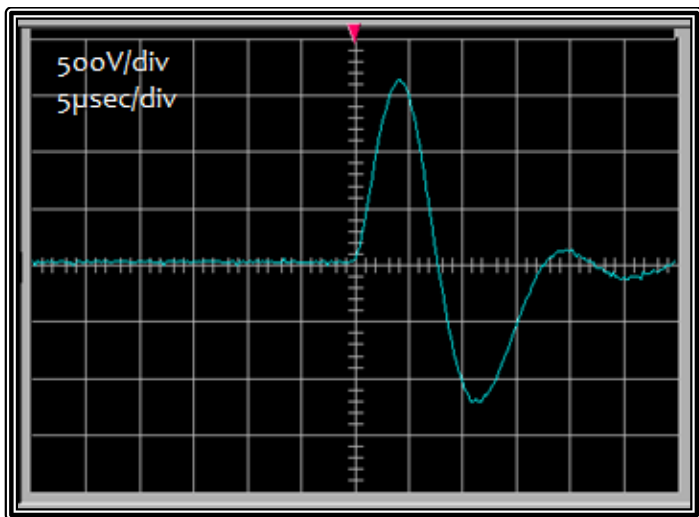
(b)

**Figure 3.1: Square trigger pulse (a) Graphical picture (b) Oscilloscope picture.**

The above square pulse has been applied to the trigger transformer, and gives pulse with positive and negative parts as shown in figure 3.2, the positive part is to ignite the main discharge. The negative part of the trigger pulse appears to be very useful; it can be used as a negative biasing to cutoff the tail of the main discharge current pulse. This leads to shorting the recovery time for the next pulse. The output trigger pulse is  $\sim 1.623\text{kV}$  in peak and frequency of  $2.2\text{ kHz}$ .



(a)



(b)

**Figure 3.2: Trigger pulse shape at the electrode (a) Graphical picture (b) Oscilloscope picture.**

In reference [75] the design of multi-gap pseudospark switch is triggered by applying a  $\sim 4$  kV positive voltage pulse to the wire (thin tungsten wire 0.25mm in diameter) trigger electrode as shown in figure 3.3. Thin wire discharges have been used for many years in diverse applications. But for very reliable plasma generators a plug igniter is used in our design. Although the plasma density generated by plug igniter discharges is somewhat limited due to the low dissipation allowed by the plug, it is adequate to trigger the device with reasonably short delay time. The switch closed at  $\sim 1\mu\text{s}$ , while our trigger pulse closes the single-gap switch at  $\sim 3\mu\text{s}$ .

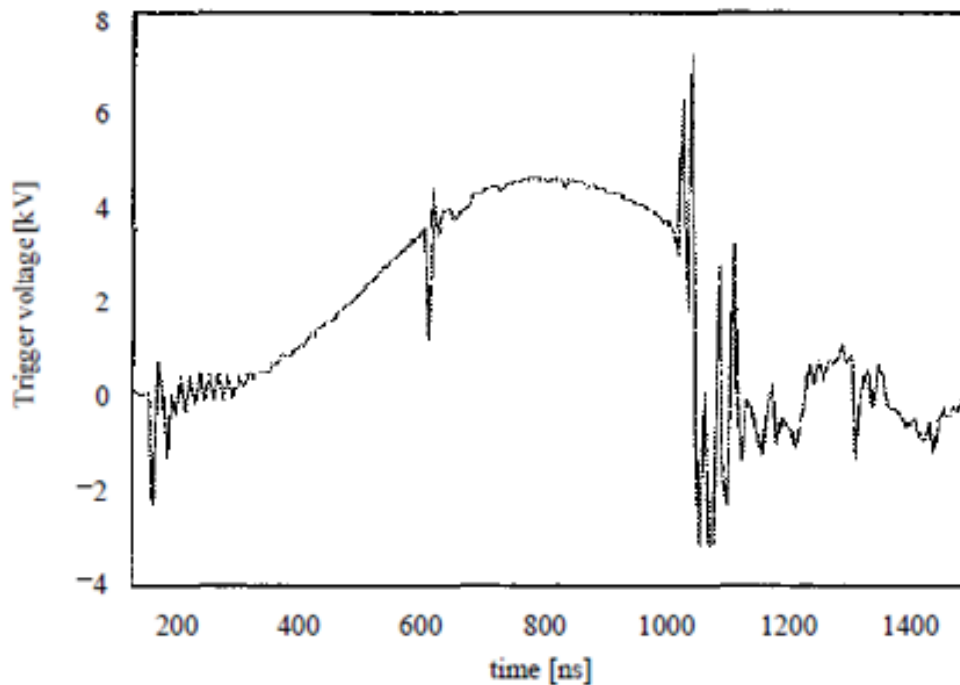


*Figure 3.3: Trigger voltage at the electrode [75].*

*de*

Figure 3.4 shows the frequency of the trigger pulse ( $\sim 2.2$  kHz) and it represents the reputation rate of PSS operation. It can be used as a criterion for the classification of the switch mode operation whether it is single shot or multi-shots. Our switch has been operated in multi-shots mode.

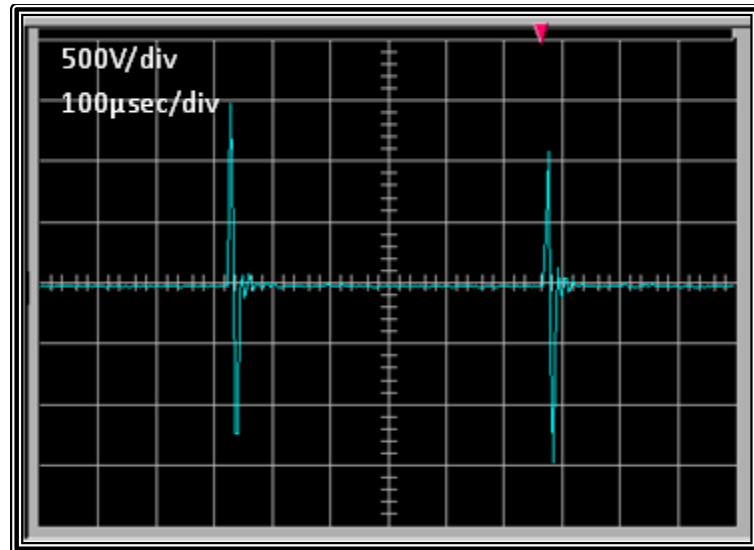


*Figure 3.4: Oscilloscope picture of repetition rate of PSS operation,.*

### **3.3. The Breakdown Voltage of the Gas:**

In order to obtain the operation region of PSS design, breakdown characteristics of the switch are measured. A practical breakdown voltage of Argon gas as a function of the pressure is shown in figure 3.5; it obeys the Paschen's law for Argon gas. It is seen that the breakdown voltage of Ar decreases with increasing the pressure values until reaching the minimum value of the curve and  $p = 1.2 \text{ mbar}$  at  $V_{\text{break}} = 3 \text{ kV}$  for charging capacitor  $C = 1.5 \text{ nF}$ , then the values of  $V_{\text{break}}$  increase with increasing the pressure values. For values of  $p > (p)_{\text{min}}$ , electrons crossing the gap makes more frequent collisions with gas molecules than at  $(p)_{\text{min}}$ , but the energy gained between collisions is lower. Hence, to maintain the desired ionization more voltage has to be applied. But, for  $p < (p)_{\text{min}}$ , electron may cross the gap without even making a collision or making only less number of collisions. Hence, more voltage has to be applied for breakdown to occur. Comparing it with the result published in reference [42] shown in figure 3.6 one can say that our results are very comparable with it.

From the breakdown characteristics of the switch, we select 0.3~ 1 mbar operating pressure for safe hold off of 18.5 kV operating voltage.

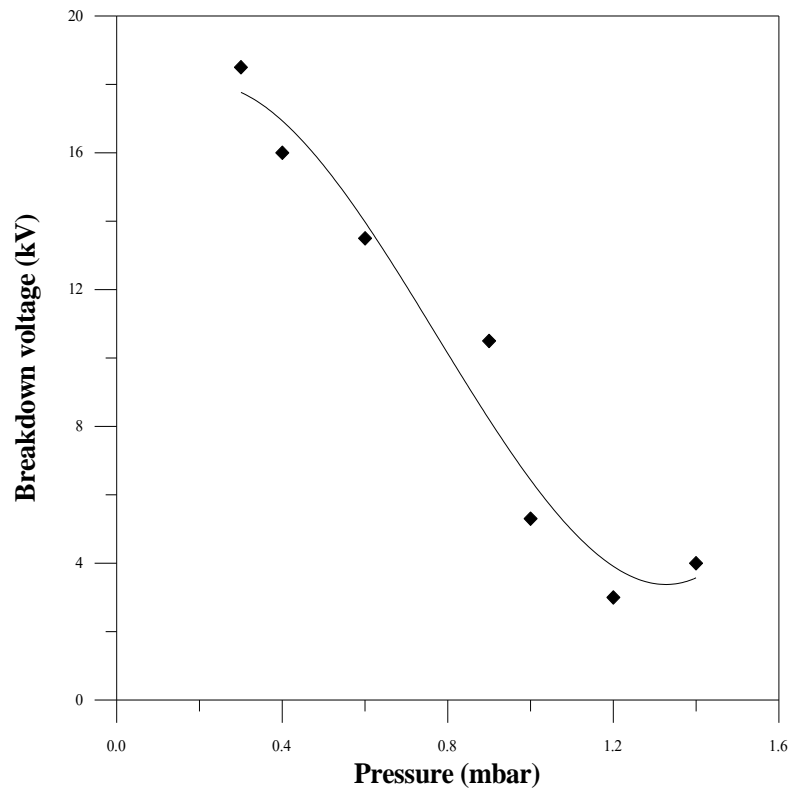


*Figure 3.5: Breakdown characteristic of the PSS as a function of gas pressure.*

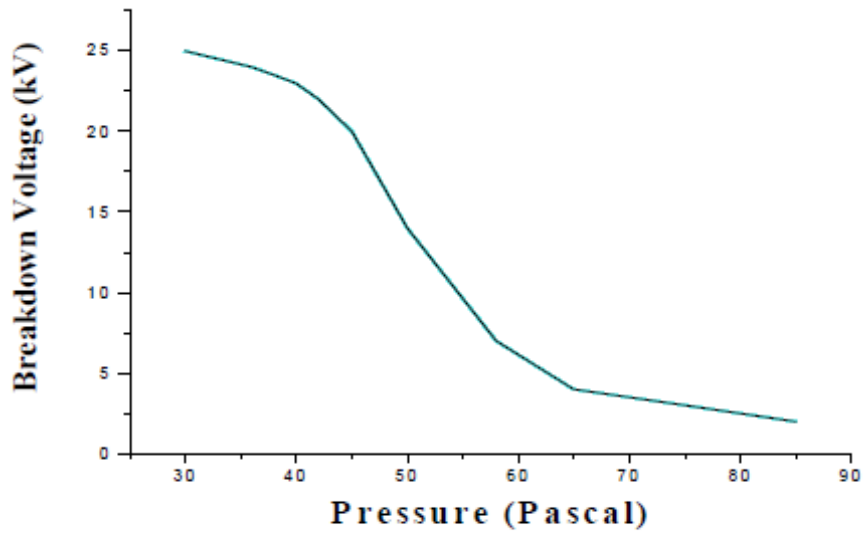


*Figure 3.6: Breakdown voltages of Argon gas [42].*

In reference [42] the breakdown test is done at different pressures to find out a suitable hold-off voltage for single stage PSS and it was found to be 25 kV breakdown voltage at 30 Pascal (1mbar=100Pa).

### **3.4. Pseudo Spark Switch Characteristic:**

#### **3.4.1. Anode Voltage Waveform:**

Figure 3.7 shows the anode voltage waveform resulting from the operation of pseudospark switch, as described in chapter two, under pressure of 0.4mbar. During the increase in voltage applied to the anode electrode of the PSS until reach in 8.5kV and due to the multi-layer air core coil, the applied voltage has been doubled reaching nearly 18.5kV. The high voltage capacitor (0.125nF) is charging continuously until the electric field strength between anode and cathode is high enough to reach the “breakdown” value at the given pressure, then the conducting plasma discharge forms between anode and cathode. Charge is carried through the plasma until the energy storage by the capacitors is drained, at which point the plasma discharge appears.

Since, the value of capacitor is very small, the inductance of the system has been dominated in the RLC discharge circuit (as mentioned in chapter two). This case will convert the discharge circuit to oscillation mode and a negative current will appear due to the negative impedance of the system. As a result voltages backward contribution, due to the passage of the current in the system across the discharge chamber, will inversely charge the capacitor with voltage raising to more than 1.6 times the charging voltage, hence the anode voltage reaches nearly 29.2kV.

By comparing the result with that of reference [75] who described the design, construction and preliminary operation of an advanced multi-gap Pseudospark switch under single mode of operation shown in figure 3.8.

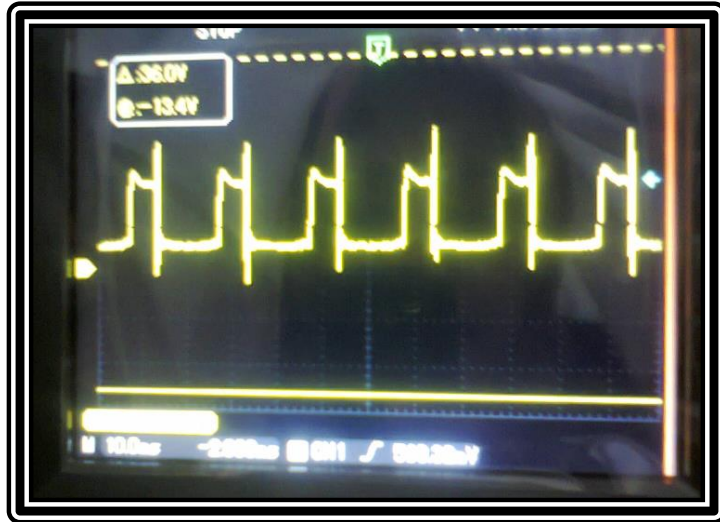


*Figure 3.7: Oscilloscope picture of anode voltage, 10kV/div with 200 $\mu$ s/div*

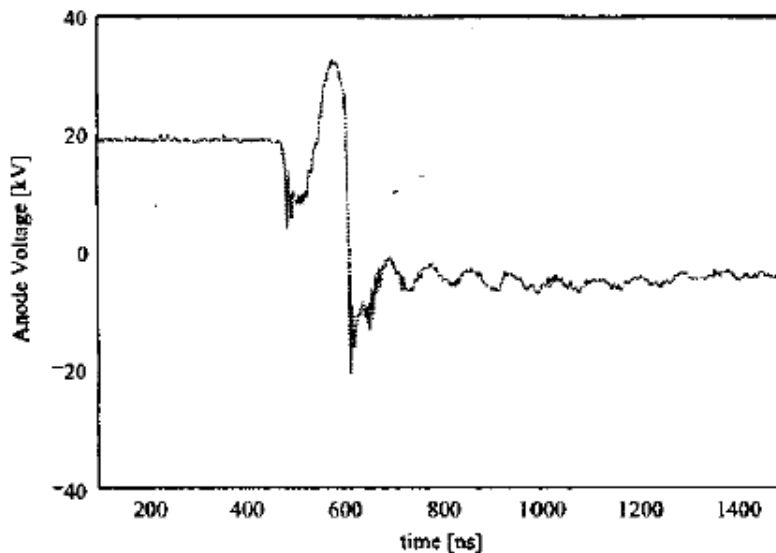


*Figure 3.8: Anode voltage showing the voltage rises to 1.5 times the charging voltage [75].*

It is found pseudo spark discharge has many unique properties. It is a pulsed gas discharge that can obtain tens to hundreds of kV voltage and kA discharge current during total time of discharge of tens to hundreds ns, and several ns rise time. The physical volume of pseudospark device, including the discharge gap and hollow cathode, is few tens of cm<sup>3</sup>. These characteristics make it suitable for a variety of applications, including high power switches and high energy e-beam sources. Most of the reported applications, especially the switch applications and laser oscillation, require the knowledge of time-dependent

characteristics of the discharge formation and development, which reveals a number of complex phenomena that are explained in chapter one. The temporal development of a pseudospark discharge can be separated into four different phases. The voltage-current characteristic that is built-up of the highly conductive plasma of the discharge is of great interest because that part of the discharge is most closely associated with its applicability in a pulsed power system.

The experimental data on discharge voltage which illustrate the principle of pseudospark operation are shown in figure 3.9, with 8.5kV applied voltage and 0.4 mbar Argon gas pressure. The main electrodes gap  $d = 5$  mm is formed by two the electrodes with a diameter of central bore hole  $D = 3$  mm.

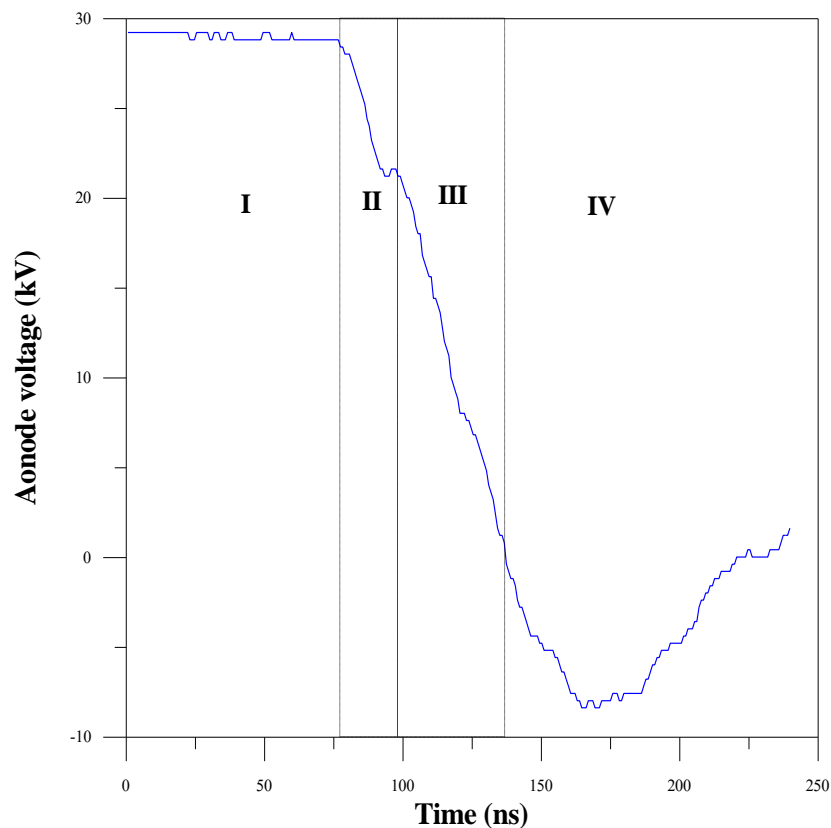


**Figure 3.9: Anode voltage waveform of PSS.**

In figure 3.9 phase I represent the maximum charging voltage value of the capacitor through the chock coil. The end of the time should be larger than the time of frequency domain. It is seen the stability of anode voltage and total

plasma vanish in the relaxation time. Because of excess space charge of the positive ions, a potential hump region appears near the anode.

A quasi-steady phase II is established, this phase is associated with a hollow-cathode dense glow discharge and represents the time between the igniter which is made by trigger plug through the gas in the hollow cathode and the appearance of the main discharge; it is named the delay time which depends on many parameters such as the type and pressure of gas and the values of the voltage/ current of trigger pulse. Normally, it doesn't exceed 40 ns. In our work it is about 11ns as shown in figure 3.14 later.

The phase II transits to phase III that is called bore-hole phase. The electrons released from the hollow cathode region generated by the particle impact depending on the trigger type cause a strong avalanche growth in the cathode backspace and accelerated into the gap between anode and cathode. It represents the time of current rise from 10% to 90% and it should be minimum value, in our work we have reached less than 13 ns. Then dense plasma emerges at the center path in the inter gap region.

Phase VI represents the time domain of current pass through the PSS. Phase VI is the relaxation plasma time where recharging of the capacitor should be started. It is seen that the voltage waveform doesn't have noisy characteristic compared to the other plasma switches as shown in figure 3.10 [45, 77].

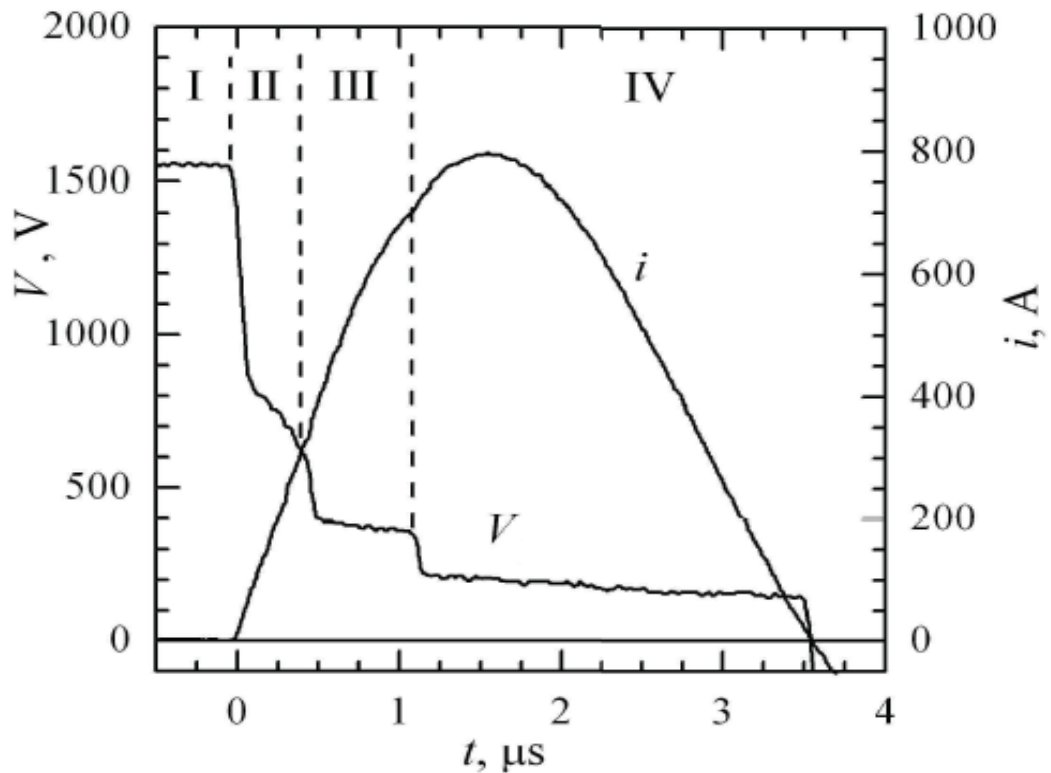


**Figure 3.10: Current and voltage waveform illustrating the different temporal stages of discharge development [45].**

### 3.4.2 Conduction Current Waveform of PSS:

Figure 3.11 shows the voltage, current and power waveforms under 0.4 mbar Argon gas pressure, it is seen that the peak current reaches, 3.6kA, with rise time 11 ns when the dc voltage is about 29.2kV. The current rate  $dI/dt$  is about  $2 \cdot 10^{11}$  A/sec, for 0.125nF discharge capacitor used. Also, the power curve has 75 MW in first peak and ~23 MW in second peak, the last one is due to the two negative peaks of current and anode voltage.

The time duration between 75 ns and 100 ns is the main discharge starting from increase in discharge current. After the voltage breakdown, the current and the voltage signals show damped oscillations, which is the typical characteristic of self-sustained pulsed gas discharges initiated from a hollow cathode discharge (HCD) [78].

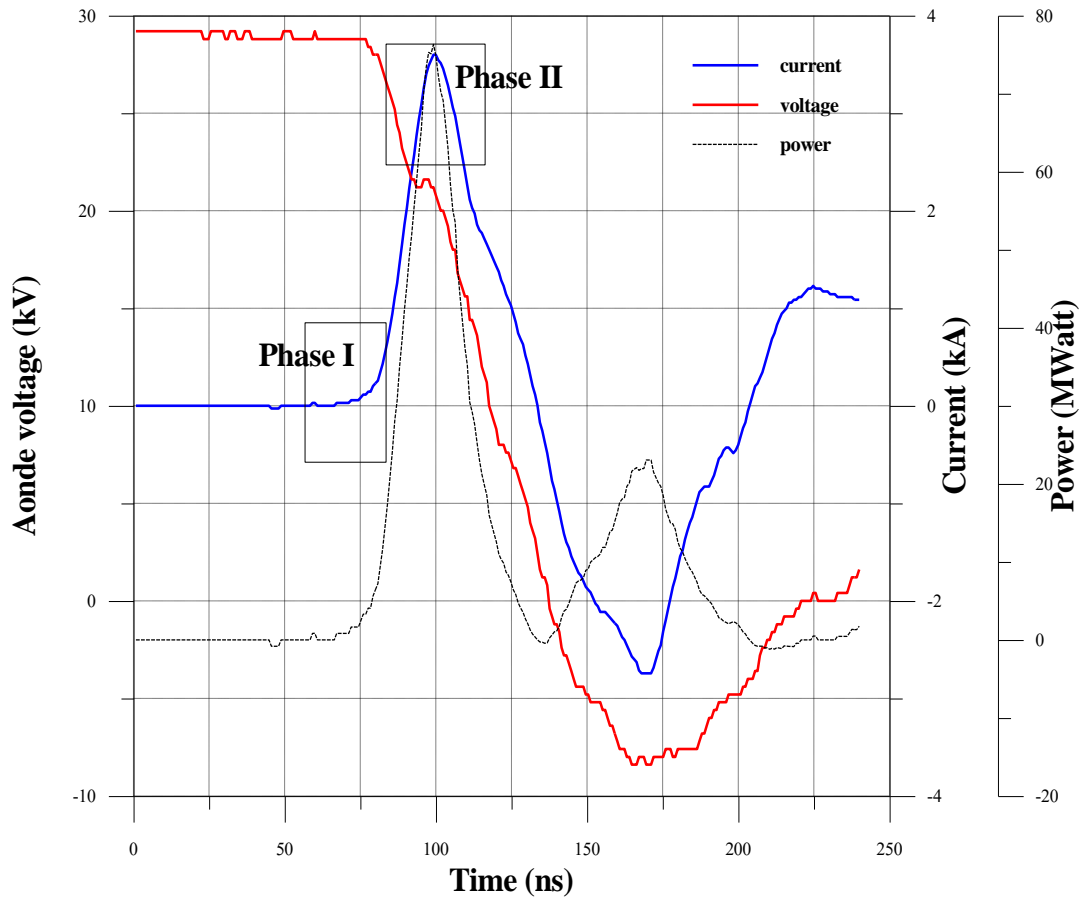


**Figure 3.11: Voltage and current waveform of pseudo-spark switch.**

In figure 3.11, Phase I is a slow current increasing phase and phase II is the fast high current build-up phase. These two different phases can be more clearly presented by time-dependent  $dI(t)/dt$  illustrated in figure 3.12. As shown in Figure 3.12, starting from 60 ns, the  $dI(t)/dt$  has a comparatively slow and flat current rising rate until 80 ns, from  $0.425 \times 10^9$  A/sec to  $2 \times 10^9$  A/sec within 20 ns. After that the temporal current rising rate keeps a fast increasing trend on the rising edge of the discharge current until reaching a maximum, increasing from  $3.1 \times 10^9$  A/sec to  $3.62 \times 10^{10}$  A/sec in 18 ns.

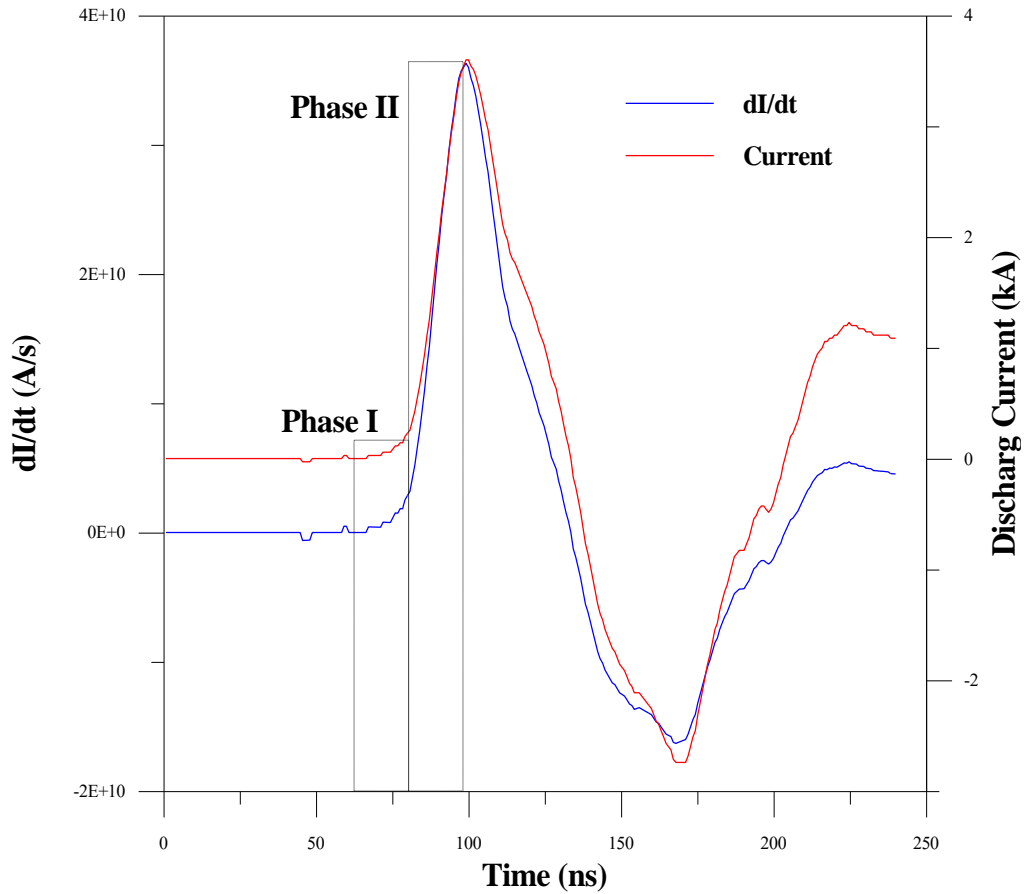


**Figure 3.12: Discharge current and time-dependent  $dI(t)/d(t)$ .**

Compared with results of reference [42], shown in figure 3.13 which shows design of pseudo spark switch with single gap for 25 kV hold off voltages and 5 kA peak currents respectively, our results are better than the results of ref.[42] because the resulting current pulse width is 40 ns, while in figure 3.13 the pulse width is about 1.5  $\mu$ s. Moreover, the current rise time of our pulse is 11ns as shown in figure 4.14, and the current rise time of ref.[42] is  $\sim$ 0.6  $\mu$ s.

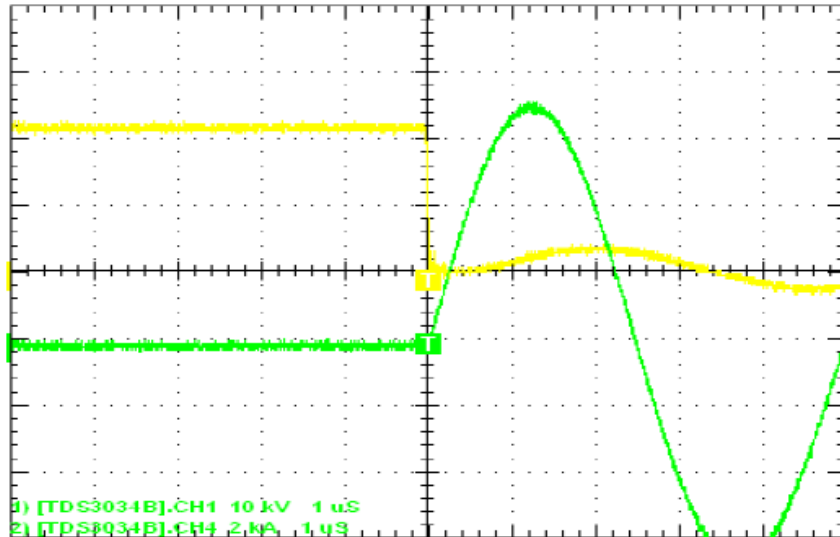


**Figure 3.13: Switch characteristic at 23kV & 7kA [Green : Ch2, 2kA/div. Current : Yellow:Ch1, 10kV/div, Voltage][42].**

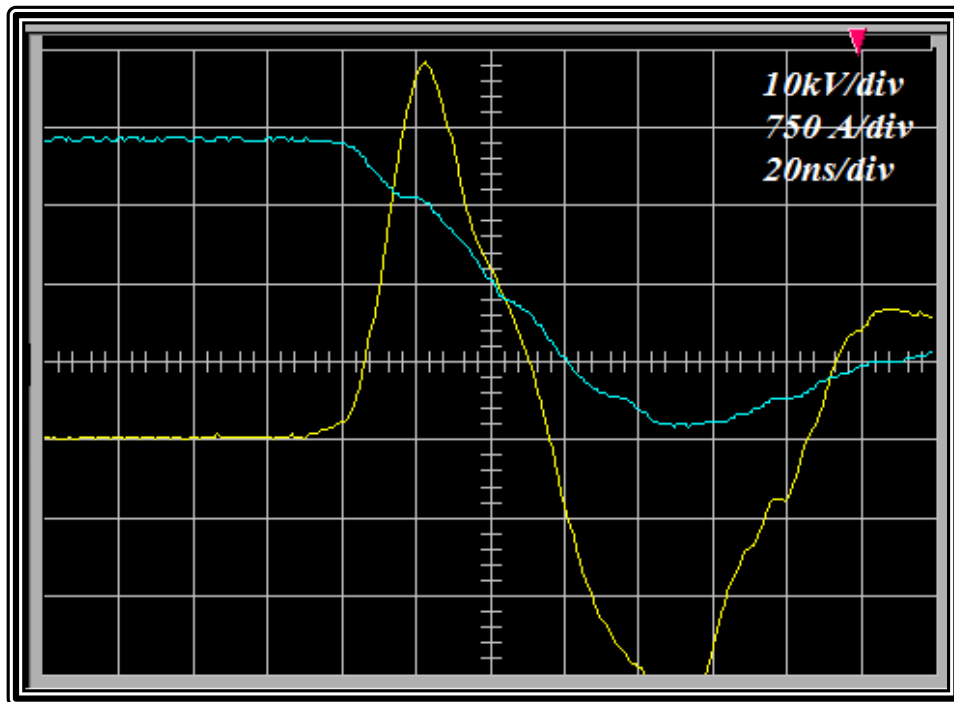


**Figure 3.14: Switching characteristics of our results at 29.2 kV & 3.6 kA [Yellow: Ch-2, 750A/div, Current, Blue: Ch-1, 10kV/div, Voltage].**

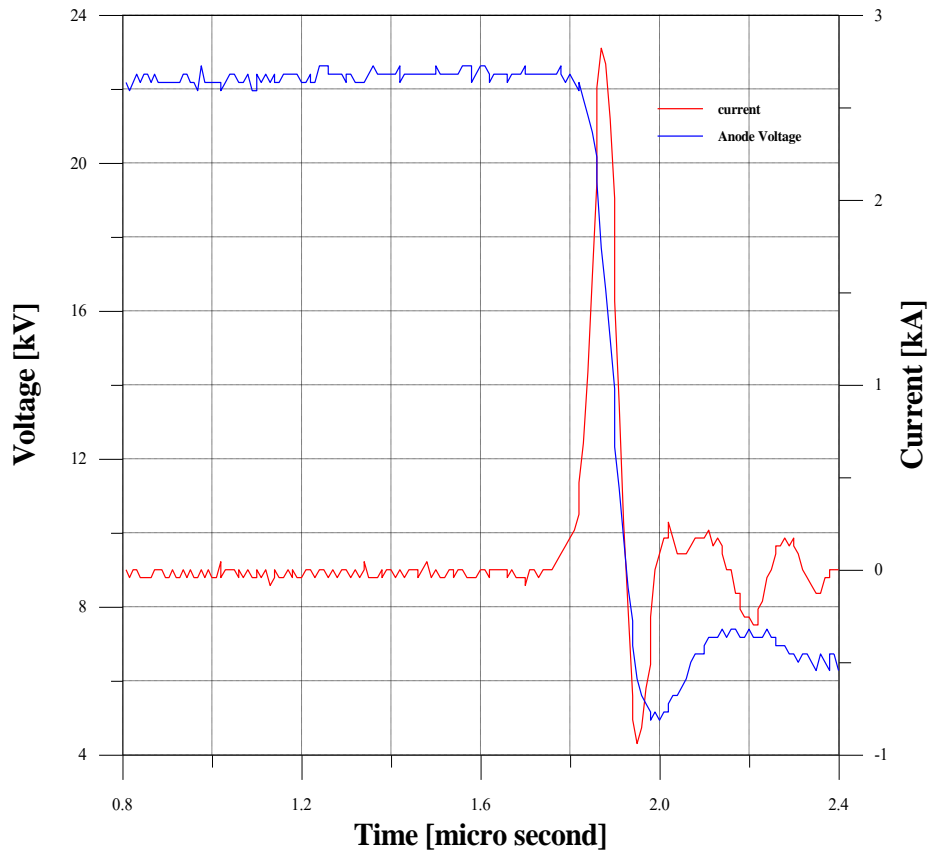
It is important to make a systematic comparison between the experimental data on the pseudo spark switch characteristics under different conditions of operation. Thus, one has to choose the gas pressure and charging capacitor values that would be an excellent comparison for PSS operation from the high

power switch point of view. Table 3.1 shows the characteristics of pseudo spark switch under different conditions.

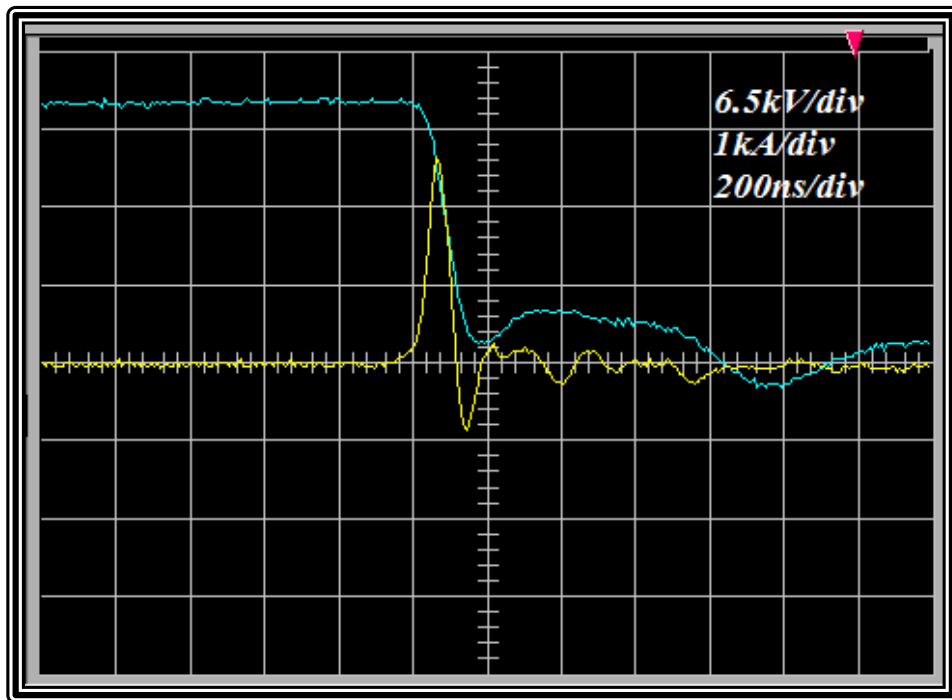
**Table 3.1: The pseudo spark switch characteristics under different conditions of operation.**

Applied Voltages (kV)	Gas Pressure (mbar)	C=0.125 (nF)		C=0.25 (nF)		C=0.5 (nF)		C = 1 (nF)		C= 1.5 (nF)	
		Anode voltage (kV)	Peak Current (kA)								
4.5	1	12.5	1.78	10	1.5	8	0.471	6.5	0.8	5.3	0.314
6.5	0.9	18.5	2.4	17	2	16	1.43	12	1.2	10.5	1.02
7.5	0.6	26	3	21	2.4	18.5	1.88	15	1.45	13.5	1.2
8.5	0.4	29	3.6	25	3.2	22	2.6	18.5	1.8	16	1.5
9.5	0.3	–	–	–	–	25	3.2	21.5	2.1	18.5	1.85

Figure 3.15 (a) and (b) shows the voltage/current waveform under 0.4mbar Argon gas pressure, 0.5 nF high voltage capacitor and 8.5 kV dc applied voltage. It is seen that, for capacitor used greater than 0.125nF such as 0.5nF in figure 3.15, the negative current peak will decrease, with increasing the positive full width half maximum current pulse (FWHM) (~85ns), this is due to the long time of discharging for high capacitor value.



(a)



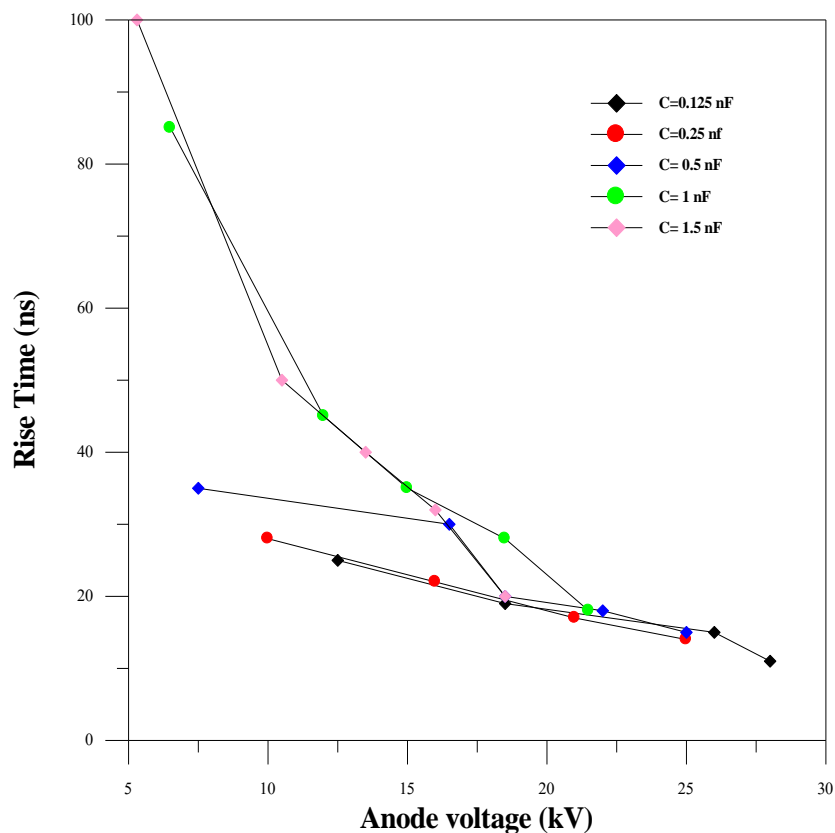
(b)

Figure 3.15: Switching Characteristics at 22 kV & 2.6 kA. (a) Graphical picture (b) Oscilloscope picture [Yellow: Ch-2, 1kA/div, Current; Blue: Ch-1, 6.5kV/div, Voltage].

### 3.5. Current Pulse Parameters:

#### 3.5.1 The Rise Time:

The current rise time is measured as the time difference between a specified low value and a specified high value (10% -90%) i.e. between the voltage drop and the maximum peak current. Shorter current rise time is a desirable parameter in a switch operation. The rise time results of different anode voltages are plotted at various values of charging capacitor (0.125, 0.25, 0.5, 1 and 1.5) nF as shown in Figure 3.16.



*Figure 4.16: The current rise time as a function of anode voltages at different values of capacitor.*

From figure 4.16 shows that the current rise time decreases as anode voltage increases for all values of the capacitors, and it is inversely proportional with charging voltages. Our new design of PSS record a very short rise time 11 ns for 29kV discharge voltage for 0.125 nF capacitor. The high current rise time~100ns has been recorded at 5.3kV discharging voltage for 1.5 nF capacitor.

With the aid of current shunt resistor or (CVR) as mentioned in chapter three, the discharge current has been measured at different values of capacitor. The current rise time is plotted as a function of peak current at different values of capacitance as shown in figure 4.17.

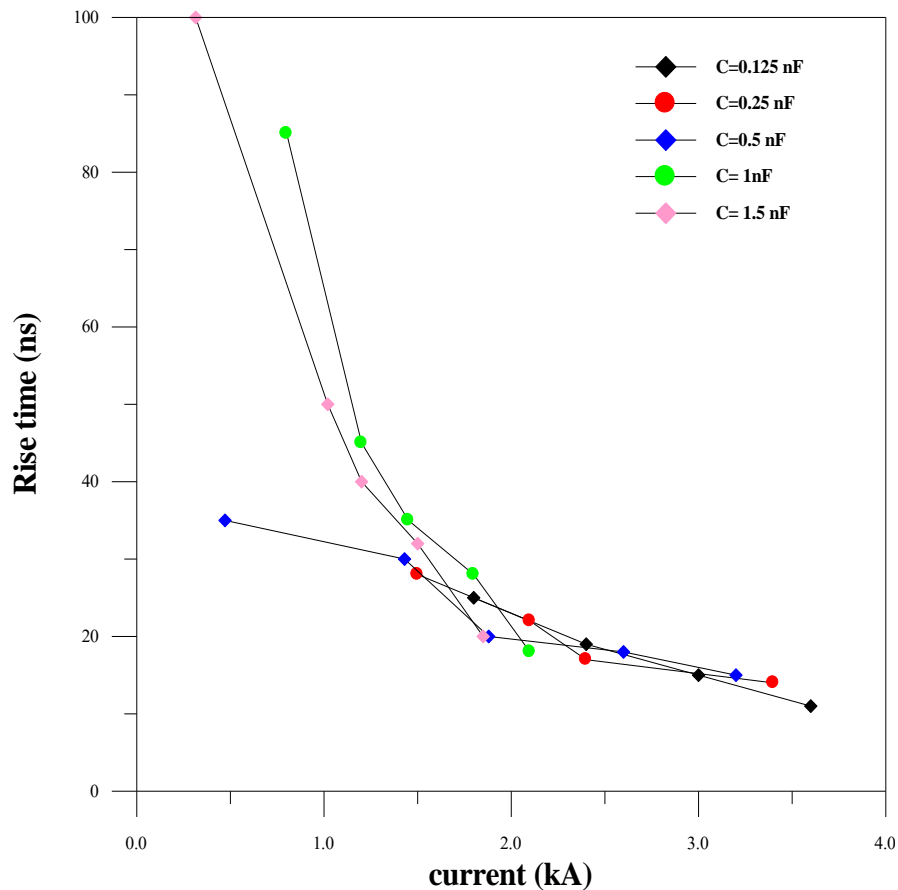


**Figure 3.17: The current rise time as a function of peak current at different values of capacitor.**

Figure 3.17 shows the current rise time decreases as the peak current increases at various values of capacitance. Also it is seen that at  $C = 0.125, 0.25$  and  $0.5$  nF, the curves of the rise time are overlapping and approximately have values smaller than the rise time values at  $C = 1$  and  $1.5$  nF. This means that the smaller capacitor value gives shorter rise time and pulsed width at the same value of applied voltage.

The behavior of the current rise time at different values of capacitance with constant charging voltage 25 kV is shown in figure 3.18 under 0.3 mbar gas pressure.

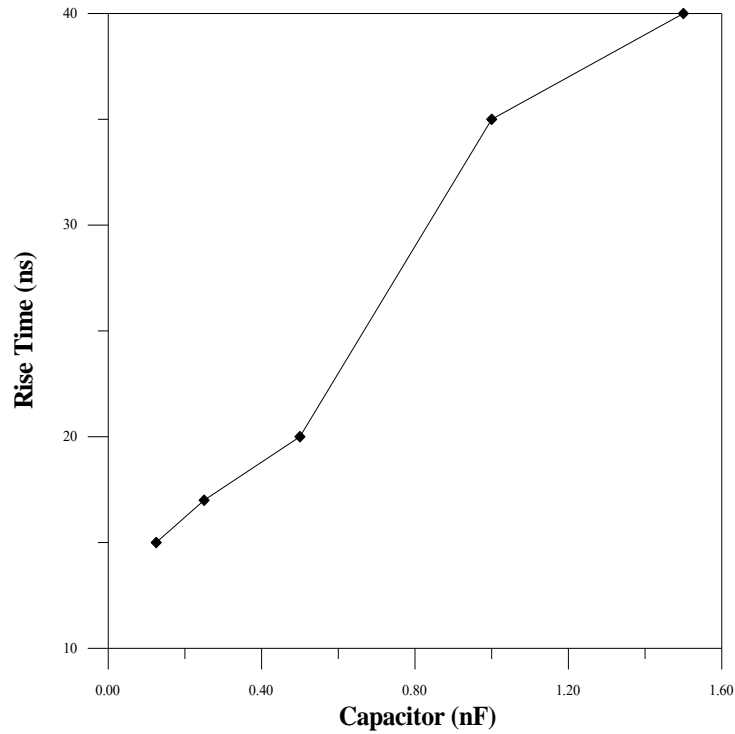


*Figure 3.18: The current rise time at different capacitance values with constant charging voltage.*

The increase in capacitor values for constant charging voltage, increase the current rise time and vice versa.

### **3.5.2. The Effect of Capacitor Values:**

The I-V characteristics of PSS operation have been considered. Figure 3.19 shows the discharge current as a function of the anode voltage at various values of capacitor.

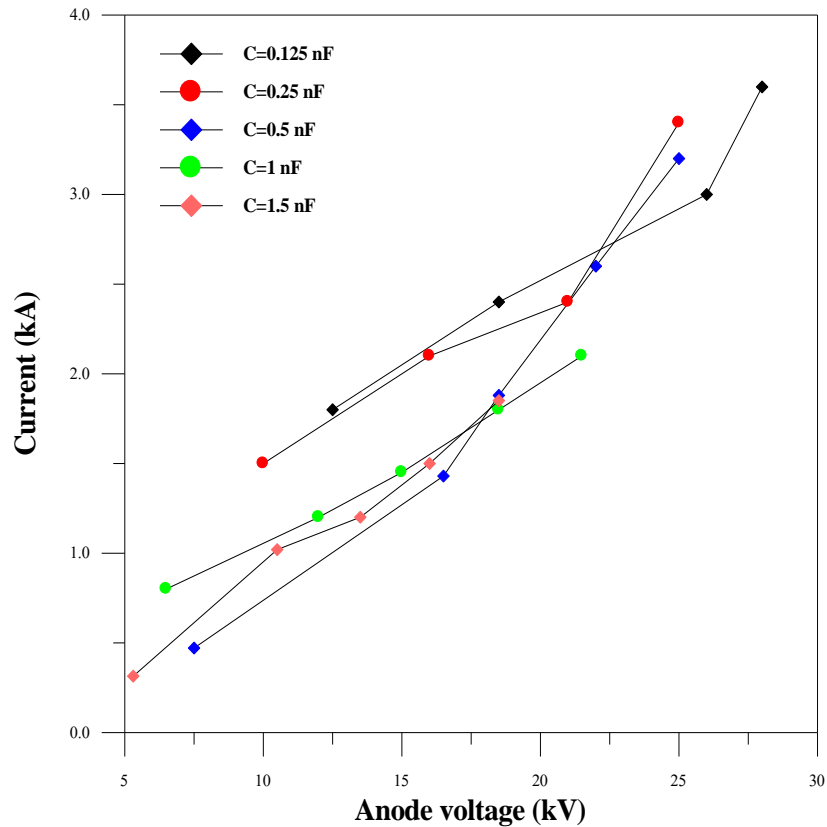


**Figure 3.19: I-V characteristics of PSS at various values of charging capacitor.**

Discharge current is found to be increasing with respect to anode charging voltage irrespective of the value of capacitance. At low values of charging capacitor (0.125, 0.25, 0.5) nF, the voltages have maximum values of more than 25 kV with maximum current of more than 3kA, and minimum values  $\geq 7.5$  kV with minimum current  $> 1$ kA. While the maximum values of voltages are  $\leq 20$  kV for capacitor of values (1, 1.5) nF in spite of similar applied voltages to all values of capacitance. This is because the excess charging voltage returns to low capacitors, causing the additional anode voltage up to 25kV.

Reference [44] designed and developed the pseudo spark switch to generate electron beam. Their results of I-V characteristic behavior are similar to our results as show in figure 3.20:

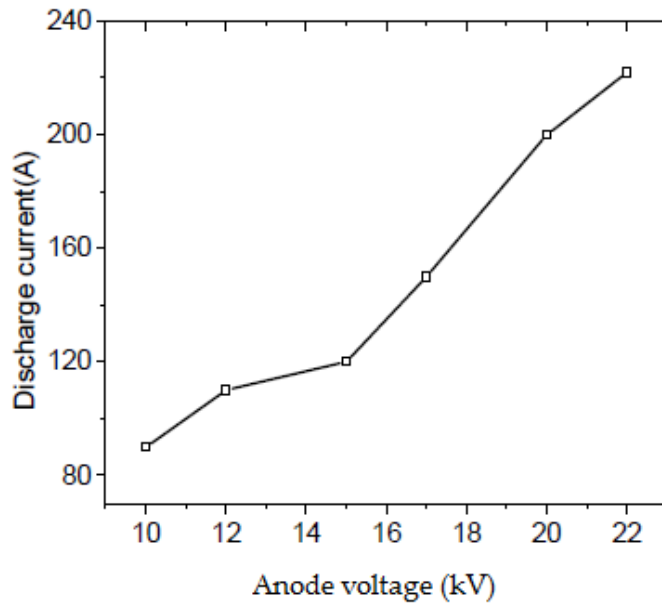


**Figure 3.20: I-V characteristics of PSS [44].** <sup>S</sup>

The effect of charging capacitor on the discharge current is shown in figure 3.21. It is seen that the current decreases with respect to capacitance value at constant applied voltage. This is due to the over voltage values that come from the chocking current in system circuit.

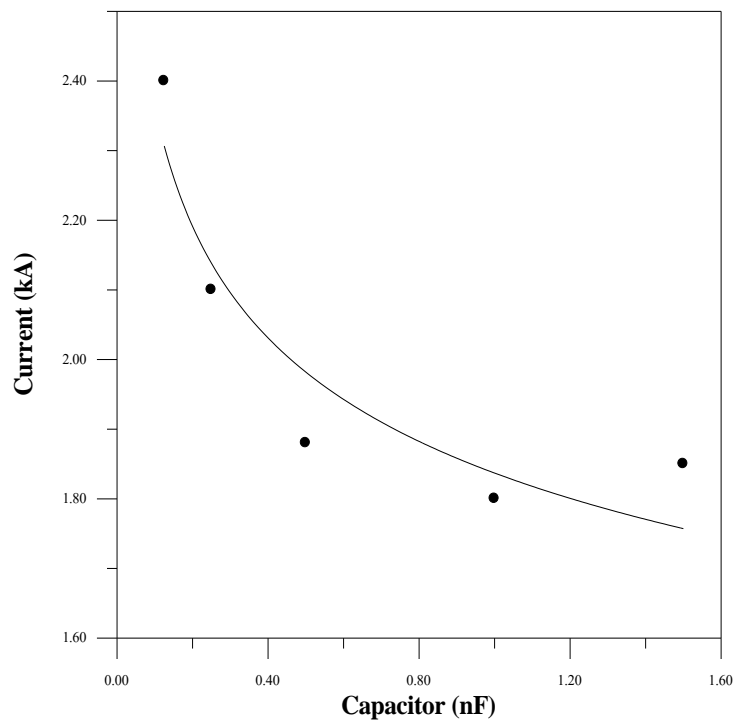


**Figure 3.21: The current as a function of charging capacitor at a constant applied voltage**

### 3.5.3. Jitter Time:

Jitter time is generally defined as any timing displacement (or error) referenced to the timing of an ideal signal. In other words, it is a signal associated with conventional waveform signal. In statistics based classification jitter time is split into two big categories: one is the deterministic jitter (DJ), and the other is the random jitter (RJ) [79]. From figure 3.22, one can measure DJ and RJ, ( $DJ = \mu_r - \mu_l$ ) and ( $RJ = (\sigma_l + \sigma_r)/2$ ) the  $\sigma$  is the values of the far left  $\sigma_l$  and far right  $\sigma_r$  Gaussian tails may and may not be the same. The total RJ value should be the average of these two, and DJ is the distance between two peaks of far left  $\mu_l$  and far right  $\mu_r$  Gaussian tails.

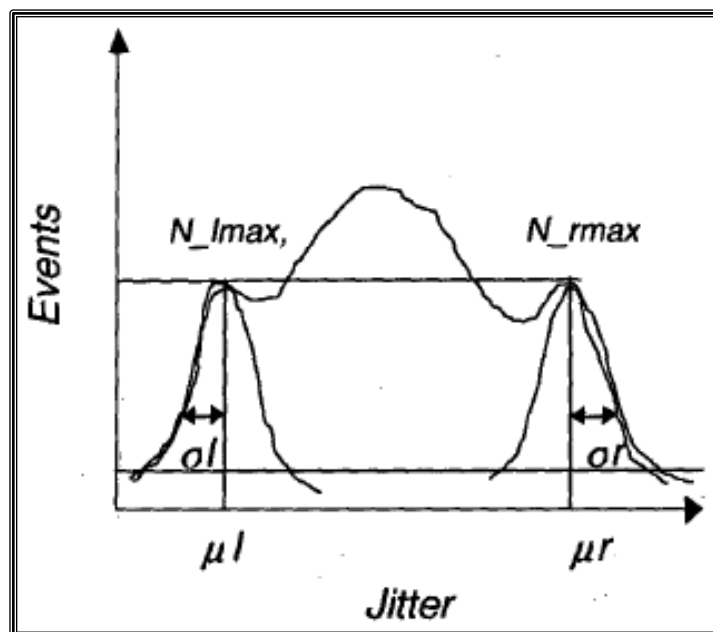
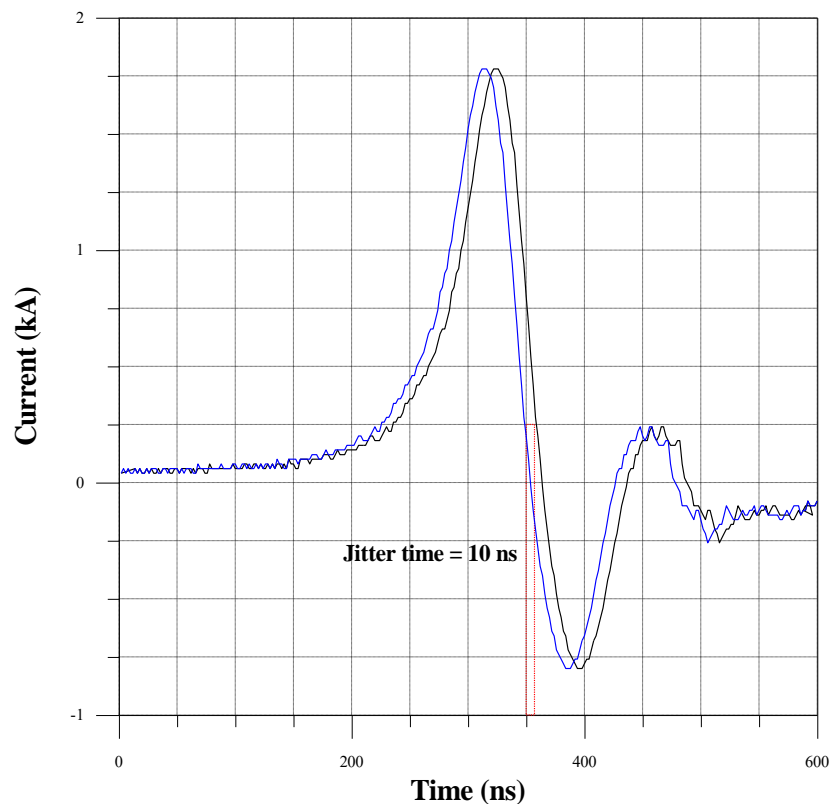


Figure 3.22: Jitter time measuring of two pulses [79].

Two pulses of current under the same condition have been recorded with constant pressure 1mbar, applied voltage 4.5kV and charging capacitor 0.125nF. The deterministic jitter time (DJ), and the random jitter time (RJ) have been measured for these two pulses as shown in figure 3.23, it is found that  $DJ = \pm 10$  ns and  $RJ = \pm 30$  ns.

Whenever the jitter time of the pulse current is small, pulse shape has the best specifications and is desirable.



*Figure 3.23: Current pulse shape at pressure gas 1mbar, anode voltage 12.5kV& charging capacitance 0.125nF.*

#### **3.5.4. The Inductance of the PSS:**

The inductance of the pseudospark switch has been calculated from equation (2-7) with the aid current pulse produced for PSS operation with dummy load connection as seen in figure 2.11,  $L_{PSS} = 241 \text{ nH}$ .

Also, the inductance of the PSS is measured with air core coil connection as seen in figure 2.12. With the aid of equations in chapter two and the data on the current pulse shape show in figure 3.24, such as peak current of 1<sup>st</sup> pulse, frequency and the time between the two successive pulses, the inductance of the PSS has been measured and it was found equal to 750 nH.

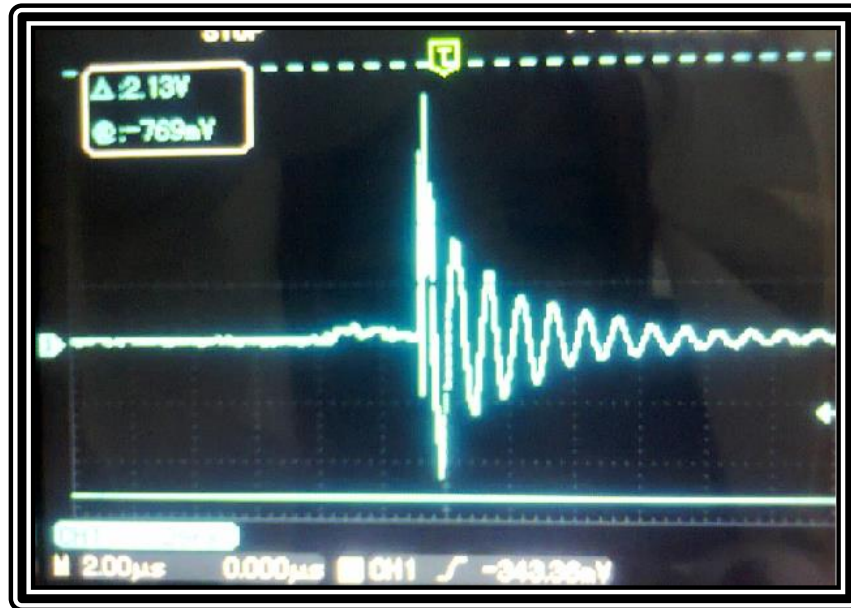


*Figure 3.24: Damping oscillation of current pulse due to air core coil connection.*

### **3.6. Conclusions:**

1. The new single-gap pseudo spark switch that is designed and fabricated as a high voltage, high current switch, gives a good results in terms of the current rise time and jitter time compared with that of other researches.
2. The appropriate operating pressure range of the switch that is 3 mm main gap is found to be  $\sim$  (0.3- 1 mbar) with Argon gas. This result shows that it follows Paschen's law, and the breakdown voltage is independent of the type of material, it depends on the type and pressure of the gas as well as the geometrical design of the chamber.
3. A new design of trigger circuit gives a typical trigger pulse with positive and negative parts. The negative part has a great effect on reducing the recovery time of plasma; it helps to cut off the unwanted current tail for the main discharge which will increase the ability of the device to work at higher repetition rate.

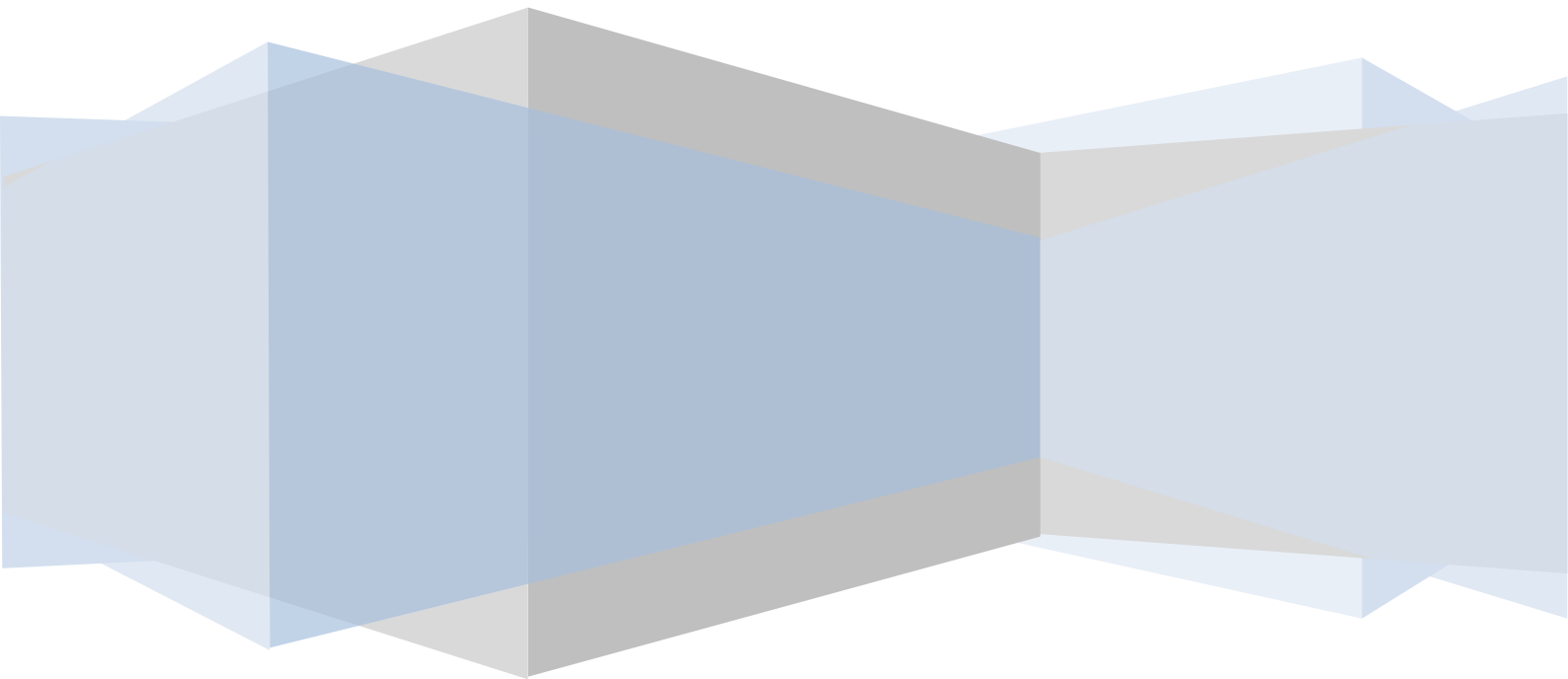
4. A non-inductive shunt resistor that as made in our laboratory gives an excellent result for measuring high currents without being affected.
5. The reliability of the work depends on the steadfastness of the insulating material in front of the high voltages; hence, we must use an insulating material with a high breakdown voltage. Also, reliable long life operation is expected to be made possible by the elimination of overvoltage breakdown across the anode.

### **3.7. Suggestions for Future Work:**

The following topics are put forward for future investigations within the framework of the present research:

- 1- Future studies aim to improve the performance of the pseudospark switch with respect to generation of short rise time ( $< 1$  ns) high quality current pulses for different gases such as  $H_2$ , He and also coupling gases.
- 2- Future experiments should be made in which the pseudospark switch generates high current to be used to generate electron, ion beams and microwaves.
- 3- Modulating the system to multi-gap pseudo spark switch for high-current pulses of up to 30 kA.
- 4- Pseudospark Switch can be used for running a copper-vapor laser instead of thyratron and also for running nitrogen laser instead of spark-gap switch.

# References



## References

- [1] J. R. Roth, "Industrial Plasma Engineering", vol.1. Bristol and Philadelphia: Institute of Physics Publishing, (1995).
- [2] A. Bogaerts, "The Glow Discharge: An Exciting Plasma," *Journal of Analytical Atomic Spectrometry*, vol. 14, pp. 1375-1384, (1999).
- [3] E. Nasser, "Fundamentals of Gaseous Ionization and Plasma Electronics:" (John Wiley & Sons press: New York), (1971).
- [4] A. A. Fridman, L. A. Kennedy, "Plasma Physics and Engineering", (Taylor & Francis press:USA), pp 453, (2004).
- [5] Y. P. Raizer, "Gas Discharge Physics", Springer: Berlin, (1991).
- [6] H. Bluhm, "Pulsed Power Systems: Principles and Applications", Springer, (2006).
- [7] Donald. H. Hale "The Townsend Ionization Coefficients for Ni and Al Cathodes in an Atmosphere of Hydrogen" *Physical Review*, Vol. 56, pp.1199-1202 (1939).
- [8] J. A. Rees, "Electric Breakdown in Gases" (John Wiley & Sons press : New York),( 1973).
- [9]D.A.Erwin and M.A.Gundersen," Measurement of Excited-State Densities During High-Current Operation of a Hydrogen Thyatron Using Laser-Induced Fluorescence", *Appl. Phys. Lett.* Vol.48, no.26,pp. 1773-1775, (1986)
- [10] R. Bischoff, K. Frank, M. Iberler, I. Petzenhauser, A. Rainer, and J. Urban, *IEEE Trans. Plasma Sci.*,vol. 32, no. 1, Special Issue on Pseudospark Physics and Applications, pp.191-195, 2004.
- [11] M. Kristiansen, "Pulsed Power Applications," in *Pulsed Power Conference, Digest of Technical Papers. Ninth IEEE International*, p.6,(1993).
- [12] T. R. Burkes, "General Switching Considerations," in *Gas Discharge Closing Switches. vol. 2*, G. Schafer, M. Kristiansen, and A. Guenther, Eds. (Plenum press : New York), pp. 1-13,(1990).

[13] M. A. Gundersen, "Gas-Phase Pulsed Power Switches," *IEEE Trans. on plasma sci.*, vol. 19, pp. 1123-1131, (1991).

[14] W. C. Nunnally and A. L. Donaldson, "Self Breakdown Gaps," in *Gas Discharge Closing Switches*. vol. 2, G. Schaefer, M. Kristiansen, and A. Guenther, Eds. (Plenum press :New York), pp. 47-61,( 1990).

[15] E. Schamiloglu, R. J. Barker, M. Gundersen, and A. A. Neuber, "Modern Pulsed Power: Charlie Martin and Beyond," *Proceedings of the IEEE Trans. on plasma sci.*, vol. 92, pp. 1014-1020,(2004).

[16] H.E.Kreffft, H. Austad and A.E.Gordon, "Design Problems of High Voltage Multi-Grid Hydrogen Thyatron Tubes",*IEEE electron devices*, pp.74-78,(1966).

[17] M. Gundersen, "Thyatron in Gas Discharge Closing Switches", vol. 2, A. Guenter and M. Kristiansen, Eds (Plenum press :New York) pp. 375-378,(1990).

[18] C. A. Pirrie and H. Menown, "The Evolution of the Hydrogen Thyatron," *IEEE conf. 24<sup>th</sup> on power modulator*, pp. 9-16. (2004).

[19] J. Christiansen, "The Pseudospark Switch," in *Gas Discharge Closing Switches*. vol. 2 (Plenum Press :New York) (1990).

[20] J. Christiansen and C. Schultheiss, "Production of High Current Particle Beams by Low Pressure Spark Discharges," *Z. Physik A.*, vol. 290,no.1, pp. 35-41, (1979).

[21] J. Christiansen and W. Hartmann, "The Pseudospark," in *Gas Discharge Closing Switches*. vol. 2, (Plenum press: New York) pp. 509-519,(1990).

[22] H. Riege and E. P. Boggasch, "High-Power, High-Current Pseudospark Switches", *Advance in pulsed power technology*, vol.2, pp.534-549,(1990)

[23] P. Choi, H. Chuaqui, J. Lunney, R. Reichle, A. J. Davies, And K. Mittag, " Plasma Formation In A Pseudospark Discharge", *IEEE Trans. Plasma Sci.* vol 17. no 5. Oct. (1989).

[24] M.A. Gundersen and G. Schaerfer, (eds) "Physics and Applications of Pseudosparks" (Plenum Press : New York), (1990).

[25] Y.D. Korolev, O.B.Frants, V.G. Geyman, N.V.Landl, R.V. Ivashov I.A. Shemyakin, R.E. Bischoff, K.Frank, and I.J. Petzenhauser, "Temporal Structure of the Fast Electron Beam Generated in the Pseudospark Discharge With External Triggering", *IEEE Trans. on Plasma Sci.*, vol.33,no.5I, pp. 1648-1653, (2005).

[26] K.Frank, and J. Christiansen, "Fundamentals of the Pseudospark and its Applications", *IEEE Trans.on Plasma Sci.*, vol.17,no.5, pp. 748-753, (1989).

[27] W.Hartmann, and G. Lins, "Spatial and Temporal Development of Pseudospark Switch Plasmas", *IEEE Trans. on Plasma Sci.*, vol.21,no.5, pp. 506-510, (1993).

[28] G.Schaefer, M.Kristiansen, and A.Guenther, (eds) "Gas Discharge Closing Switches" (Plenum Press :New York),( 1990).

[29] O.Rosier, R. Apetz, K.Bergmann, J. Jonkers, R. Wester, W. Neff, and J. Pankert, "Frequency Scaling in a Hollow-Cathode-Triggered Pinch Plasma as Radiation Source in the Extreme Ultraviolet",*IEEE Trans.on Plasma Sci.*, vol.32,no.III, pp. 240-246, (2004).

[30] D. Bloess, I. Kamber, H. Riege, G. Bittner, V. Bruckner, J. Christiansen, K. Frank, W. Hartmann, N. Lieser, C. Schultheiss, R. Seeböck and W. Steudtner, " The Trigger Pseudospark Chamber as a Fast Switch and as a High –Intensity Beam Source" *Nucl. Instrum.Methods* vol.205, no.1,pp. 173-184, (1982).

[31] G. Mechttersheimer, R. Kohler, T. Lasser, and R. Meyer, "High repetition rate, fast current rise, pseudospark switch," *J. Phys. E.: Sci. Instrum.*, vol. 19,no.6, p. 466, (1986).

[32] K. Frank, C. Kozlik, J. Christiansen, A. Gortler, W. Hartmann, and C.Braun, "High-Power Pseudospark and BLT Switches," *IEEE Trans. Plasma Sci.*, vol. 16, p. 317, (1988).

[33] C. Kozlik , K.Frank,O. Almen, J. Christiansen, A. Gortler, W. Hartmann, A. Tinschmann, and R. Tkotz, "Triggered Low-Pressure Pseudospark-Based High Power Switch," *IEEE Trans. Plasma Sci.*, vol. 17, no.5,pp. 758-761, (1989).

[34] G. Babst and M. Schwertl, "Running a Copper-Vapor Laser with a Pseudospark Switch", *IEEE Trans. on Electron Devices*, vol. 39, no. 5, May (1992)

[35] V.D. Bochkov, A.V. Kolesnikov, Yu.D. Korolev, "Investigation of the Effect of Blocking Potential on the Static Breakdown Voltage and Discharge Initiation in Pseudospark Switches," *IEEE Trans. Plasma Sci.* vol.23, no.3, pp.341-346, (1995).

[36] V.D. Bochkov, Yu.D. Korolev, and I.A. Shemyakin, "High-Current Ceramic-Metal Sealed-Off Pseudospark Switches (Designs And Applications)",*XVIIth International Symposium on Discharges and Electrical Insulation in Vacuum*, vol.2, pp. 977-980, (1996).

[37] Yu. D. Korolev, O. B. Frants, V. G. Geyman, R V. Ivashov, N. V. Landl, I. A. Shemyakin, K. Frank, M.Iberler, and J. Urban " Hollow-Cathode Auxiliary Discharge in aTrigger Unit of Pseudospark Switch", *XXth International Symposium on Discharges and Electrical Insulation in Vacuum*, pp.495-498,(2002).

[38] A. W. Cross," *Generation and Application of Pseudospark-sourced Electron Beams*", *XXVIIth ICPIG, Eindhoven, the Netherlands*, (2005).

[39] Yu.D. Korolev, O.B. Frants, V.G. Geyman, R.V. Ivashov, V.N. Landl, and I.A. Shemyakin, " Investigation of the Electric Strength Recovery Process in the Pseudospark Switch with a High Pulse Repetition Rate", *XXIIInd Int. Symp. on Discharges and Electrical Insulation in Vacuum*, vol.1, pp.25-28,(2006).

[40] K.Frank, I. Petzenhauser, and U.Blell," *Multi-gap Pseudospark Switches for High Voltage Applications*", *IEEE Trans. on Dielectrics and Electrical Insulation*, vol.14, no.4, pp.968-975, (2007).

[41] D.V. Bochkov, V.D. Bochkov, V.M. Dyagilev, and V.G. Ushich, "SN-series Pseudospark Switches Operating Completely Without Permanent Heating, New Prospects of Application in Pulsed Power", *IEEE Inter. Conf. on Plasma Sci.* pp.1-5, (2009).

[42] B. L. Meena, S. K. Rai, M. S. Tyagi, U. N. Pal, M. Kumar and A. K. Sharma," *Characterization of High Power Pseudospark Plasma Switch (PSS)*," *Journal of Physics: Conference Series* vol.208,(2010).

[43] M. Watanabe, M. Nishimura, N. Nogera, and T. Kamada, " *Small Sized Plasma Jet Based on a High Current Pseudo-Spark Discharge and its*

*Durability of the Electrodes*", APS, 63<sup>rd</sup> Annual Gaseous Electronics Conf. and 7<sup>th</sup> Inter. Conf. on Reactive Plasmas, vol.55, no.7,pp.1-3, (2011).

[44] N. Kumar, D. K. Verma, J. Prajapati, M. Kumar, B. L. Meena, M. S. Tyagi, V. Srivastava and U. N. Pal, "Experimental Investigation of Pseudospark Generated Electron Beam", *J. of Phy.: Conference Series* vol.390, (2012).

[45] Y. D. Korolev, O. B. Frants, N. V. Landl, I. A. Shemyakin, and V.G. Geyman," *High-Current Stages in a Low-Pressure Glow Discharge With Hollow Cathode*", *IEEE Trans. Plasma Sci.*, vol. 41, no. 8, pp. 2087-2096, (2013).

[46] Y. P.Raizer, "Gas Discharge Physics" (Berlin, Germany: Springer-Verlag), (1991).

[47] E. Dewald, K. Frank, D.H.H.Hoffmann, R.Stark, M.Ganciu, B.N.Mandache, M.G.Nistor, A.-M.Pointu, and I.-I.Popescu, "Pulsed Intense Electron Beams Generated in Transient Hollow Cathode Discharges: Fundamentals and Applications" *IEEE Trans. on Plasma Sci.*, vol.25, no.2, pp. 272-278, (1997).

[48] E. Dewald, K. Frank, D.H.H.Hoffmann, and A.Tauschwitz, "Comparative Studies on Intense Electron Beams Generated in Transient Hollow-Cathode Discharges" *IEEE Trans. on Plasma Sci.*, vol.30,no.5I, pp. 1820-1826, (2002).

[49] K. Frank,"Scientific and Technological Progress of Pseudospark Devices," *IEEE Trans. On Plasma Sci.*, vol.27, no.4, pp.1008 (1999).

[50] S. S. Park, Y. J. Han, Sang Hee Kim, Y. G. Kwon, Sung Han Kim, Y. J .Park, and S. H. Nam,"Study of High Voltage and High Current Pseudo-spark Switch",*International Conference on Electrical Engineering* (2002).

[51] C. Luo, X Wang, H. Zhao, and Z. Xie, "Effect of Cavity Structure on the Discharge Features of Pseudospark Switches," *IEEE Trans. on Plasma Science*, vol.30 ,no.5, (2002).

[52] K. Frank, C.Bickes, U.Ernst, M.Iberler,A.Rainer, J.Schwab, J.Urban, W.Weisser and V.Bochkov,"Design Criteria for High Performance, High

*Power Pseudospark Switch,*” 12<sup>th</sup> *Int. IEEE Pulsed Power Conf.*, vol. 1, pp.224-227 (1999).

[53] H. Taguchi, T.Sato, M. Itagaki, M. Watanabe, Y. Morikawa, Y. Abe, and T. Shimada, “Effects of Electrode Geometry on Breakdown Voltage of a Single-Gap Pseudospark Discharge,” *J. Appl. Phys.*, vol.37 no.1, pp.303 (1998).

[54] J.R.Taylor and A.C.Bull, “Ceramics Glaze Technology”, (the Institute of Ceramics & Pergamon Press: Oxford), (1986).

[55] B. L. Hertzler and M. Kaufman, “Technique for Making a Groove for an O-ring Distorted to a Non-Planar Configuration”, *Rev. Sci. Instrum.* vol.44, pp. 1779 (1973).

[56] K. Frank, E. Boggash, J. Christiansen, A. Goertler, W. Hartmann, C. Kozlik, G. Kirkman, C. Braun, V. Dominic, M. A. Gundersen, H. Riege, and G. Mechtersheimer, “High-Power Pseudospark and BLT switches,” *IEEE Trans. Plasma Sci.*, vol. 16, no. 2, pp. 317–323, Apr. (1988).

[57] “LM555CN datasheet”, *National Semiconductor Americas Customer Support Center*, (2006).

[58] D. A. Hodges, “Darlington’s Contributions to Transistor Circuit Design”, *IEEE Trans. on circuits and systems—i: fundamental theory and applications*, vol. 46, no. 1, pp. 102-104, (1999).

[59] Z. Zeng, J. C. Thomaz Jr., G. Bauville, A. Delmas, M. Legentil, F. Bendiab, C. Postel, and V. Puech, “Characterization of a Pseudospark Switch Triggered by a Corona-Plasma Electrode,” 10<sup>th</sup> *IEEE Int. Pulsed Power Conf.*, 452 (1995).

[60] T. Mehr, J. Christiansen, K. Flank, A. G”ortler, M. Stetter, and R. Tkotz, “Investigation about triggering of coaxial multichannel pseudospark switches,” *IEEE Trans. Plasma Sci.*, vol. 22, no. 1, pp. 78–82, Feb. (1994).

[61] Web site: [http://www.circuits.dk/calculator\\_multi\\_layer\\_aircore.html](http://www.circuits.dk/calculator_multi_layer_aircore.html)

[62] H. R. Bauer, G. Kirkman, and M. A. Gundersen, “A two-component model for the electron distribution function in a high current Pseudospark or back-lighted Thyatron,” *IEEE Trans. Plasma Sci.*, vol. 18, no. 2, pp. 237–246, Apr. (1990).

[63] A. Gortler, A. Schwandner, J. Christiansen, K. Flank, and H. Granzer, "Development of a high current Pseudospark switch and measurement of electron density," *IEEE Trans. Plasma Sci.*, vol. 21, no. 5, pp. 521–526, Oct. (1993).

[64] H. H. Chuaoui, M. Favre, E. S. Wyndham, L. Arroyo, and P. Choi, "Properties of a laser-initiated Pseudospark discharge," *IEEE Trans. Plasma Sci.*, vol. 29, no. 5, pp. 802–808, Oct. (2001).

[65] M. A. Gundersen and G. Schaefer, "The physics and applications of pseudosparks," in *NATO ASI, ser. B. (Plenum press:New York) vol.219*, (1990).

[66] B. Alexander, A. Charles, "Fundamentals of Electric Circuits ", McGraw-Hill pp. 387–389, (2006).

[67] K.H. Lateef, "Design and Construction of Vapor Copper Laser System as Amplifier and Oscillator", *Ph.D. Thesis, Collage of Science, Baghdad University,Iraq*,(1997).

[68] Web site: <http://www.slideshare.net/element14/current-shunt-monitors>

[69] INA138 Datasheet: <http://focus.ti.com/lit/ds/symlink/ina138.pdf>

[70] INA209 Datasheet: <http://focus.ti.com/lit/ds/symlink/ina209.pdf>

[71] Quiescent Current: <http://www.diracdelta.co.uk/science>.

[72] Electronics Industry Glossary: <http://www.uswi.com>.

[73] Y. Yin, H.H. Zhong, J.L. Liu, H.M. Ren, J.H. Yang, X.P. Zhang, and Z. Hong, "Radial Current High Power Dummy Load for Characterizing the High Power Laser Triggered Transformer-Type Accelerator", *Rev. Sci. Instrum.* vol.8,1093301, (2010).

[74] Website: [http://www.dxzone.com/catalog/Technical\\_Reference/Dummy\\_Loads/](http://www.dxzone.com/catalog/Technical_Reference/Dummy_Loads/).

[75] A. Kuthi, B. Eccles, Q. Yao, C. Jang, K. Frank and M. Gundersen, "Advanced Multi-Gap Pseudospark Switch", *Digest of Technical Papers, 14th IEEE International Pulsed Power Conf.*, vol. 2, pp.946-949, (2003).

[76] C. Torres, P. G. Reyes, F. Castillo and H. Martínez," Paschen Law for Argon Glow Discharge", *Journal of Physics: Conf. Series*, vol. 370, (2012).

[77] S.S.Park, Y.J. Han, S.H.Kim, Y.G.Kwon, S.HanKim, Y.J.Park, and S.H.Nam,"Study of High Voltage and High Current Pseudo-spark Switch", *Inter. Conf. on Elect. Eng.*, (2002).

[78] E. Dewald, K. Frank, D.H.H. Hoffmann, and A. Tauschwitz, "Plasma Development in The Low-Pressure Channel Spark for Pulsed Intense Electron Beam Generation," *IEEE Trans. on Plasma Sci.*, vol.30,no. 1III, pp. 363-374, (2002).

[79] P. L. Mike, J. Wilstrup, R. Jessen, D. Petrich," A New 'Method for Jitter Decomposition Through its Distribution Tail Fitting" *Test Conf.*, P ro. Inter.pp.788-794,(1999).

## الخلاصة :

نظراً لأهمية مفاتيح الفولتية العالية وإستخدامها في تشغيل ليزرات أبخرة المعادن ،فقد تم تصميم وتصنيع منظومات مفاتيح القدرة العالية لبلازما الومضة الكاذبة والتي بواسطتها يمكن الاستعاضة عن مفاتيح القدرة العالية المستخدمة بالليزر كالثايرترون وفجوات القذح التقليدية الاخرى، لما تمتاز به هذه المنظومات من خصائص ممتازة من حيث زمن نهوض التيار وزمن التكرارية.

في هذا البحث تم تصميم وتصنيع منظومة مفتاح الومضة الكاذبة منفرد القناة حيث تتكون حجرة المفتاح من قطبي الانود والكاثود وهما عبارة عن اسطوانتين مجوفتين مصنوعتين من مادة الحديد المقاوم للصدأ نوع (316 L) بطول 6.5 سم وسمك 2 ملم و قطر داخلي 6.5 سم وقطر خارجي 6.9 سم مُحكمتي الغلق وتحتويان على ثقب مركزي بقطر 3 ملم من جهة واحدة فقط. تم فصل القطبين بمادة عازلة بسمك 3.5 ملم من السيراميك المزجج. يتميز هذا العازل بتحمّله تفريغ الفولتية العالية عند تشغيل المنظومة لعدة ساعات، لذا امتازت هذه المنظومة بموثوقية عالية معتمدة على نوع وسمك المادة العازلة .

تم تصنيع دوائر القذح الكهربائية الملائمة لتقنية هذه المنظومة حيث تم الاعتماد على دائرة الـ master slave للمذبذب 555 نوع LM555CN وأمكن الحصول على نبضة قذح مربعة موجبة بعرض 3 مايكروثانية وفولتية 13.75 فولت وبتردد 2.2 كيلوهرتز. وبتطبيق هذه النبضة على دائرة التضخيم المعروفة بإسم (ثنائي دارلنجتون) والمربوطة بمحولة عالية الفولتية 100:30000 فولت نوع EG&G تم الحصول على نبضة قذح مثالية بفولتية 1.56 كيلو فولت بعرض 3 مايكروثانية. تم قياس نبضات التيار العالية بإستخدام مقاومة مجزئ تيار والتي تم تصميمها وتصنيعها بالمختبر اعتماداً على مادة الكرافيت من اقلام الرصاص وقيست قيمة مقاومتها بعدة طرق وكان معدل قيمة مقاومتها لا تتجاوز 7.4 ملي اوم. وبإستعمال مجس عالي الفولتية وقارئ رقمي للذبذبات تم قياس فولتية الشحن على الانود بمقدار 29~ كيلوفولت وذروة تيار 3.6 كيلوأمبير وزمن نهوض 11 نانوثانية وزمن تراوح  $\pm 10$  نانوثانية عند تشغيل المفتاح بغاز الاركون وبضغط 0.3 ملي بار عند متسعة شحن 0.125 نانوفاراد.

وُدُرست خواص المفتاح من حيث زمن نهوض التيار وفولتية شحن الانود وذروة التيار عند قيم مختلفة لمتسعة الشحن. وتم قياس إعلومات المفتاح كالمحاثّة والمقاومة حيث كانت له محاثّة قليلة أدت الى الحصول على معدل نهوض تيار وصل الى  $(2 \times 10^{11} \text{ A/sec})$ .

بِسْمِ اللَّهِ الرَّحْمَنِ الرَّحِيمِ

"سَنُرِيهِمْ آيَاتِنَا فِي الْأَفَاقِ وَفِي أَنْفُسِهِمْ حَتَّىٰ يَتَّبِعِنَ لَهُمْ أَنَّهُ  
الْحَقُّ" ۝

صدق الله العظيم

(فصلت ۵۳)



جمهورية العراق  
وزارة التعليم العالي و البحث العلمي  
جامعة النهرين - كلية العلوم  
قسم الفيزياء

# تصنيع وتوصيف مفتاح بلازما الومضة الكاذبة ذو القدرة العالية

## إطروحة

مقدمة الى كلية العلوم /جامعة النهرين

وهي جزء من متطلبات نيل درجة دكتوراه فلسفة في الفيزياء

## من قبل

بسمة حسين حمد الشمري

بكالوريوس فيزياء /كلية العلوم /جامعة النهرين 2001

ماجستير بصريات الالكترون /كلية العلوم/ جامعة النهرين 2003

## بإشراف

أ.د.أحمد كمال أحمد و د.كمال حسين لطيف